Author's response

November 5, 2020

Dear Fiona O'Connor,

thank you for overseeing the review process of our manuscript. In the following we attached our reply to the reviewer comments. The revised manuscript and supplement with all changes highlighted is included at the end of this document.

If any questions arise, please do not hesitate to contact me.

Kind regards,
Franziska Winterstein, on behalf of all co-authors

Reply to referee # 1

October 26, 2020

Dear Referee #1,

thank you for your constructive comments on the manuscript. We appreciate your eye for detail. In the following we reply to your comments point-by-point. The indicated pages of the answers relate to the discussion paper.

1 Specific comments

I don't feel that the diagrams, particularly Figure 1 and S1, are sufficiently clear enough to represent the mechanism or equations in use, and these should be included instead, or references supplied.

Thank you for this suggestion. Initially, we decided to reduce the manuscript by omitting the chemical reactions included in the submodel CH4, as they are cited in nearly every publication concerning methane (CH_4), and provided the differential equation in form of Eq. (1) instead. However, we understand that this reduces the comprehensibility of the concept and therefore include the sink reactions of CH_4 in the revised manuscript and move the differential equation to the introduction section of the CH4 submodel.

The paper describes a submodel already somewhat extensively described by Eichinger et al, 2015a, reference in this paper, and this does potentially diminish its novelty. I think it would be important to add a clear section on any differences between the implementation described here and that already in Eichinger et al.

Thank you for pointing this out. It is true that Eichinger et al, 2015a used a preliminary version of the CH4 submodel. Since then the submodel was updated and extended by the age and emission classes and by the treatment of the four most abundant isotopologues (while Eichinger et al, 2015a included deuterated methane (CH_3D) only). In the revised manuscript, we mention these unpublished developments in the introduction. Since this manuscript in GMD is meant to be a documentation of the submodel, we think it is adequate to document all features, even if some have already been described and used by Eichinger et al. (2015), yet without a full documentation.

Included paragraph in section 1:
"An early version of the simplified CH_4 chemistry (CH4) submodel has been described by Eichinger et al. (2015). The present version has been updated and extended by the additional features for simulating age and emission classes and isotopologues."

I feel the paper would be strengthened, and the assessment of the submodel for SWV simulations improved, if a further section were added on this point. I appreciate that this is difficult given the underpinning model biases, but I would suggest, in particular, that the use of instantaneous production of 2 water molecules per CH4 oxidised might be assessed further, and it may also be interesting to ask, What is the impact of the use of the CH4 submodel on radiative forcing from all relevant species, that is H2O, CH4 and O3 vs a model in which the effect of CH4 on SWV was excluded?

Yes, this is an important point. We have studied the water vapor yield of CH_4 oxidation in detail, see Frank et al. (2018) (see also the added text in a comment below). If the CH4 submodel is used alone, there is no detailed chemical mechanism solved. Thus, in these cases there is no impact on ozone (O_3). Usually for such model setups a precalculated O_3 time series or climatology is prescribed for the radiation calculation. An evaluation of the impact of the CH_4 oxidation on the radiative forcing (with or without the impact on O_3) would be a study by itself and is clearly beyond the scope of the current manuscript, which is meant as a documentation of the submodel. Instead we refer to Revell et al. (2016), who quantified the impact of CH_4 oxidation on stratospheric water vapor (SWV), Stenke and Grewe (2005), who investigated the effect of SWV trends on stratospheric O_3 chemistry and Solomon et al. (2010), who linked changes in SWV (in particular in the upper stratosphere, where CH_4 oxidation makes the biggest impact) to global warming.

I think the paper would be improved by the addition of more detail on the impact of the choices made, particularly considering the processes or feedbacks that it was necessary to omit or treat at a reduced level of detail in the submodel and how these choices impact model skill.

Thank you for this suggestion. We decided to include a discussion why the present framework of a reduced chemistry is applicable to CH_4 and which requirements have to be met so that the simulated results are meaningful.

Included paragraph in section 3:
The presented framework of the reduced CH_4 chemistry is applicable, since CH_4 is only reduced and not produced in the free atmosphere. Therefore the discretization of the four reactions, where CH_4 is involved, is sufficient to represent the chemical loss of CH_4. Nevertheless, in order to have consistent simulation results with the CH4 submodel some prerequisites have to be met. Since the educts (the hydroxyl radical (OH), chlorine (Cl) and excited oxygen ($O(^1D)$)) are prescribed, there is no feedback on them. Thus, very large variations in CH_4 mixing ratio, which would in reality influence the CH_4 sink (Winterstein et al., 2019), are not representable by the CH4 submodel. That means it is necessary to have a balanced CH_4 mixing ratio and CH_4 sink for a sufficient simulation skill.

Assessment of the correctness of the implementation of the atmospheric feedbacks is important here, and it is unfortunate that the concept of feedback is used somewhat broadly, which slightly obstructs the reader's own assessment of what the feedbacks are between or how they arise and whether they are implemented correctly. A key feedback is that of CH4 on OH, yet the specific examples do not mention OH, or the generation of species which could be the sink for OH, such as CO. Mention is made of HO2, however.
Similarly, the use of the phrase 'predefined fields' could be made more explicit to indicate the coupling.
L7: Is the oxidation always 'offline', that is the loss of OH is not returned to the chemical solver as a feedback.

Thank you for pointing this out. We see that there is need to make the phrase 'predefined fields' more clear and when we include feedbacks and when not. 'Predefined' means that they are prescribed from outside of the CH4 submodel. The CH4 submodel does not change the sink by OH (or the other sink reactants). This explains that there are no feedbacks of the CH4 submodel on the CH_4 sink educts and why we omitted the chemical processes forming or destroying these reactants. We added text to explain this in the manuscript (see next remark).

L131: the model can be coupled to, but what is the nature of the coupling? One-way(submodel receives oxidant fields) or two-way (submodel returns depleted OH, Cl fields to MECCA)?

The coupling with the Module Efficiently Calculating the Chemistry of the Atmosphere (MECCA) is one way only, as the reactant fields defined by MECCA are imported into the CH4 submodel. The CH4 submodel does not alter the reactant fields (OH, Cl and $O(^1D)$), but it optionally does alter the water vapor. We added this explanation in the manuscript.

The prescribed fields are taken either from existing simulation results with detailed chemistry, or from other data sources (e.g. reanalyses or projections). If CH4 is included in an ECHAM/MESSy Atmospheric Chemistry (EMAC) chemistry-climate model (CCM) simulation (which is possible in the Modular Earth Submodel System (MESSy) framework), the CH4 submodel can also be coupled to the reactant fields, which are on-line calculated during the same simulation by the chemical mechanism (i.e. MECCA). Although this does not save computational requirements, such a simulation configuration can be used, for example, if output of one of the additional options of the CH4 submodel (age and emission classes or isotopologues) are desired. In that case a second CH_4 tracer is treated and oxidized by the reactants solved from the kinetic solver of the comprehensive chemical mechanism. The same applies for the photolysis rate of CH_4, which can be prescribed from offline provided gridded data or on-line calculated by the submodel JVAL (Sander et al., 2014). **In either case, the CH4 submodel does not alter the reactant fields. Hence there is no feedback on the CH_4 sink by the submodel. In case of a coupling to MECCA via the reactant fields the coupling is one-way only.**

L 138: 'secondary feedback': implies that there is feedback, but of which species?

MECCA describes the full chemical mechanism, which includes the production and loss of the reactant species OH, Cl and $O(^1D)$. We rephrase this paragraph to emphasize the difference between MECCA and the CH4 submodel.

Old:

Figure 1 visualizes the conceptual differences between the MESSy submodel CH4 (left) and a CCM simulation with MECCA (right). MECCA simulates the entire chemical mechanism and therefore also includes the feedback onto the reaction partners (depicted in yellow) of CH_4. Additionally, there is also a secondary feedback by the products from the CH_4 sink reactions (e. g. water vapour (H_2O), HO_2, depicted in blue). Conversely, the CH4 submodel uses the predefined fields of the reactant species to calculate the CH_4 loss. This loss is included in the master tracer of the CH4 submodel, but does not feedback onto the sink fields or any other chemical species, except H_2O, in the case when the hydrological feedback of CH_4 oxidation is switched on. General Circulation Models (GCMs) include CH_4 foremost for its radiative impact as a greenhouse gas, but also for its influence on stratospheric water vapor (SWV, e.g. Monge-Sanz et al. (2013); ECMWF (2007); Austin et al. (2007); Boville et al. (2001); Mote (1995)). The CH4 submodel is likewise equipped with an optional feedback onto H_2O, to account for the secondary climate feedback of CH_4. It is thereby assumed that two molecules of H_2O are produced per oxidized CH_4 molecule (le Texier et al., 1988), which is, however, only a rough approximation as analyzed by Frank et al. (2018).

New:

Figure 1 visualizes the conceptual differences between the MESSy submodel CH4 (left) and a CCM simulation with MECCA (right). MECCA simulates the entire chemical mechanism and therefore also includes the feedback onto the reaction partners (depicted in yellow) of CH_4. Additionally, there is also a secondary feedback by the products from the CH_4 sink reactions (e.g., H_2O, HO_2, depicted in blue), as the subsequent chemical processes are influenced by the products from the CH_4 oxidation. Conversely, the CH4 submodel uses the prescribed fields of the reactant species to calculate the CH_4 loss. This loss is included in the master tracer of the CH4 submodel (the present CH_4 is reduced), but does not feedback onto the sink fields or any other chemical species. The only exception is H_2O, in the case when the hydrological feedback of CH_4 oxidation is switched on. GCMs include CH_4 foremost for its radiative impact as a greenhouse gas, but also for its influence on stratospheric water vapor (SWV, e.g. Monge-Sanz et al. (2013); ECMWF (2007); Austin et al. (2007); Boville et al. (2001); Mote (1995)). The CH4 submodel is likewise equipped with an optional feedback onto H_2O, to account for part of the secondary climate feedback of CH_4. It is thereby assumed that two molecules of H_2O are produced per oxidized CH_4 molecule (le Texier et al., 1988), which is, however, only a rough approximation as analyzed by Frank et al. (2018). The approximation of two molecules H_2O per oxidized CH_4 molecule overestimates the

H_2O production in the lower stratosphere and underestimates the production in the upper stratosphere. It also does not account for the chemical loss of H_2O in the mesosphere.

Figure 1: what do the green and black lines signify? What is the meaning of the differently shaded arrows? What is the meaning of yellow and red species?

We reduced to some extent the different coloring in the figure as it has no meaning. The red species is the core species CH_4. We depicted the sink reactants in yellow. Blue is reserved for the products of the oxidation of CH_4 (H_2O only, in case of the CH4 submodel).

Figure 1: caption has what I believe should be in the text 'predefined fields without feedback' but what about the effect of HO2 on OH?

In the CH4 submodel there is no feedback of HO2 on OH. In MECCA such feedbacks are included. We changed the caption to make this more clear.

L145: Would it be possible to add what the effect of this approximation is?

Yes, we added a sentence describing the most important aspects of this approximation.

Included:
The constant approximation of two molecules H_2O per oxidized CH_4 molecule overestimates the H_2O production in the lower stratosphere and underestimates the production in the upper stratosphere. It also does not account for the chemical loss of H_2O in the mesosphere.

Does H2O feedback on stratospheric ozone?

In the case of a simulation, where the CH4 submodel is the only component simulating the atmospheric chemistry, there is no feedback of H_2O on O_3, since there is no interactively calculated O_3 tracer (usually only a prescribed O_3 climatology is used).

2 Detailed comments

L13: what does 'similar to' mean here more precisely? **We used 'similar' to point out the technical similarity in adding the produced H_2O and deuterated water vapour (HDO).**

What do you mean by 'feedback' to the isotopological hydrological do you mean 'is passed back'? **Thank you for this paraphrase as it is exactly what we mean. We changed it accordingly.**

L43: remove comma between both, natural **Agreed.**

L46: what do you mean by 'not sufficiently accurate' here? Do you mean the lifetime is too short? **Our intention is to state that the lifetime - or strictly speaking OH - is an important factor for the atmospheric chemistry, however challenging to simulate accurately. We rephrased this to: The lifetime of CH_4 is in the order of magnitude of 10 years, but its exact values is still unknown and subject to uncertainties. However, CH_4 is an important precursor of the Ox/HOx chemistry in CCMs. For this reason, in most CCM setups CH_4 is prescribed at the lower model boundary to achieve a realistic CH_4 burden independent of the simulated lifetime.**

L56: reference required? **We revised the given values and added a reference.**

L60: Earth's surface **Agreed.**

L74 *and* L80: rate constant not rate, given what comes after in the text, k is usually reserved for rate constant but this is of course correct **Thank you for pointing this out. Although we decided to change the term to rate coefficient, since it is not constant. We removed this confusion of notation here and in the whole manuscript.**

L114: insert 'to' so as will read 'submodel to represent' **Agreed.**

L186: modify 'is not conform with' *and* **L193:** modify 'to be conform with' **We corrected *conform* by *consistent*.**

L200: drop comma between 'choose, whether' **Agreed.**

L220: would make more sense as a list: 1) the CH4 submodel, 2) MECCA_TAG and 3) H2O... **Agreed.**

L221-222: drop 'are treating' **We changed this to *include*.**

L231: 'doubles' is not very clear: do you mean 'duplicates'? **Thank you, we adopted this suggestion.**

L303: replace 'most and largest' with 'most importantly'? **We reduced it to "Most isotopically light emissions...", since we refer to the magnitude and extent of the emission.**

L306: sentence is rather inelegant. **We revised this to: "When CH_4 is ascending in the atmosphere it is exposed to oxidation. Due to fractionation processes heavy CH_4 isotopologues are unfavored and therefore accumulate in the remaining CH_4 content."**

L308-317: values are required for quantitative comparison. **We added more concrete results in the supplement.**

References

Austin, J., Wilson, J., Li, F., and Vömel, H.: Evolution of Water Vapor Concentrations and Stratospheric Age of Air in Coupled Chemistry-Climate Model Simulations, Am. Met. Soc., pp. 905–921, doi: 10.1175/JAS3866.1, 2007.

Boville, B. A., Kiehl, J. T., Rasch, P. J., and Bryan, F. O.: Improvements to the NCAR CSM-1 for Transient Climate Simulations, J. Climate, 14, 164–179, doi: 10.1175/1520-0442(2001)014¡0164:ITTNCF¿2.0.CO;2, 2001.

ECMWF: IFS DOCUMENTATION - Cy31r1, Part IV: Physical Processes, URL `https://www.ecmwf.int/sites/default/files/elibrary/2007/9221-part-iv-physical-processes.pdf`, 2007.

Eichinger, R., Jöckel, P., Brinkop, S., Werner, M., and Lossow, S.: Simulation of the isotopic composition of stratospheric water vapour - Part 1: Description and evaluation of the EMAC model, Atmos. Chem. Phys., 15, 5537–5555, doi: 10.5194/acp-15-5537-2015, 2015.

Frank, F., Jöckel, P., Gromov, S., and Dameris, M.: Investigating the yield of H_2O and H_2 from methane oxidation in the stratosphere, Atmos. Chem. Phys., 18, 9955–9973, doi: 10.5194/acp-18-9955-2018, URL `https://www.atmos-chem-phys.net/18/9955/2018/`, 2018.

le Texier, H., Solomon, S., and Garcia, R. R.: The role of molecular hydrogen and methane oxidation in the water vapour budget of the stratosphere, Quart. J. Roy. Meteor. Soc., 114, 281–295, doi: 10.1002/qj.49711448002, 1988.

Monge-Sanz, B. M., Chipperfield, M. P., Untch, A., Morcrette, J.-J., Rap, A., and Simmons, A. J.: On the uses of a new linear scheme for stratospheric methane in global models: water source, transport tracer and radiative forcing, Atmos. Chem. Phys., 13, 9641–9660, doi: 10.5194/acp-13-9641-2013, URL `https://www.atmos-chem-phys.net/13/9641/2013/`, 2013.

Mote, P.: The annual cycle of stratospheric water vapor in a general circulation model, J. Geophys. Res., 100, 7363–7379, doi: 10.1029/94JD03301, URL http://onlinelibrary.wiley.com/doi/10.1029/94JD03301/pdf, 1995.

Revell, L., Stenke, A., Rozanov, E., Ball, W., Lossow, S., and Peter, T.: The role of methane in projections of 21st century stratospheric water vapour, Atmos. Chem. Phys., 16, 13 067–13 080, doi: 10.5194/acp-16-13067-2016, URL www.atmos-chem-phys.net/16/13067/2016/, 2016.

Sander, R., Jöckel, P., Kirner, O., Kunert, A. T., Landgraf, J., and Pozzer, A.: The photolysis module JVAL-14, compatible with the MESSy standard, and the JVal PreProcessor (JVPP), Geosci. Model Dev., 7, 2653–2662, doi: 10.5194/gmd-7-2653-2014, URL www.geosci-model-dev.net/7/2653/2014/, 2014.

Solomon, S., Rosenlof, K. H., Portmann, R. W., Daniel, J. S., Davis, S. M., Sanford, T. J., and Plattner, G.-K.: Contributions of Stratospheric Water Vapor to Decadal Changes in the Rate of Global Warming, Science, 327, 1219–1223, doi: 10.1126/science.1182488, 2010.

Stenke, A. and Grewe, V.: Simulation of stratospheric water vapor trends: impact on stratospheric ozone chemistry, Atmos. Chem. Phys., 5, 1257–1272, URL www.atmos-chem-phys.org/acp/5/1257/, 2005.

Winterstein, F., Tanalski, F., Jöckel, P., Dameris, M., and Ponater, M.: Implication of strongly increased atmospheric methane concentrations for chemistry–climate connections, Atmos. Chem. Phys., 19, 7151–7163, doi: 10.5194/acp-19-7151-2019, URL https://www.atmos-chem-phys.net/19/7151/2019/, 2019.

Reply to referee # 2

October 26, 2020

Dear Referee # 2,

thank you very much for such positive comments on our manuscript. In the following we reply to your comments point-by-point. The indicated pages of the answers relate to the discussion paper.

1 Main concern

The CH4 model is being promoted as a useful alternative for studying methane, its isotopes, and stratospheric water vapour to the more complete and computationally expensive full chemistry scheme. As a result, I thought that the manuscript could be improved by including some verification of the CH4 model compared with the (presumably) EMAC simulation from which the sink fields used in the CH4 set up originated. How do they compare in terms of global mean methane concentration, methane lifetime, methane budget etc..? How does the modelled lifetime compare with other (fullcomplexity) models (e.g., Stevenson et al., https://acp.copernicus.org/preprints/acp-2019-1219/) and/or inversion studies? Benchmarking the CH4 model performance against EMAC and placing its performance in the context of other models/studies would be a valuable addition to the manuscript.

Thank you for this suggestion. In fact the methane (CH_4) mixing ratio of the simplified CH_4 chemistry (CH4) submodel and the Module Efficiently Calculating the Chemistry of the Atmosphere (MECCA) are by design identical, if the same CH_4 sources are applied and in CH4 the same educts are prescribed as calculated in MECCA. In that case also the CH_4 lifetime is the same, since it is defined by the sinks. Therefore, from our point of view, a comparison of CH_4 simulated by the CH4 submodel with that simulated by MECCA is not really meaningful. However, an important factor for the skill of matching the atmospheric CH_4 mixing ratio is the method of how CH_4 emissions are treated. In case of prescribing CH_4 at the lower boundary, the CH_4 mixing ratio in the troposphere represents the chosen condition. In the Earth System Chemistry integrated Modelling (ESCiMo) project (Jöckel et al., 2016) the zonally averaged marine boundary surface data provided by the National Oceanic and Atmospheric Administration/Earth System Research Laboratory (NOAA/ESRL) was used as the lower boundary condition and the simulations consequently reproduced the observations. Jöckel et al. (2016) also show that the CH_4 lifetime in the ECHAM/MESSy Atmospheric Chemistry (EMAC) model is with 8.0 ± 0.6 a rather low, but within the uncertainty range of similar studies. When using emission fluxes as lower boundary condition, reproducing (globally averaged) observations is much more challenging, as current emission inventories are subject to large uncertainties and the exact lifetime of CH_4 is still unknown. For example, we found that inventories derived by inverse modeling are quite dependent on the assumed hydroxyl radical (OH) and hence the CH_4 lifetime (Frank, 2018; Zhao et al., 2020).

The inclusion of optional region and age classes is a valuable addition to the CH4 model and this information will be useful for estimating emission strengths. The authors cite the example of using a fixed-lag Kalman Filter, which performs an inverse optimization of the emission inventory by comparing simulated and observed mixing ratios of a trace gas. However, although the example provided of the time evolution of a single region class is a nice illustration, it is by no means evidence of the suitability of the CH4 model as a tool for doing emission inventory optimization. In line with the comment above,

providing a more in-depth assessment of the model performance against observations would greatly strengthen the manuscript and provide evidence of its suitability as a tool for estimating emissions.

Yes, we also think that the estimation of emission strengths is a crucial part of modeling CH_4. The mentioned fixed-lag Kalman Filter and its application in a preproduction has been shown in Frank (2018). In the current publication we present the technical prearrangements, which are part of the CH4 submodel. As stated before, the performance of simulation results against observations is strongly influenced by the used emission inventory, which is, when targeting emission estimation, not expected to be sufficient a priori. And an in-depth analysis of the application and performance of a full inversion using the concept of the Kalman Filter would be beyond scope of the current manuscript. This will be shown elsewhere in the peer reviewed literature, since work on this is still ongoing. Nevertheless, we include the reference to Frank (2018) in the revised manuscript.

Included in section 3.1:
The third option is implemented for usage by a fixed-lag Kalman filter for inverse optimization. With this option, one age class represents one month and at the end of one month all CH_4 of one age class moves to the next. This option is specifically implemented to be consistent with the Leapfrog time stepping (c.f. option (1)). **A preliminary application of the concept of using the age and emission classes for an inverse optimization using the fixed-lag Kalman Filter has been shown in Frank (2018).**

The authors, in the context of isotopes, also state that the simulation results compare well to observations. Can you include these comparisons with observations, for example?

Yes, we added the comparisons we referred to into the revised supplement.

2 Specific comments

Page 2, line 25 and Page 2, line 33: While methane as a source of stratospheric water vapour (SWV) is unequivocal, it is important to, at least, acknowledge the role of methane as an ozone precursor. From a climate forcing perspective, this indirect forcing is much larger than that from methane-driven changes in SWV but is neglected from the MESSy/CH4 configuration presented here.

Thank you for this comment. Yes, this is indeed a drawback of the CH4 submodel and we add a discussion of this into the revised manuscript. Although we must object that the indirect forcing from influencing ozone (O_3) is much larger than that from water vapour (H_2O). From a rapid adjustments perspective the indirect forcing of O_3 and H_2O is of about the same magnitude (Winterstein et al., 2019). Considering slow climate adjustments the effect of H_2O is three times larger (Stecher et al., 2020).

Included paragraph in section 3:
Furthermore, the setup with the CH4 submodel also lacks any feedback on O_3. In the atmosphere, the O_3 chemistry is influenced by changes in the hydroxyl radical (OH) (reduced by CH_4), H_2O (produced by CH_4) and temperature (influence by radiative forcing of the abundant CH_4). The CH4 submodel alters H_2O and with that influences the radiation budget and hence the temperature, however, there is no feedback on O_3 when the setup does not include any other chemical mechanism. In a setup where the CH4 submodel is not used in parallel to MECCA, O_3 climatologies are usually prescribed for the radiation scheme.

Page 8, line 190: Can you be specific about what fraction of the age class is moved to the next class when this option is used?

Thank you for this question, since this seems not clear in the text. The fraction is defined by α. We included this note to the text.

$$M' = \alpha \cdot M, \tag{1}$$

with $\alpha = \frac{\Delta t}{\tilde{T}}$ and $\tilde{T}$ being the user-defined time-span indicating the binning width of the age class. This option carries out a quasi-continuous update of the age classes, as it moves at every time step a fraction **(i.e. defined by α)** of the current age class to the next.

Page 8, line 194: Can you comment on how significant or large is this lack of conservation?

The described procedure is done to avoid the accumulation of small (numerical) errors, which mainly arise from small non-linearities of the large scale advection scheme. The magnitude therefore depends on the applied advection scheme, but is usually of the order of floating point precision. We added this explanation to the text as well.

Included in section 3.1:
In order to reduce numerical errors, the age and emission classes are continuously constrained (i.e., in each model time step) to sum up to the master tracer and are scaled appropriately, if the sum deviates. **The described procedure is done to avoid the accumulation of such numerical errors, which mainly arise from small non-linearities of the large scale advection scheme. The magnitude therefore depends on the applied advection scheme, but is usually of the order of floating point precision.**

Page 14, line 331: Here, you refer to the temperature bias in EMAC leading to a negative bias in water vapour. Is this temperature bias even evident in simulations with specific dynamics or when EMAC is free running?

The negative temperature bias in EMAC is strongest in free running set-ups. It is reduced but is still evident in simulations with specified dynamics as long as the wave-0 (or mean) of the temperature is not included in the nudging procedure, i.e. the temperature bias is not corrected. This is the usually applied procedure for specified dynamics. As soon as the mean temperature is included in the nudging, the bias nearly disappears. For more detailed information on the nudging procedure and the temperature bias, we refer to Jöckel et al. (2016).

Included in section 5.3:
This is associated with a too cold tropopause in EMAC, where a temperature bias of -2 to -6 K is detected in the upper troposphere**, as long as the mean temperature is excluded from the nudging procedure defining the specified dynamics setup** (Jöckel et al., 2016).

A complete listing of the CH4 chemical mechanism, including isotopes, would make the description more complete rather than only showing the temperature dependent KIEs. This could be added to the Supplementary Material.

As also suggested by the other reviewer we include in the revision the CH_4 sink reactions (R1–R4) in section 1. We also include the corresponding reactions with isotopes deuterium (D) and carbon-13 (^{13}C) in the revised supplement.

3 Technical comments

Page 4, line 102: Please change The here presented new submodel for simplified CH4 chemistry (CH4) and the auxiliary submodel TRacer SYNChronization (TRSYNC) are implemented based on this framework. to Presented here is a new.... **Agreed.**

Page 7, line 160: Change which can be specified by the user via namelist to which can be specified by the user via a namelist **Agreed.**

Page 7, line 162: Change denotes thereby to thereby denotes **Agreed.**

Page 7, line 167: Change identical to identically **Agreed.**

Figure 2: The onward arrow from tracer e02 a02 should possibly be dotted to be consistent with the one from tracer e01 a02 **Thank you, we changed that for consistency.**

Page 7, line 176: Change fixed-lag to a fixed time lag **Agreed.**

Page 8, line 184: The sentence The implementation of this option is not conform with a Leapfrog time stepping with Asselin-filter and might cause numerical oscillations with negative values Is very awkwardly written please rephrase. **We changed it to: This option is not consistent with a Leapfrog time stepping using an Asselin-filter and might cause numerical oscillations and negative values.**

Page 8, line 193: Again, awkward phrasing with the use of to be conform in the phrase This option is specifically implemented to be conform with the Leapfrog timestepping (c.f. option (1)). Please re-phrase. **We corrected *conform* by *consistent*.**

Page 9, line 220: Replace the here presented CH4 submodel with the CH4 submodel presented here **Agreed.**

Page 10, line 232: Replace H2OISO doubles the hydrological cycle for the water isotopologues with H2OISO models the hydrological cycle for the water isotopologues or H2OISO represents the hydrological cycle for the water isotopologues **We changed *doubles* to *dublicates*. We want to point out that the hydrological cycle in H2OISO is in addition to the cycle in ECHAM.**

Thank you for these suggestions and corrections. We changed the manuscript accordingly.

References

Frank, F.: Atmospheric methane and its isotopic composition in a changing climate: A modelling study, Ph.D. thesis, Ludwigs Maximillian Universität München, 2018.

Jöckel, P., Tost, H., Pozzer, A., Kunze, M., Kirner, O., Brenninkmeijer, C. A. M., Brinkop, S., Cai, D. S., Dyroff, C., Eckstein, J., Frank, F., Garny, H., Gottschaldt, K.-D., Graf, P., Grewe, V., , Kerkweg, A., Kern, B., Matthes, S., Mertens, M., Meul, S., Neumaier, M., Nützel, M., Oberländer-Hayn, S., Ruhnke, R., Runde, T., Sander, R., Scharffe, D., and Zahn, A.: Earth System Chemistry integrated Modelling (ESCiMo) with the Modular Earth Submodel System (MESSy) version 2.51, Geosci. Model Dev., 9, 1153–1200, doi: 10.5194/gmd-9-1153-2016, URL `http://www.geosci-model-dev.net/9/1153/2016/gmd-9-1153-2016.html`, 2016.

Stecher, L., Winterstein, F., Dameris, M., Jöckel, P., Ponater, M., and Kunze, M.: Effects of Strongly Enhanced Atmospheric Methane Concentrations in a Fully Coupled Chemistry-Climate Model, Atmospheric Chemistry and Physics Discussions, 2020, 1–31, doi: 10.5194/acp-2020-519, URL `https://acp.copernicus.org/preprints/acp-2020-519/`, 2020.

Winterstein, F., Tanalski, F., Jöckel, P., Dameris, M., and Ponater, M.: Implication of strongly increased atmospheric methane concentrations for chemistry–climate connections, Atmos. Chem. Phys., 19, 7151–7163, doi: 10.5194/acp-19-7151-2019, URL https://www.atmos-chem-phys.net/19/7151/2019/, 2019.

Zhao, Y., Saunois, M., Bousquet, P., Lin, X., Berchet, A., Hegglin, M. I., Canadell, J. G., Jackson, R. B., Deushi, M., Jöckel, P., Kinnison, D., Kirner, O., Strode, S., Tilmes, S., Dlugokencky, E. J., and Zheng, B.: On the role of trend and variability of hydroxyl radical (OH) in the global methane budget, Atmospheric Chemistry and Physics Discussions, 2020, 1–28, doi: 10.5194/acp-2020-308, URL https://acp.copernicus.org/preprints/acp-2020-308/, 2020.

Methane chemistry in a nutshell – The new submodels CH4 (v1.0) and TRSYNC (v1.0) in MESSy (v2.54.0)

Franziska Winterstein[1] and Patrick Jöckel[1]

[1]Deutsches Zentrum für Luft- und Raumfahrt (DLR), Institut für Physik der Atmosphäre, Oberpfaffenhofen, Germany

Correspondence: Franziska Winterstein (franziska.winterstein@dlr.de)

Abstract. Climate projections including chemical feedbacks rely on state-of-the-art chemistry-climate models (CCMs). Of particular importance is the role of methane (CH_4) for the budget of stratospheric water vapor (SWV), which has an important climate impact. However, simulations with CCMs are, due to the large number of involved chemical species, computationally demanding, which limits the simulation of sensitivity studies.

To allow for sensitivity studies and ensemble simulations with a reduced demand for computational resources, we introduce a simplified approach to simulate the core of methane chemistry in form of the new Modular Earth Submodel System (MESSy) submodel CH4. It involves an atmospheric chemistry mechanism reduced to the sink reactions of CH_4 with predefined fields of the hydroxyl radical (OH), excited oxygen ($O(^1D)$), and chlorine (Cl), as well as photolysis and the reaction products limited to water vapour (H_2O). This chemical production of H_2O is optionally feed back onto the specific humidity (q) of the connected General Circulation Model (GCM), to account for the impact onto SWV and its effect on radiation and stratospheric dynamics.

The submodel CH4 is further capable of simulating the four most prevalent CH_4 isotopologues for carbon and hydrogen (CH_4 and CH_3D as well as $^{12}CH_4$ and $^{13}CH_4$), respectively. Furthermore, the production of deuterated water vapour (HDO) is, similar to the production of H_2O in the CH_4 oxidation, optionally ~~feed~~ passed back to the isotopological hydrological cycle simulated by the submodel H2OISO, using the newly developed auxiliary submodel TRSYNC. Moreover, the simulation of a user defined number of diagnostic CH_4 ~~age~~ age and emission classes is possible, which output can be used for offline inverse optimization techniques.

The presented approach combines the most important chemical hydrological feedback including the isotopic signatures with the advantages concerning the computational simplicity of a GCM, in comparison to a full featured CCM.

1 Introduction

It is beyond question that methane (CH_4) is a strong greenhouse gas (GHG), with an estimated global warming potential (GWP) of 34 times that of carbon dioxide (CO_2) on a 100 year horizon (IPCC, 2013). Therefore, most General Circulation Models (GCMs) include the effect of the radiative forcing of CH_4. However, the effect of CH_4 is underrepresented by only

using its direct radiative impact and not accounting for the water vapour (H_2O) produced by the oxidation of CH_4 due to a set-up without chemistry. Especially in the stratosphere this additional H_2O (stratospheric water vapor (SWV)) influences among others the radiative forcing, stratospheric temperature and the ozone (O_3) chemistry (Stenke and Grewe, 2005; Tian et al., 2009; Solomon et al., 2010; Revell et al., 2012; Winterstein et al., 2019). The inclusion of production of H_2O by CH_4 requires a chemical mechanism as provided by chemistry-climate models (CCMs). Current state-of-the-art CCMs include a vast amount of chemical species and reactions. By extending the chemical mechanisms, one intends to achieve an increase in accuracy of the atmospheric chemistry representation. At the same time, however, the computational demands increase. Although, available computational power increases at a certain rate, too, the availability and capacity of high performance computers is a limiting factor for sensitivity studies in climate projection simulations with CCMs.

It is hence advisable to recognize both main effects of CH_4, namely its radiative forcing and its impact on SWV, but keeping computational demands low at the same time. Therefore, our approach to simulate CH_4 includes both effects and is able to use predefined reaction partners of CH_4, which reduces computational cost to a minimum.

An early version of the simplified CH_4 chemistry submodel (CH4) has been described by Eichinger et al. (2015a). The present version has been updated and extended by the additional features for simulating age and emission classes and isotopologues.

Sections 1.1 and 1.2 introduce the sources and sinks of CH_4, and CH_4 isotopologues and their fractionation effects, respectively. In Sect. 2 we briefly present the Modular Earth Submodel System and describe the concept of the CH4 submodel in Sect. 3. Two additional options of the CH4 submodel are explained in the subsequent Sects. 3.1 and 3.2. The coupling to the hydrological cycle with the submodel TRSYNC is introduced in Sect. 4. We show three example applications using the newly presented submodels in Sect. 5 and end with a short summary. Parts of the manuscript are based on the PhD thesis of the first author (Frank, 2018).

1.1 Sources and sinks of CH_4

Methane is a GHG emitted by both ~~,~~natural, and anthropogenic sources at the Earth's surface. There are basically no known chemical sources of CH_4 in the free atmosphere.

In CCMs usually predefined lower boundary conditions instead of emission fluxes are used to describe atmospheric CH_4. This approach is mainly employed due to two major problems: (1) The ~~simulated CH_4 lifetime is not sufficiently accurate, however important for tropospheric and stratospheric chemistry~~ lifetime of CH_4 is in the order of magnitude of 10 years, but its exact value is still unknown and subject to uncertainties. However, CH_4 is an important precursor of the Ox/HOx chemistry in CCMs. For this reason, in most CCM setups, CH_4 is prescribed at the lower model boundary to achieve a realistic CH_4 burden independent of the simulated lifetime. ~~Thus, realistic climate projections with interactive chemistry and CH_4 emission fluxes are difficult.~~ (2) Despite large ongoing efforts, current emission inventories are still subject to large uncertainties, as top-down and bottom-up inventories differ significantly (e.g. EDGAR or Saunois et al. (2016)). This mismatch indicates the dilemma, that there are a lot of open questions with respect to both, the magnitude of sources, and the sinks of CH_4.

Methane is removed from the atmosphere mainly by three photochemical reactions:

$$CH_4 + OH \overset{k_{CH_4+OH}}{\rightarrow} CH_3 + H_2O \quad \text{(R1)}$$

$$CH_4 + O(^1D) \overset{k_{CH_4+O(^1D)}}{\rightarrow} products \quad \text{(R2)}$$

$$CH_4 + Cl \overset{k_{CH_4+Cl}}{\rightarrow} CH_3 + HCl \quad \text{(R3)}$$

and is also depleted by photolysis:

$$\frac{d[CH_4]}{dt} = (-k_{CH_4+OH} \cdot c_{\text{air}} \cdot [OH] - k_{CH_4+O(^1D)} \cdot c_{\text{air}} \cdot [O(^1D)] - k_{CH_4+Cl} \cdot c_{\text{air}} \cdot [Cl] - p_{CH_4+h\nu}) \cdot [CH_4],$$

~~where X denotes the mixing ratio of species X in moles of the chemical tracer per mole of air (mol mol^{-1}), c_{air} the concentration of air in cm^{-3}, k_R the reaction rate coefficient of reaction R in cm^3 s^{-1} and $p_{CH_4+h\nu}$ the photolysis rate of CH_4 in s^{-1}~~

$$CH_4 + h\nu \overset{j_{CH_4+h\nu}}{\rightarrow} products \quad \text{(R4)}$$

with (R1)–(R3) from (Sander et al., 2011) and (R4) from (Sander et al., 2014).

~~About 88~~

About 92 % of the atmospheric CH_4 removal happens in the troposphere. The largest part is thereby the reaction with the hydroxyl radical (OH) (~~95~~>90 % of the tropospheric sink), while the rest is attributed to the reaction with chlorine (Cl) in the ~~Marine Boundary Layer (MBL)~~Marine Boundary Layer (MBL, Kirschke et al. (2013)). About 8 % of CH_4 is depleted in the stratosphere, by the reactions with OH, excited oxygen ($O(^1D)$), Cl and through photolysis (IPCC, 2013).

Another sink of CH_4 is the so called soil-loss at the ~~Earths'~~Earth's surface. CH_4 is either depleted by CH_4 consuming bacteria (methanotrophs), or it is removed from the air by diffusive transport into the soil, which is mostly influenced by soil water content (King, 1997). Globally, the soil-loss accounts for approximately 4 % of the total CH_4 sink (IPCC, 2013).

1.2 Isotopologues of CH_4

A powerful and common method in the investigation of the CH_4 budget is the study of CH_4 isotopologues. Production and removal of CH_4 cause fractionation effects, which lead to distinct isotopological signals in the atmosphere. These isotopic signatures provide potentially additional insights into the role of specific CH_4 sources and depleting reactions, and are already widely used in the context of CH_4 (Hein et al., 1997; Fletcher et al., 2004; Monteil et al., 2011; Rigby et al., 2012; Nisbet et al., 2016; Schaefer et al., 2016).

Fundamentally, the stable isotopologues of CH_4 form with respect to the most abundant stable isotopes of hydrogen and of carbon. The stable isotopes of hydrogen are ^{1}H and ^{2}H (deuterium, D), and for carbon, carbon-12 (^{12}C) and carbon-13 (^{13}C). This results in the first order stable isotopologues $^{12}CH_4$, $^{13}CH_4$, and CH_3D. The corresponding sink reactions are shown in the supplement section S1. The relative abundances of higher substituted and mixed isotopologues (e.g. CH_2D_2 or $^{13}CH_3D$) are less than 0.0007% (compared to 0.0616% of CH_3D) (Stolper et al., 2014) and hence neglected.

The chemical fractionation is based on the fact that isotopologues of the same molecule have different ~~reaction rates~~rate coefficients, i.e. they react with different speed or probability. This difference in ~~reaction rates~~ rate coefficients is described as

the so called Kinetic Isotope Effect (KIE) and becomes apparent during the chemical reaction of a specific molecule X:

$$X_L + E \quad \overset{k_L}{\rightarrow} P \tag{R5}$$

$$X_H + E \quad \overset{k_H}{\rightarrow} P' \tag{R6}$$

with X_L being its light (major), and X_H its heavy (minor) isotopologue. E and P/P' denote the reaction partner(s) and product(s), respectively. The value of the KIE is thereby defined as the ratio of the ~~reaction rates~~ rate coefficients k_L and k_H (Bigeleisen, 2005) and its inverse is called the fractionation factor α:

$$\text{KIE} := \frac{k_L}{k_H} = \frac{1}{\alpha}\,. \tag{1}$$

The KIEs of the sink reactions of CH_4 have been, among others, determined by Saueressig et al. (1995, 1996, 2001) and Crowley et al. (1999) in laboratory measurements (see Table 1). Since the KIEs of CH_4 isotopologues are partly temperature dependent, the KIEs are described by two parameters A and B and are calculated as

$$\text{KIE} = \text{A} \cdot \exp(\text{B}/T), \tag{2}$$

with T being the temperature in [K].

The largest KIE and therefore strongest fractionation effect is found for the reaction with Cl, which especially influences the isotopic composition of CH_4 in the middle and upper stratosphere (Saueressig et al., 1996; Bergamaschi et al., 1996). Conversely, the reaction with $O(^1D)$ shows the lowest KIE, which furthermore does not show any temperature dependence. The KIE of the reaction with OH is temperature dependent with respect to deuterated methane (CH_3D) but not with respect to methane containing ^{13}C ($^{13}CH_4$) (Saueressig et al., 2001). Nair et al. (2005) estimated the rate coefficients of the photodissociation of CH_4 and its major isotopologues for planet Mars, which results in a calculated KIE$= 1.005$ for CH_3D and a negligible isotopic fractionation for the ^{13}C isotopologue (Nixon et al., 2012). There is, especially for deuterium, a non-negligible fractionation during the soil-loss for CH_4 (Snover and Quay, 2000; Maxfield et al., 2008). An average value for the overall soil-loss is estimated as $\text{KIE}^{\text{soil}}_{CH_3D} = 1.0825$ and $\text{KIE}^{\text{soil}}_{^{13}CH_4} = 1.0196$ (Snover and Quay, 2000; Holmgren, 2006; Maxfield et al., 2008).

2 The Modular Earth Submodel System (MESSy)

The framework of the Modular Earth Submodel System (MESSy, used in the second version MESSy2, Jöckel et al. (2010)) is based on the idea to modularize a climate model in a way, that single components can be switched on and off independently, depending on the desired set-up, meeting the demands of current Earth System Modeling in terms of flexibility and computational performance. The modularization enables the user to pick suitable submodels or expand the model easily with new ones. ~~The here presented new submodel for~~ Presented here are the submodel CH4 and the auxiliary submodel TRacer SYNChronization (TRSYNC), which are implemented based on this framework.

For the application examples of the new ~~submodel~~submodels, MESSy is used together with the ~~core atmospheric model~~ 5th generation European Centre Hamburg general circulation model (ECHAM5, Roeckner et al. (2006)). The ECHAM/MESSy

Table 1. Temperature dependent KIEs of the sink reactions of CH_4 described as $\mathrm{KIE} = \mathrm{A} \cdot \exp(\mathrm{B}/T)$. The KIEs are valid in the given temperature range (T in [K]).

reaction	A	B	T	reference
$KIE^{OH}_{^{13}CH_4}$	1.0039	0.0	200–300	(Saueressig et al., 2001)
$KIE^{O(^1D)}_{^{13}CH_4}$	1.013	0.0	223–295	(Saueressig et al., 2001)
$KIE^{Cl}_{^{13}CH_4}$	1.043	6.455	223–297	(Saueressig et al., 1995; Crowley et al., 1999)
$KIE^{OH}_{CH_3D}$	1.097	49.0	249–422	(Saueressig et al., 2001)
$KIE^{O(^1D)}_{CH_3D}$	1.060	0.0	224–295	(Saueressig et al., 2001)
$KIE^{Cl}_{CH_3D}$	1.278	51.31	223–295	(Saueressig et al., 1996)

Atmospheric Chemistry (EMAC) model is a numerical chemistry and climate simulation system that includes sub-models describing tropospheric and middle atmosphere processes and their interaction with oceans, land and human influences (Jöckel et al., 2010). EMAC (ECHAM5 version 5.3.02, MESSy version 2.54, Jöckel et al. (2010, 2016)) is applied in the given examples in the T42L90MA-resolution, i.e. with a spherical truncation of T42, which corresponds to a quadratic Gaussian grid of approx. 2.8 by 2.8 degrees in latitude and longitude, and includes 90 vertical hybrid pressure levels from the Earth surface up to 0.01~~hPa~~ hPa. MESSy allows the configuration of EMAC in several operational modes. The two basic ones are the GCM set-up without chemistry and the CCM set-up with fully interactive chemistry, using, among other components, the Module Efficiently Calculating the Chemistry of the Atmosphere (~~MECCA~~MECCA, Sander et al. (2005)) ~~. MECCA~~ and the SCAVenging (SCAV, Tost et al. (2006)) submodel to represent the chemical kinetics of EMAC in gas phase and in aqueous phase, respectively. They define the underlying chemical reaction mechanisms in troposphere, stratosphere, and lower mesosphere. MECCA and SCAV provide comprehensive mechanisms, combining state-of-the-art reactions and rate coefficients. ~~The~~ The kinetic chemistry tagging technique (MECCA_TAG, Gromov et al. (2010)) enables the user to tag selected chemical elements, without modifying the underlying standard chemical mechanism of MECCA. It can be applied for simulating isotopologues of trace gases with respect to selected isotopes. In order to do so, rare and abundant isotopologues of the species of interest (e.g., those containing atomic hydrogen (H)) are created in an extended set of reactions in the same chemical mechanism.

MESSy and its application in EMAC has been used in multiple studies (see the special issue in Atmospheric Chemistry and Physics https://www.atmos-chem-phys.net/special_issue22.html) and includes several submodels from contributing institutions. Further information on EMAC, MESSy and its submodels can be found in Jöckel et al. (2010, 2016), on the web-site https://www.messy-interface.org/, or accompanying papers documenting the specific submodels.

3 The submodel CH4

The MESSy submodel CH4 aims to close the gap between the operational modes of EMAC as a GCM without chemistry and as a CCM with the comprehensive chemical mechanisms of MECCA and SCAV. The basic concept of the submodel is to limit

the chemical mechanism to the loss-processes of methane and use predefined fields of the reaction partners OH, O(^{1}D) and Cl to reduce the computational demands. ~~The predefined~~

The sink reactions (R1)–(R4) in the CH4 submodel are parameterized as follows:

$$\frac{d[CH_4]}{dt} = (-k_{CH_4+OH} \cdot c_{\text{air}} \cdot [OH] - k_{CH_4+O(^1D)} \cdot c_{\text{air}} \cdot [O(^1D)] - k_{CH_4+Cl} \cdot c_{\text{air}} \cdot [Cl] - j_{CH_4+h\nu}) \cdot [CH_4], \quad (3)$$

where [X] denotes the mixing ratio of species X in [mol mol^{-1}], c_{air} the concentration of air in [cm^{-3}], k_R the reaction rate coefficient of reaction R in [cm^3 s^{-1}] and $j_{CH_4+h\nu}$ the photolysis rate of CH_4 in [s^{-1}].

The prescribed fields are taken either from existing simulation results with detailed chemistry, or from other data sources (e.g. reanalyses or projections). If CH4 is included in an EMAC CCM simulation (which is possible in the MESSy framework), the CH4 submodel can also be coupled to the reactant fields, which are on-line calculated during the same simulation by the chemical mechanism (i.e. MECCA). Although this does not save computational requirements, such a simulation configuration can be used, for example, if output of one of the additional options of the CH4 submodel ~~are desired together with a coupled~~ (age and emission classes or isotopologues) are desired. In that case a second CH_4 tracer is treated and oxidized by the reactants provided by the kinetic solver of the comprehensive chemical mechanism. ~~Same~~ The same applies for the photolysis rate of CH_4, which can be ~~predefined~~ prescribed from offline provided gridded data or on-line calculated by the submodel JVAL (Sander et al., 2014). In either case, the CH4 submodel does not alter the reactant educts. Hence there is no feedback onto the CH_4 sink by the submodel. In case of coupling to MECCA via the educts the coupling is one-way only.

Figure 1 visualizes the conceptual differences between the MESSy submodel CH4 (left) and a CCM simulation with MECCA (right). MECCA simulates the entire chemical mechanism and therefore also includes the feedback onto the reaction partners (depicted in yellow) of CH_4. Additionally, there is also a secondary feedback by the products from the CH_4 sink reactions (e.g., H_2O, HO_2, depicted in blue), as the subsequent chemical processes are influenced by the products from the CH_4 oxidation. Conversely, the CH4 submodel uses the ~~predefined~~ prescribed fields of the reactant species to calculate the CH_4 loss. This loss is included in the master tracer of the CH4 submodel (the present CH_4 is reduced), but does not feedback onto the sink fields or any other chemical species~~, except~~. The only exception is H_2O, in the case when the hydrological feedback of CH_4 oxidation is switched on. GCMs include CH_4 foremost for its radiative impact as a greenhouse gas, but also for its influence on stratospheric water vapor (SWV, e.g. Monge-Sanz et al. (2013); ECMWF (2007); Austin et al. (2007); Boville et al. (2001); Mote (1995)). The CH4 submodel is ~~likewise~~ therefore equipped with an optional feedback onto H_2O, to account for part of the secondary climate feedback of CH_4. It is thereby assumed that two molecules of H_2O are produced per oxidized CH_4 molecule (le Texier et al., 1988), which is, however, only a rough approximation as analyzed by Frank et al. (2018). The approximation of two molecules H_2O per oxidized CH_4 molecule overestimates the H_2O production in the lower stratosphere and underestimates the production in the upper stratosphere. It also does not account for the chemical loss of H_2O in the mesosphere.

Note that soil loss is not explicitly included in the CH4 submodel, since the concept of dry deposition is already part of the EMAC submodel DDEP (Kerkweg et al., 2006a). An example how to use DDEP to simulate the soil loss of CH_4 is included in the supplement of this paper.

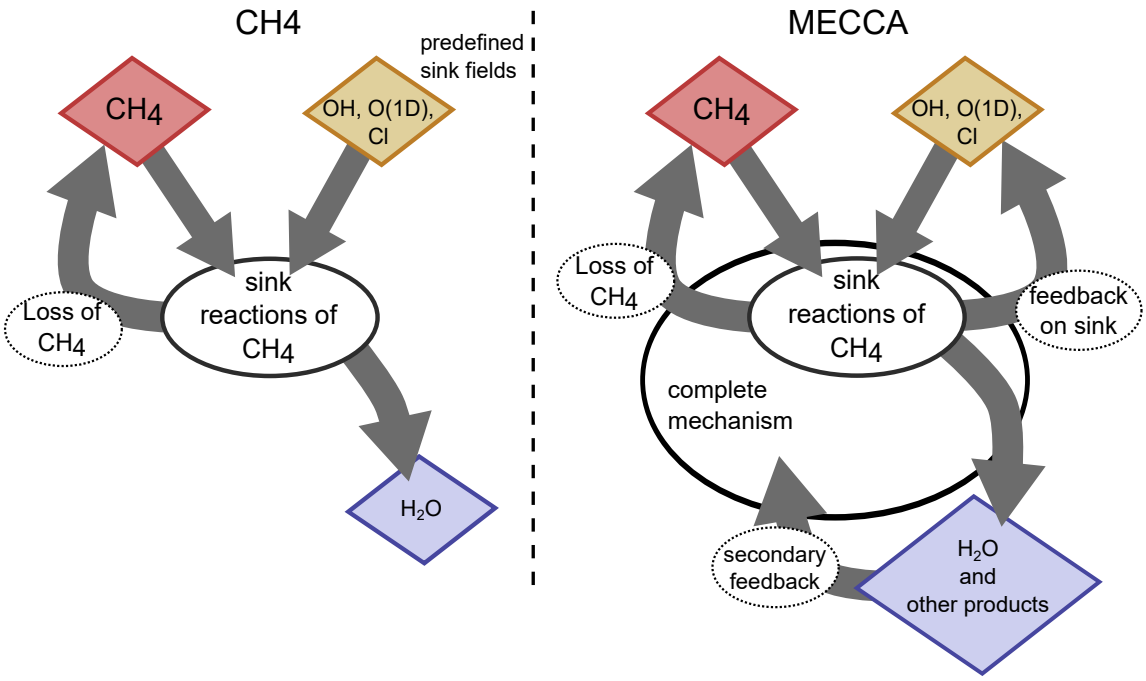

Figure 1. Sketch visualizing the concepts of parameterizing CH_4 sink reactions in the MESSy submodels CH4 (left) and MECCA (right). The red species is the core species CH_4. The chemical mechanism in CH4 is reduced to the sink reactions of CH_4 and ~~gives optional~~ optionally includes the feedback to H_2O (blue) only. In MECCA a complete chemical mechanism is included, which feeds back among others on H_2O and other products of the CH_4 sink reactions ~~. Reaction~~ including the reaction partners ~~are depicted in yellow, whose feedback is included in MECCA~~(educts) of CH_4. The reaction partners (yellow) in the CH4 submodel are ~~predefined fields without feedback~~prescribed and not changed by the CH4 submodel.

The submodel CH4, with its four sink reactions of CH_4, is considerably computationally cheaper, compared to a fully interactive chemistry simulation using MECCA, which represents (depending on the chosen set-up) several hundred reactions (e.g., more than 300 in the base simulations of Earth System Chemistry integrated Modelling (ESCiMo) project (Jöckel et al., 2016)). For example, a reference set-up with MECCA requires about 250 node-h[1] per simulated year, while a set-up with the CH4 submodel without MECCA requires only 30 node-h per year (these numbers are calculated for simulations conducted on the high performance computer (HPC) Mistral at the *Deutsches Klimarechenzentrum* (DKRZ)).

The presented framework of the reduced CH_4 chemistry is applicable, since CH_4 is only reduced and not produced in the free atmosphere. Therefore the discretization of the four reactions, where CH_4 is involved, is sufficient to represent the chemical loss of CH_4. Nevertheless, in order to achieve meaningful simulation results with the CH4 submodel some prerequisites have to be met. Since the educts (OH, Cl and $O(^1D)$) are prescribed, there is no feedback on them. Thus, very large variations

[1]node-h: required wall-clock hours times applied high performance computer (HPC) nodes.

in CH_4 mixing ratio, which would in reality influence the CH_4 sink (Winterstein et al., 2019), are not representable by the CH4 submodel.

Furthermore, the setup with the CH4 submodel also lacks any feedback on O_3. In the atmosphere, the O_3 chemistry is influenced by changes in OH (reduced by CH_4), H_2O (produced by CH_4) and temperature (influenced by the radiatively active CH_4). The CH4 submodel alters H_2O and with that influences the radiation budget and hence the temperature, however, there is no feedback on O_3 when the setup does not include any other chemical mechanism. In a setup where the CH4 submodel is not used in parallel to MECCA, O_3 time series or climatologies are usually prescribed for the radiation scheme.

First simulations using the CH4 submodel are presented in studies by Eichinger et al. (2015a, b), it was included in the simulations of the ESCiMo project (Jöckel et al., 2016) and it has been used for the CH_4 forecast system presented by Nickl et al. (2019).

3.1 Option I: Age and Emission classes

The CH_4 submodel includes an option for simulating age and emission classes. These classes, which can be specified by the user via a namelist, enable a precise distinction between CH_4 source sectors and/or regions (emission classes), as well as further insight into the CH_4 distribution over time (age classes). The term "emission class" ~~denotes thereby~~ thereby denotes a CH_4-like tracer defined by the CH4 submodel. The assignment of specific emission fluxes (sectors and regions) to the tracers of the emission classes is handled by the submodel OFFEMIS (Kerkweg et al., 2006b). In our present application example these classes are subject to emissions being a combination of an emission sector (like wetlands, biomass burning, anthropogenic etc.) and a region (e.g. continents or countries). One tracer, for example, thus traces anthropogenic CH_4 emitted from Africa, as shown in Sect. 5.1. These additional diagnostic tracers are transported ~~identical~~ identically to the master CH_4 tracer of the CH4 submodel and also experience the same sink reactions.

The time period represented by one age class can be chosen by the user. How the age and emission classes evolve over time is depicted in Fig. 2. Methane of each emission class is propagated through a specific number of age classes. The emitted CH_4 of a specific emission class is added to the tracer which corresponds to the first age class. After the selected time span it moves to the next "older" age class until it reaches the oldest. The oldest age class represents the background, since CH_4 does not proceed further.

It is further selectable which age evolving method is applied. The CH4 submodel offers three options: (1) CH_4 is passed on in one step after a user-defined time-span, (2) CH_4 is continuously passed on with respect to an user-defined time-span, and (3) CH_4 is passed on monthly with ~~fixed-lag~~fixed time lag.

We define the state vector for emission class i and age classes 1 to N as:

$$f_i = \begin{pmatrix} f_{i1} \\ f_{i2} \\ \vdots \\ f_{iN} \end{pmatrix} \tag{4}$$

The first two options are implemented according to

$$\Delta f_i = \frac{M \cdot f_i}{\Delta t}, \tag{5}$$

with Δf_i being the tendency of f_i, Δt being the time step length, and M being a matrix defining the ageing step according to the chosen option. For option (1) this matrix looks like

$$M = \begin{pmatrix} -1 & 0 & & \cdots & & 0 \\ 1 & -1 & & & & \\ & 1 & -1 & & & \vdots \\ & & & \ddots & \ddots & \\ 0 & & \cdots & & 1 & 0 \end{pmatrix}. \tag{6}$$

This moves the current values of one age class tracer after a user-defined time-span to the next older one. ~~The implementation of this~~ This option is not ~~conform~~ consistent with a Leapfrog time stepping ~~with~~ using an Asselin-filter and might cause numerical oscillations ~~with~~ and negative values. It was implemented solely for testing purposes during development, but it is not recommended for real applications. The ageing step matrix M for option (2) is M'

$$M' = \alpha \cdot M, \tag{7}$$

with $\alpha = \frac{\Delta t}{\tilde{T}}$ and $\tilde{T}$ being the user-defined time-span indicating the binning width of the age class. This option carries out a quasi-continuous update of the age classes, as it moves at every time step a fraction (α) of the current age class to the next.

The third option is implemented for usage by a fixed-lag Kalman filter for inverse optimization. With this option, one age class represents one month and at the end of one month all CH_4 of one age class moves to the next. This option is specifically implemented to be ~~conform~~ consistent with the Leapfrog time stepping (c.f. option (1)). A preliminary application of the concept of using the age and emission classes for an inverse optimization using the fixed-lag Kalman Filter has been shown by Frank (2018).

In order to reduce numerical errors, the age and emission classes are continuously constrained (i.e., in each model time step) to sum up to the master tracer and are scaled appropriately, if the sum deviates. This procedure is done to avoid the accumulation of such numerical errors, which mainly arise from small non-linearities of the large scale advection scheme. The magnitude therefore depends on the applied advection scheme, but is usually of the order of floating point precision.

3.2 Option II: Isotopologues

Additional to solving the basic CH_4 kinetics, the submodel CH4 further allows for the simulation of CH_4 isotopologues, which are a potent diagnostic measure in the source and sink attribution. The submodel CH4 is able to simulate the abundant and first order rare isotopologues and defines these as tracers additional to the master tracer. Higher substituted isotopologues are neglected. The user can choose ~~,~~whether isotopologues are simulated with respect to carbon (methane containing ^{12}C ($^{12}CH_4$) and $^{13}CH_4$), or hydrogen (CH_4 (containing ^{1}H isotopes only) and CH_3D), or both. The abundant (with ^{12}C or ^{1}H isotopes

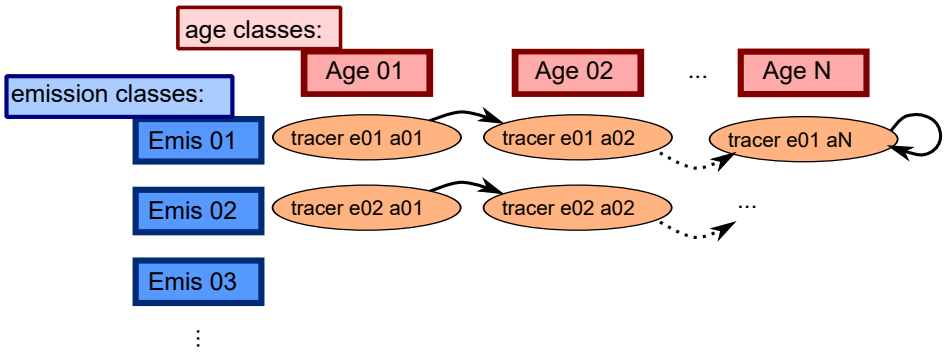

Figure 2. Sketch showing the advancing of the age classes in the CH4 submodel. Each tracer represents one specific emission and age class. After the defined length of time, the age classes proceed to the next "older" age class. The last class represents the background CH_4, where the CH_4 is only subject to transport and the chemically defined sink reactions, but not propagated to an older age class, which is indicated by the circled arrow.

only) and rare (with ^{13}C or D) isotopologues are thereby simulated in parallel. During the simulation it is taken care that each isotopologue family sums up to the master tracer CH_4 tracer of the CH4 submodel (`CH4_fx`). The isotopic signatures of CH_4 emission sources are included by splitting the emission fluxes into an abundant and a rare fraction. This is handled via the OFFEMIS namelist (Kerkweg et al. (2006b), see example namelists in the supplement).

The ~~reaction rates~~ rate coefficients of the CH_4 isotopologues with their reaction partners are adjusted with respect to the KIE factors, e.g.:

$$\mathrm{KIE} = k_{\mathrm{CH_4+OH}} / k_{\mathrm{CH_3D+OH}} \,, \tag{8}$$

and similar for reactions with $O(^1D)$, Cl, and photolysis. The applied reaction partners are thereby the same as those used for the master tracer.

The oxidation of CH_3D produces to a certain extent deuterated water vapour (HDO). If the feedback of CH_4 oxidation onto the hydrological cycle and the simulation of D containing isotopologues is switched on in the CH4 submodel, an additional tracer for HDO is created by the submodel and filled by the produced HDO from CH_3D oxidation. There are two options available: (1) one oxidized CH_3D produces one HDO molecule, or (2) the tendency of the HDO tracer is calculated by Eq. (9) (Eichinger et al., 2015a):

$$\frac{\partial(HDO)}{\partial t} = \frac{-\frac{\partial(CH_3D)}{\partial t} + 6.32 \times 10^{-5} \cdot \frac{\partial(CH_4)}{\partial t}}{\frac{M_{air}}{M_{HDO}} \left(\frac{1}{1-HDO}\right)^2} \,, \tag{9}$$

with M_{air} and M_{HDO} being the molar masses of air (28.987 g mol^{-1}) and HDO (19.02 g mol^{-1}), respectively. This empirical equation accounts for the D, which stays in deuterated molecular hydrogen (HD), as it builds up to an equilibrium with HDO via the HOx-cycle.

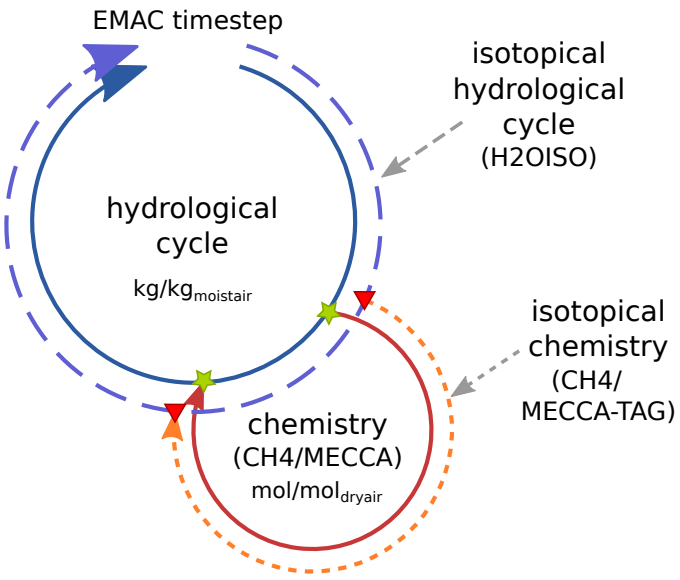

Figure 3. Sketch showing the coupling of the hydrological cycle and the chemistry (either CH4 or MECCA) with respect to H_2O isotopologues in one time step of EMAC. Green stars indicate the points of the hydrological cycle, where (1) the current value of the water vapor master tracer is taken, and (2) the chemical tendencies are added onto the water vapor master tracer. Red triangles indicate the synchronization points of the corresponding isotopical tracers by the TRSYNC submodel. Synchronization of the isotopological cycles accounts also for the appropriate unit conversion and adds the tendency of chemical processes to the fractionation in the physical hydrological cycle.

4 Coupling to the hydrological cycle with the new submodel TRSYNC

In EMAC three different submodels are included dealing with isotopologues of H_2O in the vapor phase: ~~the here presented~~ (1) the CH4 submodel ~~,~~ presented here, (2) MECCA_TAG, and (3) H_2O ISOtopologues (H2OISO, Eichinger et al. (2015a)). CH4 and MECCA_TAG ~~are treating~~ include the chemical fractionations, while H2OISO is responsible for the physical fractionations in the hydrological cycle of the underlying GCM. All three create independent tracers of H_2O isotopologues, which need to be synchronized to be able to combine physical and chemical fractionation effects of H_2O and its isotopologues. The chemical fractionation is thereby considered either from MECCA_TAG or from CH4, although both submodels can be concurrently included in a simulation and compute the isotopic fractionation independently.

In principal, if EMAC is applied in GCM mode, only the master hydrological cycle is present (see Fig. 3, inner solid blue cycle). Adding MECCA or CH4 to the set-up expands the model into a CCM, or a simple "CH_4-only" CCM, respectively (red solid circle). The chemistry submodels use water vapor as a chemical tracer (first green star) and calculate the contribution from CH_4 oxidation (second green star). This chemical feedback onto water vapor was already implemented as an option in previous EMAC versions. By including the isotopological submodels into the set-up, H2OISO ~~doubles~~ duplicates the hydrological cycle for the water isotopologues and CH4 or MECCA_TAG create the chemical tracers of the water isotopologues (outer

dashed circles). This results in several physical and chemical H_2O isotopologue tracers. While the master chemical process adds its feedback directly to the specific humidity of the hydrological cycle (there is no need for a chemical water tracer), the synchronization of the physical isotopological tracers in the isotopic hydrological cycle (H2OISO) and the chemical isotopological tracers (CH4 or MECCA_TAG) is done via the new auxiliary submodel TRSYNC. In brief, TRSYNC guarantees that the physical H_2O tracers (incl. their isotopologues) receive also the correct tendencies of the corresponding chemical tracers. Since isotopological water vapor tracers of MECCA_TAG and the HDO tracer created by CH4 are transported in EMAC in the same way as every other tracer, they are subject to some of the physical processes, but not to all hydrological fractionation effects. Thus, at the first synchronization point the chemical tracer is synchronized to represent the current value of the physical tracer. In the following, chemical tendencies including fractionation effects are calculated and are added via the second synchronization point to the physical tracer. By doing so, chemical and physical fractionation processes are strictly separated and the tendencies of the chemical tracers represent the chemical tendencies in addition to the previous physical fractionations in the current time step.

Water vapor in the physical hydrological cycle (regarding ECHAM5 and H2OISO) are defined in units of kg of the tracer per kg of moist air (kg $kg^{-1}_{\text{moist air}}$), while the chemical tracers are defined in mol mol^{-1}_{dryair}. This also holds for the corresponding isotopologue tracers. Parameterizations of physical processes in ECHAM5 are by design formulated with specific humidity (per moist air). Conversely, chemical reactions are necessarily calculated with species concentrations. This requires the individual chemical and physical isotopologue tracers, which have, for the sake of correct process formulations, distinct units, and motivated the development of the auxiliary submodel TRSYNC in order to be able to synchronize these tracers accordingly and in a common way for CH4 and MECCA_TAG, respectively.

In addition to that, the application of MECCA_TAG creates the basis to investigate various other isotopes in the interactive chemical mechanism. While CH4 feedbacks on H_2O with respect to hydrogen isotopes only, MECCA_TAG can also be used to simulate oxygen isotopes (^{16}O, ^{17}O and ^{18}O) in the chemical mechanism. It is therefore also possible to couple MECCA_TAG with oxygen isotopes to the corresponding oxygen related isotopologue tracers in H2OISO. Last but not least, for MECCA_TAG tracer names are not standardized. Therefore, the namelist of the submodel TRSYNC can be adjusted according to the actual tracer names used in MECCA_TAG.

5 Example applications

The following examples are simulations carried out with EMAC in a GCM-like mode including the newly presented CH4 and TRSYNC submodels. Other involved MESSy submodels are OFFEMIS (Kerkweg et al., 2006b) and DDEP (Kerkweg et al., 2006a). OFFEMIS manages the emissions of CH_4 from prescribed sources. It reads predefined fields with emission data and adds these fluxes to the chemical tracers. DDEP simulates the dry deposition for gases and aerosols and is used in the present context to simulate the soil-loss of CH_4, which is not done in the CH4 submodel itself.

Monthly mean sink fields are used in the simulation set-up in the examples below. Higher frequencies are technically possible, this would, however, increase the computational demands due to the larger amount of data read from disk. Monthly mean

fields smooth the diurnal cycle, which is especially strong in OH. However, in order to investigate long-term global trends of CH_4, which has a tropospheric lifetime of 8–10 years, variations on time scales of less than one month are negligible and monthly mean fields are assumed to suffice for such applications. Furthermore in the examples, photolysis rates are calculated by the submodel JVAL in the presented examples, but predefined data can be used as well.

The H2OISO submodel (Eichinger, 2014; Eichinger et al., 2015a) simulates the stable water isotopologues with respect to H and D, as well as ^{16}O, ^{17}O and ^{18}O. Overall, it represents a second hydrological cycle, which includes water isotopologues in their three phases: gas, liquid and ice. H2OISO accounts for fractionation processes during phase transitions in large scale and convective clouds, during vertical diffusion, and during evaporation from the ocean (evaporation from soil, biosphere and snow are not considered to have a significant fractionation).

We simulated the years 1989 to 2012 and applied a specified dynamics set-up to represent the reanalyzed meteorology of this time. Specified dynamics means here that the prognostic variables divergence, vorticity, temperature and (logarithm of) surface pressure are nudged by Newtonian relaxation towards ECMWF ERA-Interim reanalysis data (Dee et al., 2011).

5.1 Application of the CH4 submodel for inverse optimization of CH_4 emission inventories

Current estimates of CH_4 emission inventories still include large uncertainties. In order to reduce these, new estimates of inventories must be able to represent temporal and spatial resolutions in greater detail (e.g., seasonal cycle, distinct regions). One statistical method to estimate CH_4 emission strengths is the fixed-lag Kalman Filter, which performs an inverse optimization of the emission inventory by comparing simulated and observed mixing ratios of a trace gas (see e.g., Bruhwiler et al. (2005)). This "off-line" inversion algorithm requires data from a forward simulation including temporal and spatial information of the simulated CH_4 tracer.

In order to provide the necessary data, the CH4 submodel with the option of age and emission classes is applied. The combination of chosen regions and emission sectors in this example results in 48 emission classes altogether. These 48 emission classes are simulated with 5 age classes for ages up to 1, 2, 3, 4, and $\geq$5 months since emission release. Figure 4 shows exemplarily the evolution of one emission class (i.e., anthropogenic emissions in Africa) from age class to age class. Panel (a) shows the emissions of the year 2000 in g(CH_4) m^{-2} per year (y^{-1}). The other panels (b)–(f) show the age classes in ascending order and display the distribution of the CH_4 mixing ratio onto the 5 age classes in January 2000 (the simulation has started in 1989). In the fourth age class the CH_4 from anthropogenic African sources is almost evenly distributed mostly in the Northern Hemisphere (NH). Eventually, the fifth (i.e. the last age class) shows the accumulated background of all CH_4 from anthropogenic African sources. Applied is an a priori emission inventory.

Overall, the temporal evolution of the age classes in Fig. 4 confirms that the 5 age classes in this set-up sufficiently track the spread of CH_4 towards a fairly uniform distribution, which is a prerequisite for a successful application of the inverse optimization method.

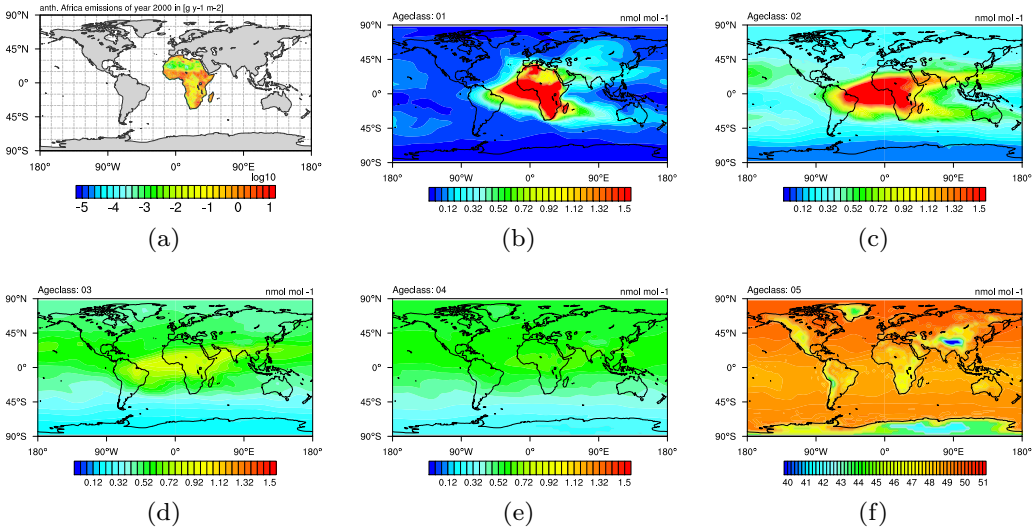

Figure 4. Panel (a): anthropogenic emissions in Africa (taken from EDGARv4.2 2010 fast track database (Olivier and Janssens-Maenhout, 2012)). Panels (b)–(f): Methane as pressure weighted column up to 200 hPa of anthropogenic origin from Africa, distributed into 5 age classes, i.e. up to 1, 2, 3, and 4, and $\geq$5 months after emission release. Shown are exemplarily all age classes of January 2000 after the simulation has run for 12 years.

5.2 Simulating CH_4 isotopologues

We further present a simulation using the CH4 submodel, which includes all four CH_4 isotopologues. For this simulation, we applied a global a posteriori emission inventory provided by Dominik Brunner (pers. communication) and a set of isotopic emission signatures prepared from data from literature (see Table S1 in the supplement). Figure 5 shows zonal mean climatologies (2000–2009) of CH_4 in [nmol mol^{-1}] and the corresponding isotopic signature in [‰]. The isotopologues are displayed in the δ-notation with respect to the reference isotope ratios Vienna-PeeDee Belemnite (VPDB) for $^{13}CH_4$, and Vienna Standard Mean Ocean Water (VSMOW) for CH_3D, respectively. In the troposphere the NH is isotopically depleted compared to the Southern Hemisphere (SH). Most ~~and largest,~~ isotopically light emissions, as for example wetlands and rice, are located in the NH, while isotopical heavy sources like biomass burning are mostly located in the SH. This results in the prevalent tropospheric North-South gradient. In the stratosphere CH_4 becomes isotopically enriched towards higher altitudes. ~~This can be ascribed to fractionation processes, as heavier CH_4 isotopologues likely remain when CH_4 is~~ When CH_4 is ascending in the atmosphere it is exposed to oxidation~~during the ascend in the troposphere~~. Due to fractionation processes heavy CH_4 isotopologues are unfavored and therefore accumulate in the remaining CH_4.

~~These~~ Our simulation results compare well to observations. For example isotopic observations from the National Oceanic and Atmospheric Administration/Earth System Research Laboratory (NOAA/ESRL) sampling sites (White et al., 2016, 2017) and airborne samples taken during the Comprehensive Observation Network for TRace gases by AIrLiner (CONTRAIL)

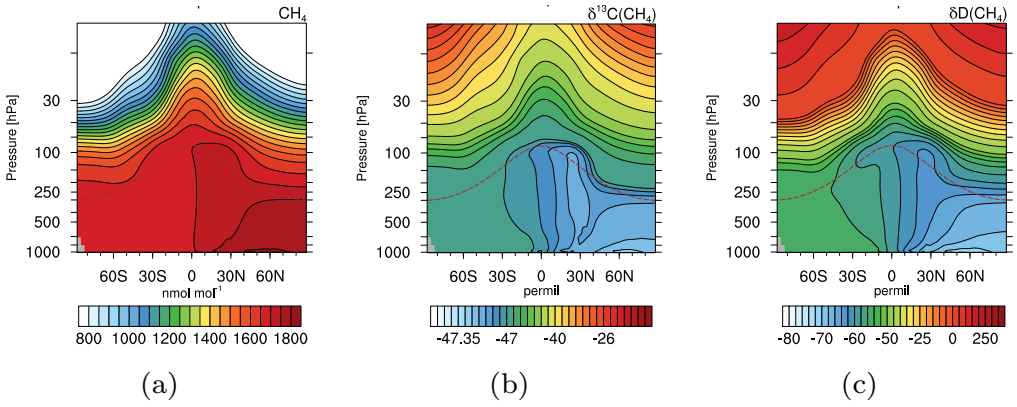

(a) (b) (c)

Figure 5. Zonal mean climatologies of 2000–2009 for CH_4 in [nmol mol^{-1}] (a), $\delta^{13}C(CH_4)$ in [‰] (b), and $\delta D(CH_4)$ in [‰] (c) of the simulation with EMAC and the CH4 submodel. The dashed brown lines indicate the height of the climatological tropopause.

project (Umezawa et al., 2012) verify the North-South gradient ~~.~~(shown in the supplement Sects. 2.1 and 2.2). The values of the signature of ^{13}C in CH_4 ($\delta^{13}C(CH_4)$), for example, are within the uncertainty of the CONTRAIL observations. The the signature of D in CH_4 ($\delta D(CH_4)$) is isotopological depleted in D compared to the CONTRAIL observations, however, still capture the gradient well~~(not shown)~~. The vertical gradient (i.e. isotopical enrichment in the stratosphere) can be verified by comparing with balloon borne observations by Röckmann et al. (2011). Our simulation results are thereby within the local and temporal uncertainties (~~not shown~~ shown in the supplement Sect. 2.3). Note that an optimization with respect to source signatures are yet to be made and requires an optimized emission inventory. However, the capturing of the respective gradients indicates that the isotopical fractionation is sufficiently implemented.

5.3 Coupling of the CH_4 isotopologues to the isotopological hydrological cycle

The previously shown results were achieved with the CH4 submodel including the option to simulate CH_4 isotopologues. The produced HDO (by oxidation of CH_3D) is connected via the TRSYNC submodel to the isotopological hydrological cycle represented by the H2OISO submodel. We carried out an additional simulation in which we applied MECCA and MECCA_TAG to simulate the atmospheric chemistry and the CH_4 isotopologues instead of the CH4 submodel. In this simulation TRSYNC connects the produced HDO likewise to the isotopological water tracers of H2OISO.

In Figure 6 we compare the results obtained with submodel CH4 (left) and those obtained with the submodel MECCA_TAG (right) to vertical profiles of H_2O and HDO (middle) provided by the Michelson Interferometer for Passive Atmospheric Sounding (MIPAS) instrument mounted on the ENVIronmental SATellite (ENVISAT) satellite (Steinwagner et al., 2007; Lossow et al., 2011). The ENVISAT satellite is on a sun-synchronous orbit around the Earth, completing the circuit 14 times a day. The presented observational and simulated data comprise the time period July 2002 to March 2004. The vertical range of the observations extends from 6 to 68 km (i.e. approx. the range 100–1~~hPa~~ hPa) with a vertical resolution of 3–8 km. Simulation

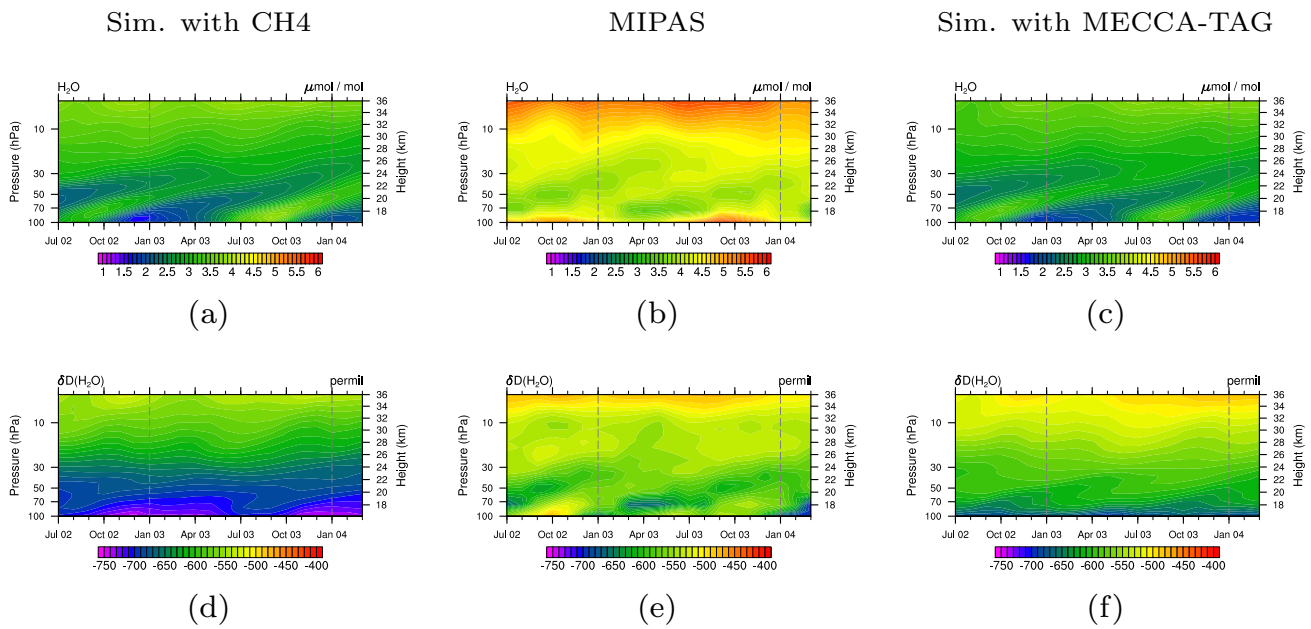

Figure 6. Tropical stratospheric tape recorder signal of H_2O (upper) and in $\delta D(H_2O)$ (lower) in MIPAS data (middle column) and the simulations with the CH4 submodel (left column) and with the MECCA_TAG submodel (right column) in the time period July 2002 to March 2004. Simulation data is averaged monthly, zonally and over the tropics between 23° S–23° N and are displayed between 100 and 1~~hPa~~ hPa. The grey dashed lines are included for eye guidance in the comparison of the tape recorder signal.

and observation data is monthly and zonally averaged over the tropics. Similar to the conclusions of Eichinger et al. (2015a) it is observed that the EMAC model underestimates the H_2O mixing ratio (see Figs. 6a and 6c). This is associated with a too cold tropopause in EMAC, where a temperature bias of -2 to -6 K is detected in the upper troposphere, as long as the mean temperature is excluded from the nudging procedure defining the specified dynamics setup (Jöckel et al., 2016). This reduces the H_2O transported into the stratosphere since more gas phase H_2O freezes and sediments. Comparing Fig. 6d with 6f indicates a better agreement concerning the signature of D in H_2O ($\delta D(H_2O)$) in the simulation using the submodel MECCA_TAG with the MIPAS observations, which suggests that although the absolute H_2O and HDO mixing ratios are not met, the relative composition is well represented. The differences in HDO in the simulation with the CH4 submodel compared to the one with the MECCA_TAG submodel and MIPAS are potentially caused by (1) the Eq. (9) from Eichinger et al. (2015a) used in the simulation using the CH4 submodel, which possibly does not capture important fractionation processes in the oxidation chain of CH_3D, and (2) the HD, produced in the troposphere and propagating into the stratosphere, which is not included in the simplified chemistry, but represents an additional source of HDO. For an accurate simulation of stratospheric HDO this source needs to be considered as well in future simulations.

6 Summary

The submodel CH4 provides a reduced chemical set-up focusing on the CH_4 sink reactions, using predefined data of reaction partners, and optionally includes the feedback on SWV. This reduces the computational demands for sensitivity simulations of climate projections without neglecting the main source of chemically induced SWV.

We ~~presented~~ present two additional options of the CH4 submodel. The age and emission classes allow the inverse optimization of emission inventories using a fixed-lag Kalman filter. The simulation of CH_4 isotopologues provides further insight into the variability and distribution of CH_4 from its source (via emission signatures and fractionation effects) to its sink (coupling to the isotopic content of H_2O). The latter is implemented in form of the new submodel TRSYNC, which takes care of the correct and time integration conform synchronization of the various H_2O isotopologue tracers in the model.

Example use cases show specific applications of the CH4 submodel as well as the coupling to the isotopological hydrological cycle via the TRSYNC submodel, which is especially helpful for the closure of the isotopic content in SWV.

Code and data availability. The Modular Earth Submodel System (MESSy) is continuously further developed and applied by a consortium of institutions. The usage of MESSy and access to the source code is licensed to all affiliates of institutions which are members of the MESSy Consortium. Institutions can become a member of the MESSy Consortium by signing the MESSy Memorandum of Understanding. More information can be found on the MESSy Consortium Web-site (http://www.messy-interface.org). The new submodels presented in this paper have been implemented based on MESSy v2.53.0 and are available since v2.54.0. The exact code version used to produce the examples is archived at the German Climate Computing Center (DKRZ) and can be made available to members of the MESSy community upon request.

Author contributions. FW and PJ worked on the development of the CH4 and TRSYNC submodel and wrote the manuscript.

Competing interests. The authors declare that they have no conflict of interest.

Acknowledgements. We acknowledge the DLR internal project KliSAW (Klimarelevanz von atmosphärischen Spurengasen, Aerosolen und Wolken), which provided the financial basis for the presented model developments, and the Helmholtz-Gemeinschaft e.V. (HGF) "Project Advanced Earth System Modelling Capacity (ESM)". The model simulations have been performed at the German Climate Computing Centre (DKRZ) through support from the Bundesministerium für Bildung und Forschung (BMBF). We further thank Theresa Klausner ~~for her~~ and two anonymous reviewers for their supportive comments on the manuscript.

References

Austin, J., Wilson, J., Li, F., and Vömel, H.: Evolution of Water Vapor Concentrations and Stratospheric Age of Air in Coupled Chemistry-Climate Model Simulations, Am. Met. Soc., pp. 905–921, https://doi.org/10.1175/JAS3866.1, 2007.

Bergamaschi, P., Brühl, C., Brenninkmeijer, C. A. M., Saueressig, G., Crowley, J. N., Grooß, J. U., Fischer, H., and Crutzen, P. J.: Implications of the large carbon kinetic isotope effect in the reaction CH_4 + Cl for the $^{13}C/^{12}C$ ratio of stratospheric CH_4, Geophys. Res. Lett., 23, 2227–2230, https://doi.org/10.1029/96GL02139, 1996.

Bigeleisen, J.: Isotope Effects in Chemistry and Biology, chap. Chapter 01 Theoretical Basis of Isotope Effects from an Autobiographical Perspective, pp. 1–40, Taylor & Taylor & Francis Group, LLC, https://doi.org/10.1201/9781420028027.ch1, http://dx.doi.org/10.1201/9781420028027.ch1, 2005.

Boville, B. A., Kiehl, J. T., Rasch, P. J., and Bryan, F. O.: Improvements to the NCAR CSM-1 for Transient Climate Simulations, J. Climate, 14, 164–179, https://doi.org/10.1175/1520-0442(2001)014<0164:ITTNCF>2.0.CO;2, 2001.

Bruhwiler, L. M. P., Michalak, A. M., Peters, W., Baker, D. F., and Tans, P.: An improved Kalman Smoother for atmospheric inversions, Atmos. Chem. Phys., 5, 2691–2702, https://doi.org/10.5194/acp-5-2691-2005, https://www.atmos-chem-phys.net/5/2691/2005/, 2005.

Crowley, J. N., Saueressig, G., Bergamaschi, P., Fischer, H., and Harris, G. W.: Carbon kinetic isotope effect in the reaction CH_4+Cl: a relative rate study using FTIR spectroscopy, Chem. Phys. Lett., 303, 268–274, https://doi.org/10.1016/S0009-2614(99)00243-2, 1999.

Dee, D. P., Uppala, S. M., Simmons, A. J., Berrisford, P., Poli, P., Kobayashi, S., Andrae, U., Balmaseda, M. A., Balsamo, G., Bauer, P., Bechtold, P., Beljaars, A. C. M., van de Berg, L., Bidlot, J., Bormann, N., Delsol, C., Dragani, R., Fuentes, M., Geer, A. J., Haimberger, L., Healy, S. B., Hersbach, H., Hólm, E. V., Isaksen, L., Kållberg, P., Köhler, M., Matricardi, M., McNally, A. P., Monge-Sanz, B. M., Morcrette, J.-J., Park, B.-K., Peubey, C., de Rosnay, P., Tavolato, C., Thépaut, J.-N., and Vitart, F.: The ERA-Interim reanalysis: configuration and performance of the data assimilation system, Quart. J. Roy. Meteor. Soc., 137, 553–597, https://doi.org/10.1002/qj.828, http://dx.doi.org/10.1002/qj.828, 2011.

ECMWF: IFS DOCUMENTATION - Cy31r1, Part IV: Physical Processes, https://www.ecmwf.int/sites/default/files/elibrary/2007/9221-part-iv-physical-processes.pdf, 2007.

Eichinger, R.: Investigation of stratospheric water vapour by means of the simulation of water isotopologues, Ph.D. thesis, Ludwig Maximilian Universität München, 2014.

Eichinger, R., Jöckel, P., Brinkop, S., Werner, M., and Lossow, S.: Simulation of the isotopic composition of stratospheric water vapour - Part 1: Description and evaluation of the EMAC model, Atmos. Chem. Phys., 15, 5537–5555, https://doi.org/10.5194/acp-15-5537-2015, 2015a.

Eichinger, R., Jöckel, P., and Lossow, S.: Simulation of the isotopic composition of stratospheric water vapour - Part 2: Investigation of HDO / H_2O variations, Atmos. Chem. Phys., 15, 7003–7015, https://doi.org/10.5194/acp-15-7003-2015, http://www.atmos-chem-phys.net/15/7003/2015/, 2015b.

Fletcher, M., E., S., Tans, P. P., Bruhwiler, L. M., Miller, J. B., and Heimann, M.: CH_4 sources estimated from atmospheric observations of CH_4 and its $^{13}C/^{12}C$ isotopic ratios: 2. Inverse modeling of CH_4 fluxes from geographical regions, Glob. Biogeochem. Cycles, 18, 1–15, https://doi.org/10.1029/2004GB002224, 2004.

Frank, F.: Atmospheric methane and its isotopic composition in a changing climate: A modelling study, Ph.D. thesis, Ludwigs Maximillian Universität München, 2018.

Frank, F., Jöckel, P., Gromov, S., and Dameris, M.: Investigating the yield of H_2O and H_2 from methane oxidation in the stratosphere, Atmos. Chem. Phys., 18, 9955–9973, https://doi.org/10.5194/acp-18-9955-2018, https://www.atmos-chem-phys.net/18/9955/2018/, 2018.

Gromov, S., Jöckel, P., Sander, R., and Brenninkmeijer, C. A. M.: A kinetic chemistry tagging technique and its application to modelling the stable isotopic composition of atmospheric trace gases, Geosci. Model Dev., 3, 337–364, https://doi.org/10.5194/gmd-3-337-2010, www.geosci-model-dev.net/3/337/2010/, 2010.

Hein, R., Crutzen, P. J., and Heimann, M.: An inverse modeling approach to investigate the global atmospheric methane cycle, Glob. Biogeochem. Cycles, 11, 43–76, 1997.

Holmgren, P.: Global land use area change matrix, Working Paper 134, Forest Resources Assessment Programme, Food and Agriculture Organization of the United Nations, 2006.

IPCC: Climate Change 2013: The Physical Science Basis. Contribution of Working Group I to the Fifth Assessment Report of the Intergovernmental Panel on Climate Change, Cambridge University Press, Cambridge, United Kingdom and New York, NY, USA, https://doi.org/10.1017/CBO9781107415324, www.climatechange2013.org, 2013.

Jöckel, P., Kerkweg, A., Pozzer, A., Sander, R., Tost, H., Riede, H., Baumgaertner, A., Gromov, S., and Kern, B.: Development cycle 2 of the Modular Earth Submodel System MESSy2, Geosci. Model Dev., 3, 717–752, https://doi.org/10.5194/gmd-3-717-2010, manual, 2010.

Jöckel, P., Tost, H., Pozzer, A., Kunze, M., Kirner, O., Brenninkmeijer, C. A. M., Brinkop, S., Cai, D. S., Dyroff, C., Eckstein, J., Frank, F., Garny, H., Gottschaldt, K.-D., Graf, P., Grewe, V., , Kerkweg, A., Kern, B., Matthes, S., Mertens, M., Meul, S., Neumaier, M., Nützel, M., Oberländer-Hayn, S., Ruhnke, R., Runde, T., Sander, R., Scharffe, D., and Zahn, A.: Earth System Chemistry integrated Modelling (ESCiMo) with the Modular Earth Submodel System (MESSy) version 2.51, Geosci. Model Dev., 9, 1153–1200, https://doi.org/10.5194/gmd-9-1153-2016, http://www.geosci-model-dev.net/9/1153/2016/gmd-9-1153-2016.html, 2016.

Kerkweg, A., Buchholz, J., Ganzeveld, L., Pozzer, A., Tost, H., and Jöckel, P.: Technical Note: An implementation of the dry removal processes DRY DEPosition and SEDImentation in the Modular Earth Submodel System (MESSy), Atmos. Chem. Phys., 6, 4617–4632, https://doi.org/10.5194/acp-6-4617-2006, https://www.atmos-chem-phys.net/6/4617/2006/, 2006a.

Kerkweg, A., Sander, R., Tost, H., and Jöckel, P.: Technical note: Implementation of prescribed (OFFLEM), calculated (ONLEM), and pseudo-emissions (TNUDGE) of chemical species in the Modular Earth Submodel System (MESSy), Atmos. Chem. Phys., 6, 3603–3609, https://doi.org/10.5194/acp-6-3603-2006, https://www.atmos-chem-phys.net/6/3603/2006/, 2006b.

King, G.: Responses of atmospheric methane consumption by soils to global climate change, Global Change Biology, 3, 351–362, https://doi.org/10.1046/j.1365-2486.1997.00090.x, http://dx.doi.org/10.1046/j.1365-2486.1997.00090.x, 1997.

Kirschke, S., Bousquet, P., Ciais, P., Saunois, M., Canadell, J. G., Dlugokencky, E. J., Bergamaschi, P., Bergmann, D., Blake, D. R., Bruhwiler, L., Cameron-Smith, P., Castaldi, S., Chevallier, F., Feng, L., Fraser, A., Heimann, M., Hodson, E. L., Houweling, S., Josse, B., Fraser, P. J., Krummel, P. B., Lamarque, J.-F., Langenfelds, R. L., Le Quèrè, C., Naik, V., O'Doherty, S., Palmer, P. I., Pison, I., Plummer, D., Poulter, B., Prinn, R. G., Rigby, M., Ringeval, B., Santini, M., Schmidt, M., Shindell, D. T., Simpson, I. J., Spahni, R., Steele, L. P., Strode, S. A., Sudo, K., Szopa, S., van der Werf, G. R., Voulgarakis, A., van Weele, M., Weiss, R. F., Williams, J. E., and Zeng, G.: Three decades of global methane sources and sinks, Nature Geoscience, 6, 813–823, https://doi.org/10.1038/ngeo1955, https://www.nature.com/articles/ngeo1955#supplementary-information, 2013.

le Texier, H., Solomon, S., and Garcia, R. R.: The role of molecular hydrogen and methane oxidation in the water vapour budget of the stratosphere, Quart. J. Roy. Meteor. Soc., 114, 281–295, https://doi.org/10.1002/qj.49711448002, 1988.

Lossow, S., Steinwagner, J., Urban, J., Dupuy, E., Boone, C. D., Kellmann, S., Linden, A., Kiefer, M., Grabowski, U., Glatthor, N., Höpfner, M., Röckmann, T., Murtagh, D. P., Walker, K. A., Bernath, P. F., von Clarmann, T., and Stiller, G. P.: Comparison of

HDO measurements from Envisat/MIPAS with observations by Odin/SMR and SCISAT/ACE-FTS, Atmos. Meas. Tech., 4, 1855–1874, https://doi.org/10.5194/amt-4-1855-2011, https://www.atmos-meas-tech.net/4/1855/2011/, 2011.

Maxfield, P. J., Evershed, R. P., and Hornibrook, E. R. C.: Physical and Biological Controls on the In Situ Kinetic Isotope Effect Associated with Oxidation of Atmospheric CH_4 in Mineral Soils, Environ. Sci. Technol., 42, 7824–7830, https://doi.org/10.1021/es800544q, http://dx.doi.org/10.1021/es800544q, pMID: 19031867, 2008.

Monge-Sanz, B. M., Chipperfield, M. P., Untch, A., Morcrette, J.-J., Rap, A., and Simmons, A. J.: On the uses of a new linear scheme for stratospheric methane in global models: water source, transport tracer and radiative forcing, Atmos. Chem. Phys., 13, 9641–9660, https://doi.org/10.5194/acp-13-9641-2013, https://www.atmos-chem-phys.net/13/9641/2013/, 2013.

Monteil, G., Houweling, S., Dlugockenky, E. J., Maenhout, G., Vaughn, B. H., White, J. W. C., and Rockmann, T.: Interpreting methane variations in the past two decades using measurements of CH_4 mixing ratio and isotopic composition, Atmos. Chem. Phys., 11, 9141–9153, 2011.

Mote, P.: The annual cycle of stratospheric water vapor in a general circulation model, J. Geophys. Res., 100, 7363–7379, https://doi.org/10.1029/94JD03301, http://onlinelibrary.wiley.com/doi/10.1029/94JD03301/pdf, 1995.

Nair, H., Summers, M. E., Miller, C. E., and Yung, Y. L.: Isotopic fractionation of methane in the martian atmosphere, ICARUS, 175, 32–35, https://doi.org/10.1016/j.icarus.2004.10.018, 2005.

Nickl, A.-L., Mertens, M., Roiger, A., Fix, A., Amediek, A., Fiehn, A., Gerbig, C., Galkowski, M., Kerkweg, A., Klausner, T., Eckl, M., and Jöckel, P.: Forecasting of regional methane from coal mine emissions in the Upper Silesian Coal Basin using the on-line nested global regional chemistry climate model MECO(n)(MESSy v2.53), Geosci. Model Dev. Discuss., 2019, 1–29, https://doi.org/10.5194/gmd-2019-303, https://www.geosci-model-dev-discuss.net/gmd-2019-303/, 2019.

Nisbet, E. G., Dlugokencky, E. J., Manning, M. R., Lowry, D., Fisher, R. E., France, J. L., Michel, S. E., Miller, J. B., White, J. W. C., Vaughn, B., Bousquet, P., Pyle, J. A., Warwick, N. J., Cain, M., Brownlow, R., Zazzeri, G., Lanoisellé, M., Manning, A. C., Gloor, E., Worthy, D. E. J., Brunke, E.-G., Labuschangne, C., W., W. E., and Ganesan, A. L.: Rising atmospheric methane: 2007–2014 growth and isotopic shift, Glob. Biogeochem. Cycles, 30, 1–15, https://doi.org/10.1002/2015GB005326.Received, 2016.

Nixon, C. A., Temelso, B., Vinatier, S., Teanby, N. A., B'ezard, B., Achterberg, R. K., Mandt, K. E., Sherrill, C. D., Irwin, P. G. J., Jennings, D. E., Romani, P. N., Coustenis, A., and Flasar, F. M.: Isotopic ratios in titan's methane: measurements and modeling, The Astrophysical Journal, 749, 159, https://doi.org/10.1088/0004-637X/749/2/159, http://stacks.iop.org/0004-637X/749/i=2/a=159, 2012.

Olivier, J. and Janssens-Maenhout, G.: CO2 Emissions from Fuel Combustion 2012, chap. Part III, Greenhouse-Gas Emissions, p. 540, International Energy Agency, https://doi.org/https://doi.org/https://doi.org/10.1787/co2_fuel-2012-en, https://www.oecd-ilibrary.org/content/publication/co2_fuel-2012-en, 2012.

Revell, L. E., Bodeker, G. E., Huck, P. E., Williamson, B. E., , and Rozanov, E.: The sensitivity of stratospheric ozone changes through the 21st century to N_2O and CH_4, Atmos. Chem. Phys., 12, 11 309–11 317, https://doi.org/10.5194/acp-12-11309-2012, www.atmos-chem-phys.net/12/11309/2012/, 2012.

Rigby, M., Manning, A. J., and Prinn, R. G.: The value of high-frequency high-precision methane isotopologue measurements for source and sink estimation, J. Geophys. Res., 117, D12 312, https://doi.org/10.1029/2011JD017384, 2012.

Röckmann, T., Brass, M., Borchers, R., and Engel, A.: The isotopic composition of methane in the stratosphere: high-altitude balloon sample measurements, Atmos. Chem. Phys., 11, 13 287–13 304, https://doi.org/10.5194/acp-11-13287-2011, 2011.

Roeckner, E., Brokopf, R., Esch, M., Giorgetta, M., Hagemann, S., Kornblueh, L., Manzini, E., Schlese, U., and Schulzweida, U.: Sensitivity of Simulated Climate to Horizontal and Vertical Resolution in the ECHAM5 Atmosphere Model, American Meterological Society, 19, 3771–3791, 2006.

Sander, R., Kerkweg, A., Jöckel, P., and Lelieveld, J.: Technical note: The new comprehensive atmospheric chemistry module MECCA, Atmos. Chem. Phys., 5, 445–450, 2005.

Sander, R., Jöckel, P., Kirner, O., Kunert, A. T., Landgraf, J., and Pozzer, A.: The photolysis module JVAL-14, compatible with the MESSy standard, and the JVal PreProcessor (JVPP), Geosci. Model Dev., 7, 2653–2662, https://doi.org/10.5194/gmd-7-2653-2014, www.geosci-model-dev.net/7/2653/2014/, 2014.

Sander, S. P., Abbatt, J., Barker, J. R., Burkholder, J. B., Friedl, R. R., Golden, D. M., Huie, R. E., Kolb, C. E., Kurylo, M. J., Moortgat, G. K., Orkin, V. L., and Wine, P. H.: Chemical Kinetics and Photochemical Data for Use in Atmospheric Studies, Evaluation No. 17, JPL Publication 10-6, Jet Propulsion Laboratory, https://doi.org/10.1002/kin.550171010, http://jpldataeval.jpl.nasa.gov/, 2011.

Saueressig, G., Bergamaschi, P., Crowley, J. N., and Fischer, H.: Carbon kinetic isotope effect in the reaction of CH_4 with Cl atoms, Geophys. Res. Lett., 22, 1225–1228, 1995.

Saueressig, G., Bergamaschi, P., Crowley, J., and Fischer, H.: D/H kinetic isotope effect in the reaction CH_4 + Cl, Geophys. Res. Lett., 23, 3619–3622, 1996.

Saueressig, G., Crowley, J. N., Bergamaschi, P., Brühl, C., Brenninkmeijer, C. A. M., and Fischer, H.: Carbon 13 and D kinetic isotope effects in the reactions of CH_4 with $O^1(D)$ and OH: New laboratory measurements and their implications for the isotopic composition of stratospheric methane, J. Geophys. Res., 106, 23 127–23 138, 2001.

Saunois, M., Bousquet, P., Poulter, B., Peregon, A., Ciais, P., Canadell, J. G., Dlugokencky, E. J., Etiope, G., Bastviken, D., Houweling, S., Janssens-Maenhout, G., Tubiello, F. N., Castaldi, S., Jackson, R. B., Alexe, M., Arora, V. K., Beerling, D. J., Bergamaschi, P., Blake, D. R., Brailsford, G., Brovkin, V., Bruhwiler, L., Crevoisier, C., Crill, P., Covey, K., Curry, C., Frankenberg, C., Gedney, N., Höglund-Isaksson, L., Ishizawa, M., Ito, A., Joos, F., Kim, H.-S., Kleinen, T., Krummel, P., Lamarque, J.-F., Langenfelds, R., Locatelli, R., Machida, T., Maksyutov, S., McDonald, K. C., Marshall, J., Melton, J. R., Morino, I., Naik, V., O'Doherty, S., Parmentier, F.-J. W., Patra, P. K., Peng, C., Peng, S., Peters, G. P., Pison, I., Prigent, C., Prinn, R., Ramonet, M., Riley, W. J., Saito, M., Santini, M., Schroeder, R., Simpson, I. J., Spahni, R., Steele, P., Takizawa, A., Thornton, B. F., Tian, H., Tohjima, Y., Viovy, N., Voulgarakis, A., van Weele, M., van der Werf, G. R., Weiss, R., Wiedinmyer, C., Wilton, D. J., Wiltshire, A., Worthy, D., Wunch, D., Xu, X., Yoshida, Y., Zhang, B., Zhang, Z., and Zhu, Q.: The global methane budget 2000–2012, Earth Syst. Sci. Data, 8, 697–751, https://doi.org/10.5194/essd-8-697-2016, https://www.earth-syst-sci-data.net/8/697/2016/, 2016.

Schaefer, H., Fletcher, S. E. M., Veidt, C., Lassey, K. R., Brailsford, G. W., Bromley, T. M., Dlugokencky, E. J., Michel, S. E., Miller, J. B., Levin, I., Lowe, D. C., Martin, R. J., Vaughn, B. H., and White, J. W. C.: A 21st century shift from fossil-fuel to biogenic methane emissions indicated by $^{13}CH_4$, Science (New York, N.Y.), 352, 80–84, https://doi.org/10.1126/science.aad2705, http://science.sciencemag.org/content/352/6281/80.abstract, 2016.

Snover, A. and Quay, P.: Hydrogen and carbon kinetic isotope effects during soil uptake of atmospheric methane and a temperate grassland, Glob. Biogeochem. Cycles, 14, 25–39, 2000.

Solomon, S., Rosenlof, K. H., Portmann, R. W., Daniel, J. S., Davis, S. M., Sanford, T. J., and Plattner, G.-K.: Contributions of Stratospheric Water Vapor to Decadal Changes in the Rate of Global Warming, Science, 327, 1219–1223, https://doi.org/10.1126/science.1182488, 2010.

Steinwagner, J., Milz, M., von Clarmann, T., Glatthor, N., Grabowski, U., Höpfner, M., Stiller, G. P., and Röckmann, T.: HDO measurements with MIPAS, Atmos. Chem. Phys., 7, 2601–2615, https://doi.org/10.5194/acp-7-2601-2007, https://www.atmos-chem-phys.net/7/2601/2007/, 2007.

Stenke, A. and Grewe, V.: Simulation of stratospheric water vapor trends: impact on stratospheric ozone chemistry, Atmos. Chem. Phys., 5, 1257–1272, www.atmos-chem-phys.org/acp/5/1257/, 2005.

Stolper, D., Sessions, A., Ferreira, A., Neto, E. S., Schimmelmann, A., Shusta, S., Valentine, D., and Eiler, J.: Combined C–D and D–D clumping in methane: Methods and preliminary results, Geochim. Cosmochim. Acta, 126, 169–191, https://doi.org/10.1016/j.gca.2013.10.045., http://www.sciencedirect.com/science/article/pii/S0016703713006170, 2014.

Tian, W., Chipperfield, M. P., and Lü, D.: Impact of increasing stratospheric water vapor on ozone depletion and temperature change, Advances in Atmospheric Sciences, 26, 423–437, https://doi.org/10.1007/s00376-009-0423-3, https://doi.org/10.1007/s00376-009-0423-3, 2009.

Tost, H., Jöckel, P., Kerkweg, A., Sander, R., and Lelieveld, J.: Technical note: A new comprehensive SCAVenging submodel for global atmospheric chemistry modelling, Atmos. Chem. Phys., 6, 565–574, https://doi.org/10.5194/acp-6-565-2006, https://www.atmos-chem-phys.net/6/565/2006/, 2006.

Umezawa, T., MacHida, T., Ishijima, K., Matsueda, H., Sawa, Y., Patra, P. K., Aoki, S., and Nakazawa, T.: Carbon and hydrogen isotopic ratios of atmospheric methane in the upper troposphere over the Western Pacific, Atmos. Chem. Phys., 12, 8095–81 113, https://doi.org/10.5194/acp-12-8095-2012, 2012.

White, J., Vaughn, B., and Michel, S.: University of Colorado, Institute of Arctic and Alpine Research (INSTAAR), Stable Isotopic Composition of Atmospheric Methane (^{2}H) from the NOAA ESRL Carbon Cycle Cooperative Global Air Sampling Network, 2005-2009, Version: 2016-04-26, ftp://aftp.cmdl.noaa.gov/data/trace_gases/ch4h2/flask/, 2016.

White, J., Vaughn, B., and Michel, S.: University of Colorado, Institute of Arctic and Alpine Research (INSTAAR), Stable Isotopic Composition of Atmospheric Methane (^{13}C) from the NOAA ESRL Carbon Cycle Cooperative Global Air Sampling Network, 1998-2016, Version: 2018-01-31, ftp://aftp.cmdl.noaa.gov/data/trace_gases/ch4c13/flask/, 2017.

Winterstein, F., Tanalski, F., Jöckel, P., Dameris, M., and Ponater, M.: Implication of strongly increased atmospheric methane concentrations for chemistry–climate connections, Atmos. Chem. Phys., 19, 7151–7163, https://doi.org/10.5194/acp-19-7151-2019, https://www.atmos-chem-phys.net/19/7151/2019/, 2019.

Supplement of:
Methane chemistry in a nutshell – The new submodels CH4 (v1.0) and TRSYNC (v1.0) in MESSy (v2.54.0)

Franziska Winterstein[1] and Patrick Jöckel[1]

[1]Deutsches Zentrum für Luft- und Raumfahrt (DLR), Institut für Physik der Atmosphäre, Oberpfaffenhofen, Germany

Correspondence: Franziska Winterstein (franziska.winterstein@dlr.de)

Contents

1 Chemical processes and reaction rate coefficients concerning CH_4 3

1.1 Sink reactions . . . 3

1.2 Reaction rate coefficients . . . 3

2 Evaluation of simulated CH_4 isotopologues with observations 4

2.1 Surface sampling sites . . . 5

2.2 Airborne observations . . . 7

2.3 Balloon borne observations . . . 8

3 Documentation of the CH4 submodel 12

3.1 Introduction . . . 12

3.2 MODULE messy_ch4_si: Subroutines in the submodel interface layer (SMIL) . . . 12

3.3 MODULE messy_ch4: Subroutines in the submodel core layer (SMCL) . . . 14

3.4 Private subroutines . . . 16

3.5 User interface . . . 19

3.5.1 CH4 CTRL namelist . . . 19

3.5.2 CH4 CPL namelist . . . 19

3.6 Example namelist . . . 20

4 Documentation of the TRSYNC submodel 22

4.1 Introduction . . . 22

4.2 MODULE messy_trsync_si: Subroutines in SMIL . . . 24

4.3 MODULE messy_trsync: Subroutines in SMCL . . . 26

4.4 Private subroutines . . . 27

4.5 User interface 29
4.5.1 TRSYNC CPL namelist 29
4.6 Example namelist 29

5 Example namelist entries for other submodels corresponding to CH4 set-up 30
5.1 TRACER 30
5.2 DDEP 30
5.3 IMPORT 31
5.4 OFFEMIS 34
5.5 TNUDGE 37
5.6 H2OISO 38

6 ~~Isotopic signatures of emission sources~~ 38

1 Chemical processes and reaction rate coefficients concerning CH_4

1.1 Sink reactions

General sink reactions:

$$CH_4 + OH \xrightarrow{k_{CH_4+OH}} CH_3 + H_2O \quad \text{(SR1)}$$

$$CH_4 + O(^1D) \xrightarrow{k_{CH_4+O(^1D)}} products \quad \text{(SR2)}$$

$$CH_4 + Cl \xrightarrow{k_{CH_4+Cl}} CH_3 + HCl \quad \text{(SR3)}$$

$$CH_4 + h\nu \xrightarrow{k_{CH_4+h\nu}} products \quad \text{(SR4)}$$

Sink reactions with isotopologues containing carbon-13 (^{13}C) :

$$^{13}CH_4 + OH \xrightarrow{k_{^{13}CH_4+OH}} {}^{13}CH_3 + H_2O \quad \text{(SR5)}$$

$$^{13}CH_4 + O(^1D) \xrightarrow{k_{^{13}CH_4+O(^1D)}} products \quad \text{(SR6)}$$

$$^{13}CH_4 + Cl \xrightarrow{k_{^{13}CH_4+Cl}} {}^{13}CH_3 + HCl \quad \text{(SR7)}$$

$$^{13}CH_4 + h\nu \xrightarrow{k_{^{13}CH_4+h\nu}} products \quad \text{(SR8)}$$

Sink reactions with isotopologues containing deuterium (D):

$$CH_3D + OH \xrightarrow{k_{CH_3D+OH}} CH_2D + H_2O \quad \text{(SR9)}$$

$$CH_3 + HDO \quad \text{(SR10)}$$

$$CH_3D + O(^1D) \xrightarrow{k_{CH_3D+O(^1D)}} products \quad \text{(SR11)}$$

$$CH_3D + Cl \xrightarrow{k_{CH_3D+Cl}} CH_2D + HCl \quad \text{(SR12)}$$

$$CH_3 + DCl \quad \text{(SR13)}$$

$$CH_3D + h\nu \xrightarrow{k_{CH_3D+h\nu}} products \quad \text{(SR14)}$$

1.2 Reaction rate coefficients

The reaction rates for the reaction (SR1–SR3) applied in this study are:

$$k_{CH_4+OH} \approx 1.85 \times 10^{-20} \cdot \exp(2.82 \cdot \log(T) - \frac{987}{T}) \quad (1)$$

$$\approx 1.85 \times 10^{-20} \cdot T^{2.82} \cdot \exp(-\frac{987}{T}) \quad (2)$$

$$k_{CH_4+Cl} \approx 6.6 \times 10^{-12} \cdot \exp(\frac{-1240}{T}) \quad (3)$$

$$k_{CH_4+O1D} \approx 1.75 \times 10^{-10} \quad (4)$$

Eq. (3) and (4) are from Sander et al. (2011) and Eq. (1) from Atkinson (2003). The temperature in [K] is denoted as T.

The reaction rate coefficients for the isotopologues (SR5–SR14) are achieved by multiplying the inverse of the corresponding Kinetic Isotope Effect (KIE) from Table 1 in the main manuscript. For example:

$$k_{^{13}CH_4+OH} \approx k_{CH_4+OH} \cdot \mathrm{KIE}^{\mathrm{OH}-1}_{^{13}CH_4} \quad (5)$$

2 Evaluation of simulated CH_4 isotopologues with observations

The following section shows comparisons of simulation results with atmospheric observations from stationary surface sampling sites of the National Oceanic and Atmospheric Administration/Earth System Research Laboratory (NOAA/ESRL, White et al. (2016, 2017) with airborne observations taken during the Comprehensive Observation Network for TRace gases by AIrLiner (CONTRAIL) project (Umezawa et al., 2012), and with balloon borne observations by Röckmann et al. (2011). The study is based on work by Frank (2018) and observations are thereby compared to two simulations (1) EMAC-apos-02 and (2) EMAC-apos-03.

In the simulation EMAC-apos-02, the CH4 submodel together with its isotopologue extension is applied. This includes isotopologues concerning both, carbon, and hydrogen isotopes. The submodel is set up with the KIEs as introduced in Table 1 (see main manuscript). The comprehensive interactive chemistry simulation EMAC-apos-03 is conducted with the kinetic chemistry tagging hydrogen isotopologues, only. This configuration is chosen to investigate the pathways of deuterium from the source towards the end-product of deuterated methane (CH_3D), i.e. deuterated water vapour (HDO). This requires to include KIEs for the intermediates, too, as well as to apply adequate branching ratios and isotope transfer probabilities. The inclusion of carbon isotopologues with MECCA_TAG is omitted due to the fact that MECCA_TAG introduces additionally nearly twice as many chemical reactions and species as included in the basic chemical mechanism. To maintain a computational efficient simulation, the CH4 submodel is in EMAC-apos-03 additionally applied to simulate the carbon related methane (CH_4) isotopologues. In this case, the CH_4 tracer of the simplified CH_4 chemistry (CH4) submodel (`CH4_fx`), acting as the master tracer for the CH_4 isotopologues in the CH4 submodel, is in each model time step reset to the CH_4 tracer in the Module Efficiently Calculating the Chemi ensure an identical overall CH_4 budget. The CH4 submodel also uses directly the on-line calculated the hydroxyl radical (OH), excited oxygen ($O(^1D)$) and chlorine (Cl) distribution from MECCA.

Table S1. The isotopic signature of the emission sources as used in the model simulations with ECHAM/MESSy Atmospheric Chemistry (EMAC). All δ-values and ranges are given in [permil (‰)].

	$\delta^{13}C(CH_4)_{VPDB}$			$\delta D(CH_4)_{VSMOW}$		
Natural sources	δ-value	$\pm$	references	δ-value	$\pm$	references
wetlands	-59.4	1.5	[1,2,3,4,6]	-336.2	23.8	[3,4,6]
other						
wildanimals	-61.5	0.5	[1]	-319.0	/	[5]
termites	-63.3	6.5	[1,2,3]	-390.0	35.5	[3]
volcanoes	-40.9	0.9	[1,2]	-253.4	53.4	[3,7]
ocean (hydrates)	-59.0	1.0	[1,2,3]	-220.0	/	[3]
Anthropogenic sources						
anthropogenic (collective)	-46.8	10.3	[3,4,6,8]	-223.5	23.5	[3,4,6]
rice	-63.0	1.0	[1,2,3,4,6]	-324.3	5.5	[3,4,6]
biomass burning	-23.9	1.6	[1,2,3,4,6]	-213.0	7.5	[3,4,6]

references: (1) (Monteil et al., 2011) (2) (Fletcher et al., 2004) (3) (Whiticar and Schaefer, 2007) (4) (Snover and Quay, 2000) (5) (Rigby et al., 2012) (6) (Quay et al., 1999) (7) (Kiyosu, 1983) (8) (Zazzeri et al., 2015)

The applied emission inventory in the presented simulations is an a posteriori inventory derived using an inverse optimization technique (Frank, 2018; Bruhwiler et al., 2005). The specific isotopic signatures of the emission sources used in the model are listed in Table S1.

The isotopic signatures are given in the δ-notation (McKinney et al., 1950). We use the standard isotopic signature of Vienna Standard Mean Ocean Water (VSMOW) for the signature of D in CH_4 ($\delta D(CH_4)$) and Vienna-PeeDee Belemnite (VPDB) for the signature of ^{13}C in CH_4 ($\delta^{13}C(CH_4)$).

2.1 Surface sampling sites

To start with the evaluation of the simulation results, isotopic observations from NOAA/ESRL sampling sites (White et al., 2016, 2017) are compared to the surface mixing ratios and δ-values of the simulations. For the comparison a climatological mean of 2000–2009 is used, since this time period is represented by most of the stations and the dynamic equilibrium of the simulated isotopic composition (as visible especially in EMAC-apos-03, Frank (2018)) has been reached.

EMAC-apos-03 agrees well with the stations regarding the CH_4 mixing ratio. Interesting is that the $\delta^{13}C(CH_4)$ values are slightly better represented in EMAC-apos-02 compared to EMAC-apos-03, although the agreement is overall quite well in both simulations. This suggests that the emission signatures are a bit too low for methane containing ^{13}C ($^{13}CH_4$) in connection with the OH concentration in EMAC-apos-03. On the other hand, in case of $\delta D(CH_4)$, EMAC-apos-03 agrees better, however, is

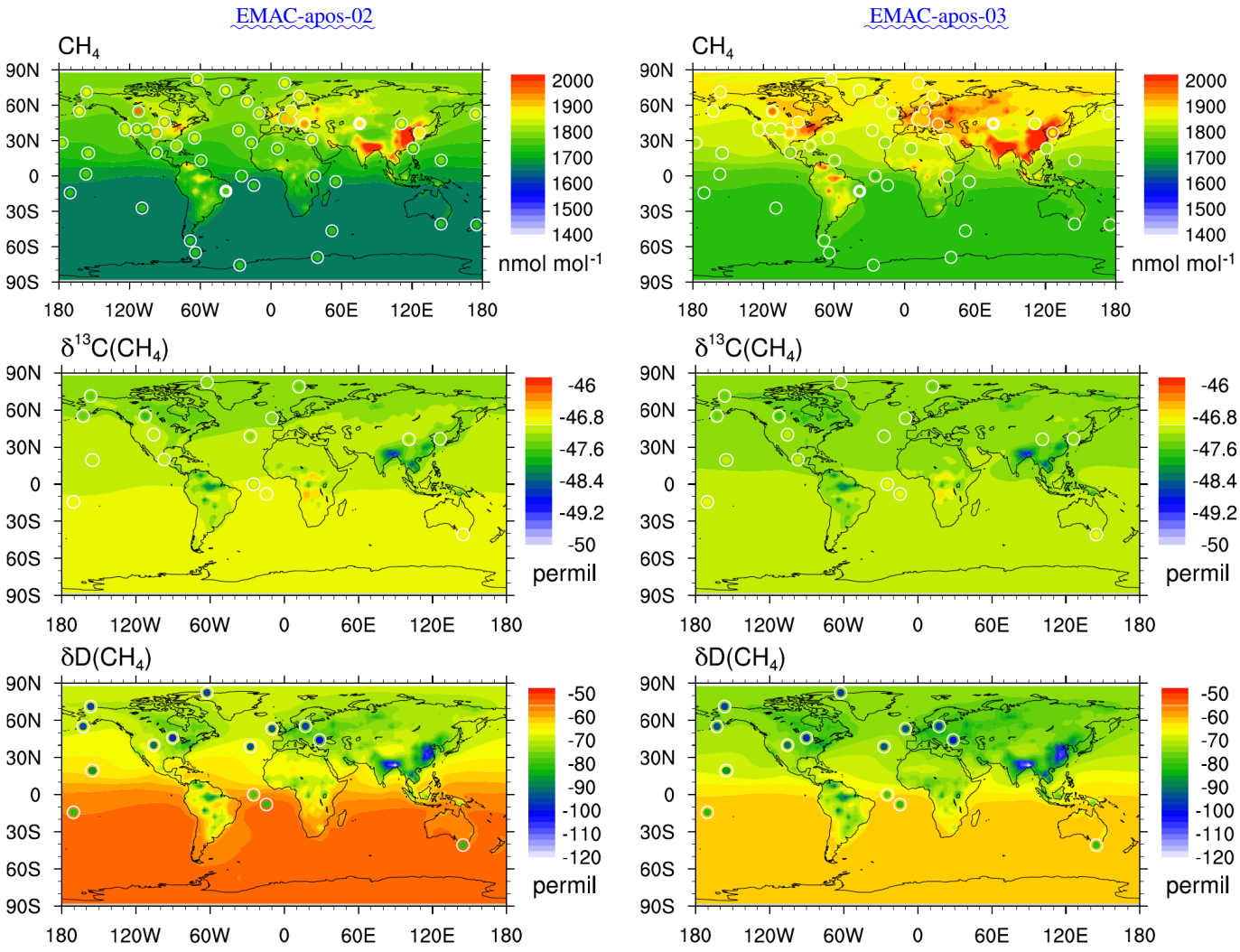

Figure S1. Simulated multi-annual (2000–2009) surface mixing ratio of CH_4 in [nmoles of the chemical tracer per mole of air (mol mol^{-1})] (upper), corresponding $\delta^{13}C(CH_4)_{VPDB}$ in [‰] (middle), and $\delta D(CH_4)_{VSMOW}$ in [‰] (lower). The left column shows results of EMAC-apos-02 and the right column those from EMAC-apos-03. The colored dots indicate the surface observations from NOAA/ESRL. The circles around the dots are the value of the simulation at the specific sampling height of the observation (in order to account for sub-grid orographic differences between simulation and observation).

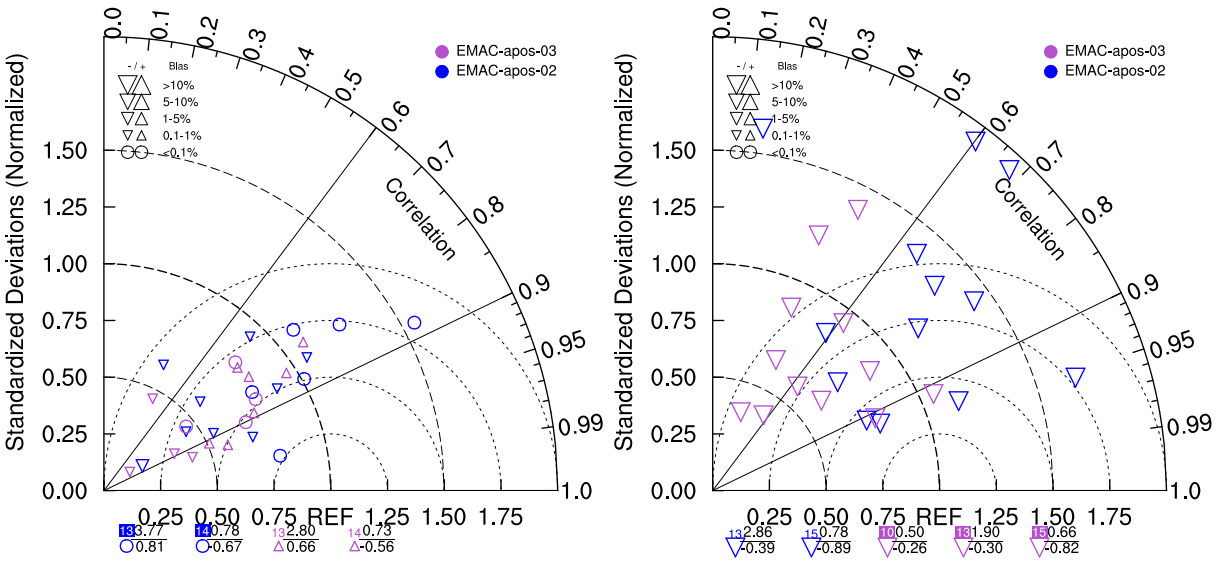

Figure S2. Taylor diagrams of the comparison between observations and the simulations EMAC-apos-02 (blue) and EMAC-apos-03 (purple) at various surface sampling sites. The Taylor diagram is shown for $\delta^{13}C(CH_4)_{VPDB}$ (a) and for $\delta D(CH_4)_{VSMOW}$ (b) with respect to the representation of the annual cycle during the considered time period 2000–2009. The size of the triangles indicates the bias in percent with upward oriented triangles indicating a positive and downward oriented triangles a negative bias, respectively. Circles indicate a bias of less than 0.1%. The symbols below the diagram are stations outside the displayed range of the Taylor diagram and are indicated by the colored number. The normalized standard deviation is displayed by the upper black number and the correlation coefficient by the lower black number on the right hand side of the symbol.

still isotopically enriched compared to the station samples. This indicates that the chosen emission signatures for CH_3D are too heavy.

In addition to that, the annual cycle of the observations is generally fairly well represented in both simulations (see Fig. S2). However, the trend of the signatures at the stations over the years could not be captured yet. The reason for this is that the simulations fail to represent the general trend of the CH_4 mixing ratio and that the emission signatures of the individual sources are still uncertain.

2.2 Airborne observations

During the CONTRAIL project, atmospheric air samples were taken with an Automatic air Sampling Equipment (ASE) mounted on a commercial aircraft (Umezawa et al., 2012). These air samples were later measured concerning the isotopic composition of CH_4 using a gas chromatography system and a flame ionization detector. The here presented sampling data comprise several flights between 2006 and 2010, with each flight providing up to 12 air samples.

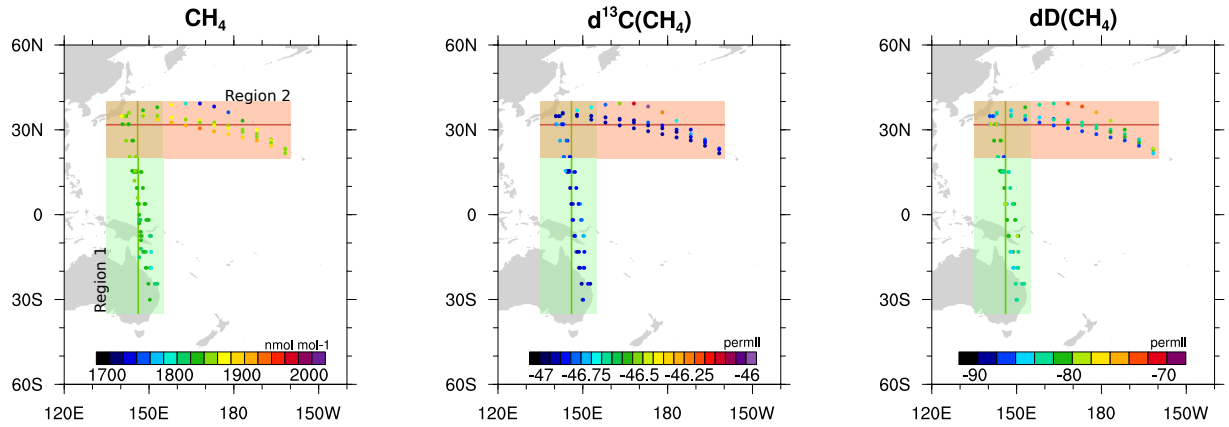

Figure S3. Observations provided by the CONTRAIL project (Umezawa et al., 2012). The green shaded area indicates region 1, and the red shaded area indicates region 2.

The presented flights are seperated into two regions, as depicted in Fig. S3. The first region (green) indicates the flights on a north-south route, bound from Narita airport (Japan) to Sydney, Brisbane (Australia) or Guam, and the second region (red) represents those flights on an east-west route, bound from Narita to Honolulu (Hawaii).

Especially the first region provides the opportunity to investigate the representation of the meridional gradient and the north-south imbalance in the δ-values in the model as it nicely spans over the tropics (40° S−40° N). Simulation results and the airborne observations in this region are depicted in Fig. S4, where green dots indicate the observations. The dark green line indicates the mean of the observations and the shaded green area is the corresponding standard deviation. Simulated values are included as the red and blue dots respectively.

It is apparent from the shown results that the meridional gradient in the simulations concerning CH_4 and both isotopic signatures are well represented, although the absolute values differ. This indicates that the implemented KIE in the model is reasonable and that adjustments to the signatures of the emission inventory are required.

2.3 Balloon borne observations

The presented airborne observations are used to infer tropospheric chemical compositions. The high-altitude range of balloon borne observations enables to investigate the stratospheric isotopic signatures, as well.

The observational data are provided by Röckmann et al. (2011) and were obtained by altogether 13 balloon flights between 1987 and 2003 at four launch stations: Hyderabab in India (HYD), Aire sur l'Adour in France (ASA), Gap in France (GAP) and Kiruna in Sweden (KIR). The balloon-borne high-altitude air samples are obtained up to 10 hPa (35 km) and were later examined with respect to CH_4 mixing ratios as well as its isotopic composition concerning $^{13}CH_4$ and CH_3D using a high precision continuous flow isotope ratio mass spectrometer (Brass and Röckmann, 2010).

The observations shown in Fig. S5 indicate two features:

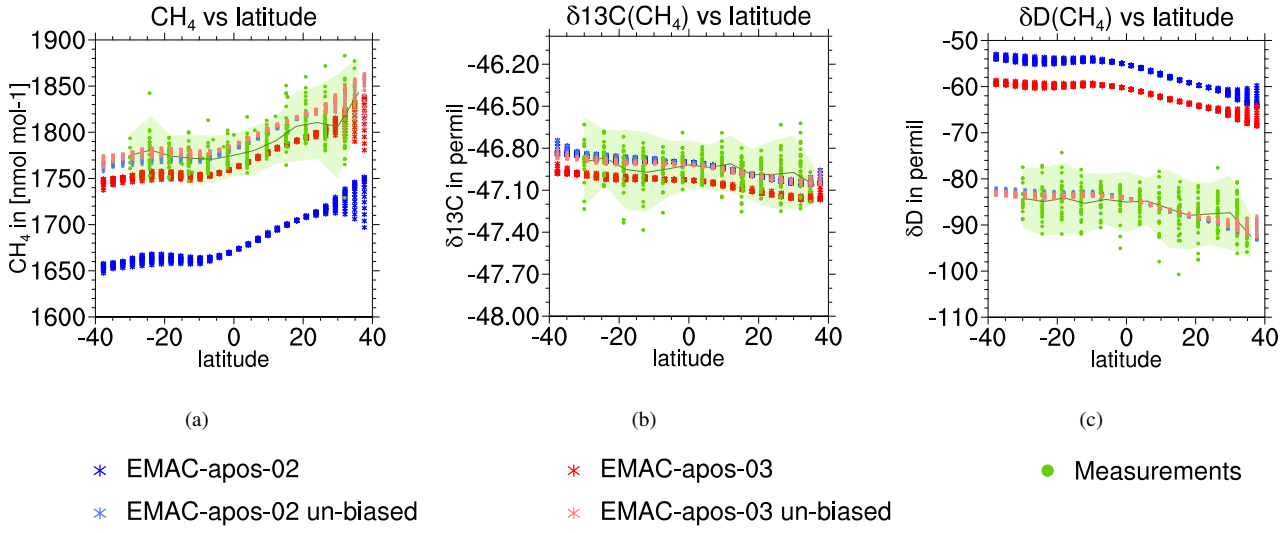

Figure S4. Comparison of airborne observations (green) in the meridionally aligned region 1 with simulation data from EMAC-apos-02 (blue) and EMAC-apos-03 (red). CH_4 (a), $\delta^{13}C(CH_4)_{VPDB}$ (b) and $\delta D(CH_4)_{VSMOW}$ (c). The lighter red and blue colored markers indicate the de-biased simulation data for the direct comparison to the meridional gradient of the observations. The dark green line indicates the mean of the observations with the greenish shaded area being the corresponding single standard deviation.

- First, while CH_4 gets reduced towards higher altitudes, the isotopic content gets enriched (both, in $\delta^{13}C(CH_4)$ and $\delta D(CH_4)$). This occurs due to fractionation processes, which prefer lighter isotopologues in the sink reactions over heavier isotopologues.
- Secondly, again, a meridional gradient is visible. Polar regions tend to have less CH_4 than tropical regions, indicating to some extent the older age of the polar air masses. Consequently, polar regions are isotopically enriched compared to regions at mid and low latitudes.

The balloon-borne observations are compared to the simulations in Fig. S5 at pressure levels from 200 hPa to 10 hPa and separated into polar, mid-latitude and tropical regions. For the comparison, the monthly averaged data of the simulation is sampled at the specific year, month and location of the observation and interpolated from model levels to pressure levels. The plots in Fig. S5 further show the single standard deviation of the observations by the grey shaded areas and the standard deviation of all vertical profiles in the corresponding latitudinal region of the simulations as the shaded area in the color of the respective simulation.

The presented comparisons of observations to simulation results show that the global isotopic features of the meridional isotopic gradient and the isotopic gradient with altitude is captured well by both simulations (EMAC-apos-02, only with

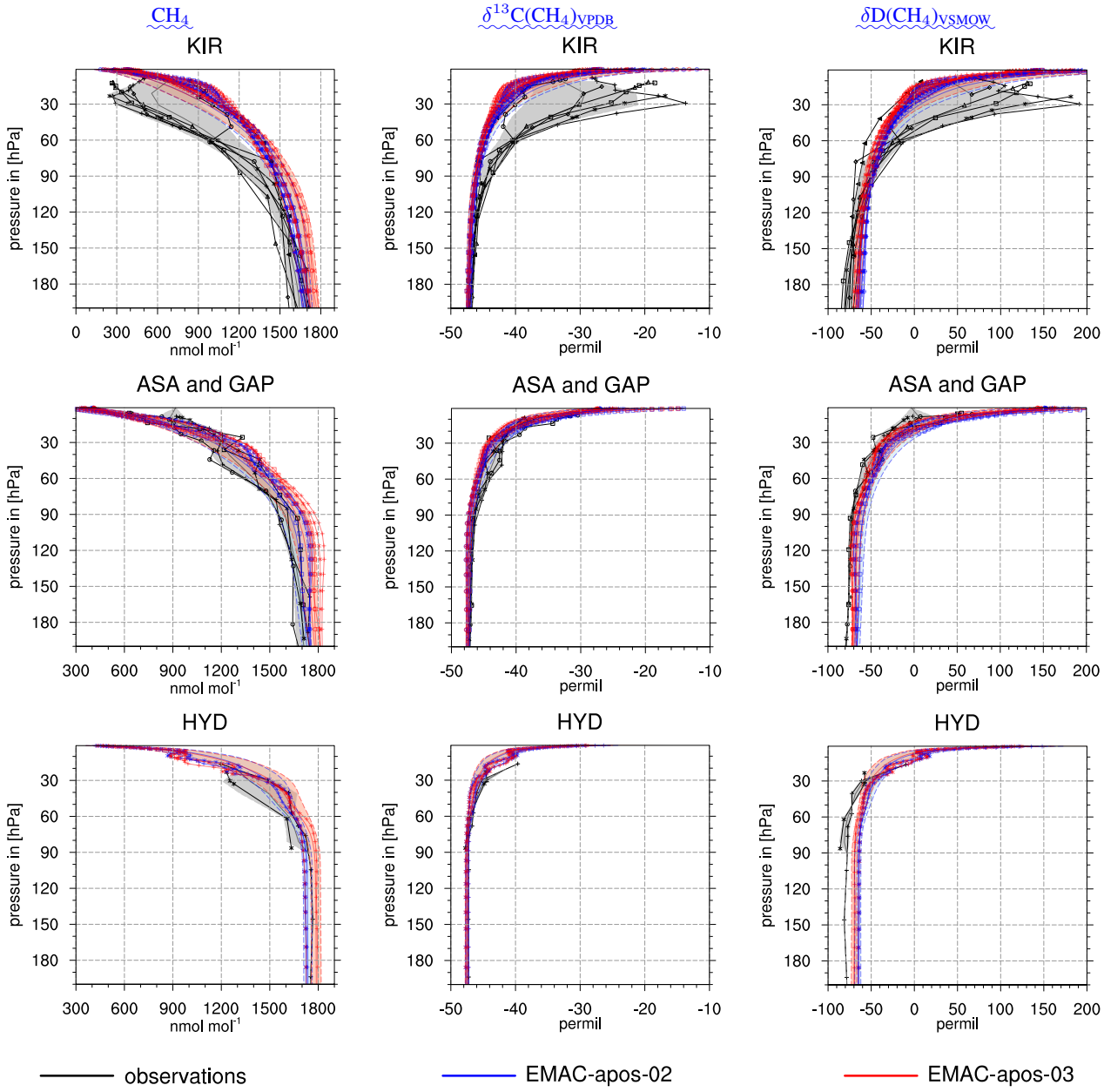

Figure S5. Balloon borne observations from Röckmann et al. (2011, black) together with simulation results from EMAC-apos-02 (blue) and EMAC-apos-03 (red). The rows of panels from top to bottom present balloon launches in the polar region from Kiruna in Sweden (KIR), in the mid-latitude region from Aire sur l'Adour in France (ASA) and Gap in France (GAP), and in the tropical region from Hyderabab in India (HYD). The profiles of the simulations are taken from monthly averaged data in the specific year, month and at the location of the observation. For observations taken before the simulation start, the simulated year 1990 is shown. Shaded areas indicate the single standard deviation of the observations (grey) and the simulations (blue and red, respectively) with respect to the variations within the specific latitudinal region and the interannual variation in the years 1990–2003.

CH4 submodel, and EMAC-apos-03, with MECCA and the CH4 submodel). This indicates that the implementation of the simulation of CH_4 isotopologues is sufficiently realized and also confirms the suitability of the chosen KIE values. Absolute values and the inter-annual trend of the observations, however, are not captured well, which is mainly caused by uncertainties in the CH_4 emission fluxes and the applied source signatures.

3 Documentation of the CH4 submodel

3.1 Introduction

The CH4 submodel represents a simplified CH_4 chemistry. It defines the tracer `CH4_fx`, which gets reduced via the four CH_4 sink reactions. The tracer is initialized from external data via the submodel TRACER (Jöckel et al., 2008) and modified by either emissions, which need to be introduced via the submodel OFFline EMISsions (OFFEMIS) (Kerkweg et al., 2006) or by Newtonian relaxation towards a lower boundary condition with the submodel TNUDGE (Kerkweg et al., 2006). Example namelist entries concerning the configuration of these submodels are found in Section 5.

Additional to that, the CH4 submodel provides two further options. One is the simulation of the CH_4 isotopologues, and the second is the representation of ~~age-~~age and emission classes of CH_4, which, to some extent, are able to resolve an additional spatial and temporal information of the CH_4 emissions.

The option concerning the CH_4 isotopologues can be applied with respect to ^{13}C isotopologues, D isotopologues, or both. The submodel defines the following tracers for the given isotopologues: `CH4_12C` (methane containing carbon-12 (^{12}C, $^{12}CH_4$)), `CH4_13C` ($^{13}CH_4$), `CH4_D0` (CH_4), and `CH4_D1` (CH_3D).

The option to simulate ~~age-~~age and emission classes introduces additional tracers depending on the chosen number of ~~age-~~age and emission classes. For every combination of ~~age-~~age and emission class one tracer is defined, thus, if N is the number of age classes and M is the number of emission classes, in total $N \times M$ additional tracers are defined. The tracers are denoted by the names `CH4_fx_e[mm]_a[nn]`, with `[mm]` being the identifying number of the emission class and `[nn]` the number of the age class.

The following section documents the subroutines, which are part of the CH4 submodel and in the section "User interface" the entries in the corresponding namelists are explained.

3.2 MODULE messy_ch4_si: Subroutines in the submodel interface layer (SMIL)

These subroutines follow the general structure mandatory for Modular Earth Submodel System (MESSy) submodels. Note that _gp and _lg denote the Gaussian grid point and Lagrangian mode (see Brinkop and Jöckel (2019) for more information). In the presented examples solely the Gaussian grid point mode is used.

- `SUBROUTINE ch4_initialize`: Initializes the submodel, reads the control and coupling namelists and broadcasts the information to all parallel tasks.
- `SUBROUTINE ch4_new_tracer`: Defines the new tracers, which also includes the additional tracers regarding the submodel extensions (if applied).
- `SUBROUTINE ch4_init_memory`: Defines the channel objects and allocates memory.
- `SUBROUTINE ch4_init_coupling`: Sets pointers for coupling to the basemodel and other submodels.

- `SUBROUTINE ch4_global_start`: Sets values of internal variables with respect to the applied ageing method, if the option of ~~age~~ age and emission classes is switched on.
- `SUBROUTINE ch4_vdiff`: Currently not used.
- `SUBROUTINE ch4_physc`: This subroutine calls the integration step of the submodel, i.e. `ch4_integrate`. It further accounts for the water vapour (H_2O) feedback, if it is switched on. The tendencies for the ~~age~~ age and emission class tracers and the isotopologue tracers are calculated in separate integration routines, namely `class_integrate_gp/lg` and `iso_integrate_gp/lg`.
- `SUBROUTINE ch4_global_end`: Entry point in time loop for LG calculations; not used for the presented examples.
- `SUBROUTINE ch4_free_memory`: Deallocation of allocated memory.

3.3 MODULE messy_ch4: Subroutines in the submodel core layer (SMCL)

The following subroutines represent the core layer of the submodel.

SUBROUTINE ch4_integrate			(CH4_te, CH4, OH, O1D, Cl, j_CH4, temp, press, spechum, iso_id)
name	type	intent	description
mandatory arguments:			
CH4_te	REAL	OUT	CH_4 tendency
CH4	REAL	IN	CH_4 mixing ratio
OH	REAL	IN	OH mixing ratio
O1D	REAL	IN	$O(^1D)$ mixing ratio
Cl	REAL	IN	Cl mixing ratio
j_CH4	REAL	IN	photolysis rate of CH_4
temp	REAL	IN	temperature
press	REAL	IN	pressure
spechum	REAL	IN	specific humidity
iso_id	INTEGER	IN	ID of isotopologue

description:

This subroutine executes the integration step of the submodel. It applies the functional (i.e. temperature dependent) reaction rate coefficients of the sink reactions of CH_4 and accounts for the KIE in the case of rare isotopologues.

SUBROUTINE sca_tend			(m, mte, s, ste, dt, a)
name	type	intent	description
mandatory arguments:			
m	REAL	IN	master tracer
mte	REAL	IN	tendency of master tracer
s	REAL	IN	sum of fractional tracers
ste	REAL	IN	sum of fractional tracer tendencies
dt	REAL	IN	time step length
a	REAL	OUT	resulting correction factor

description:

Calculates the necessary correction factor so that the fractional tracers including their tendencies add up to the master tracer (incl. its current tendency).

SUBROUTINE adj_tend			(f, t, a, dt, tadj)
name	type	intent	description
mandatory arguments:			
f	REAL	IN	fractional tracer
t	REAL	IN	tendency of fractional tracer
a	REAL	IN	correction factor
dt	REAL	IN	time step length
tadj	REAL	OUT	resulting additional tendency for adjustment

description:

Calculates the necessary additional tendency to adjust for the given correction factor.

SUBROUTINE ch4_read_nml_ctrl			(status, iou)
name	type	intent	description
mandatory arguments:			
status	INTEGER	OUT	error status info
iou	INTEGER	IN	I/O unit

description:

This subroutine is used to read the CTRL-namelist of the submodel.

3.4 Private subroutines

Private subroutines in `messy_ch4_si`

SUBROUTINE ch4_read_nml_cpl			(status, iou)
name	type	intent	description
mandatory arguments:			
status	INTEGER	OUT	error status info
iou	INTEGER	IN	I/O unit

description:

This subroutine is used to read the CPL-namelist of the submodel.

SUBROUTINE class_integrate_gp			(temp, press, spechum)
name	type	intent	description
mandatory arguments:			
temp	REAL, DIMENSION(:,:)	IN	temperature
press	REAL, DIMENSION(:,:)	IN	pressure
spechum	REAL, DIMENSION(:,:)	IN	specific humidity

description:

This subroutine calls `ch4_integrate` for every age and emission class tracer separately.

SUBROUTINE class_age_move_gp			(CH4c, CH4c_te)
name	type	intent	description
mandatory arguments:			
CH4c	REAL, DIMENSION(:,:)	IN	current CH_4 tracer mixing ratio
CH4c_te	REAL, DIMENSION(:,:)	IN	current CH_4 tracer tendency

description:

Accounts for the shifting from one age class to the next.

SUBROUTINE class_adj_tend_gp			(CH4c, CH4c_te)
name	type	intent	description
mandatory arguments:			
CH4c	REAL, DIMENSION(:,:)	IN	current CH_4 tracer mixing ratio
CH4c_te	REAL, DIMENSION(:,:)	IN	current CH_4 tracer tendency

description:

Adjusts the tendencies of the age and emission class tracers so that the tracers sum up to the master tracer CH4_fx, which is required to correct for potential numerical inaccuracies.

SUBROUTINE iso_integrate_gp			(temp, press, spechum, CH4_te)
name	type	intent	description
mandatory arguments:			
temp	REAL, DIMENSION(:,:)	IN	temperature
press	REAL, DIMENSION(:,:)	IN	pressure
spechum	REAL, DIMENSION(:,:)	IN	specific humidity
CH4_te	REAL, DIMENSION(:,:)	IN	current CH_4 tracer tendency

description:

Calls ch4_integrate for every isotopologue tracer separately. It further calculates the tendency added to the HDO, either by the simple assumption that one HDO molecule is produced by one oxidized CH_3D molecule, or by the function

$$\frac{\partial(HDO)}{\partial t} = \frac{-\frac{\partial(CH_3D)}{\partial t} + 6.32 \times 10^{-5} \cdot \frac{\partial(CH_4)}{\partial t}}{\frac{M_{air}}{M_{HDO}} \left(\frac{1}{1-HDO}\right)^2} , \tag{6}$$

proposed by Eichinger et al. (2015).

SUBROUTINE class_adj_tend_gp			(CH4c, CH4c_te, idt_gp_iso_adj)
name	type	intent	description
mandatory arguments:			
CH4c	REAL, DIMENSION(:)	IN	current CH_4 tracer mixing ratio
CH4c_te	REAL, DIMENSION(:)	IN	current CH_4 tracer tendency
idt_gp_iso_adj	REAL, DIMENSION(:)	IN	list of tracer IDs

description:

Adjusts the tendencies of the isotopologue tracers so that the tracers regarding the isotopes of the same element sum up to the master tracer CH4_fx, which is required to correct for potential numerical inaccuracies.

Private subroutines in `messy_ch4`

SUBROUTINE calc_KIE			(KIE_AB_val, temp_t, KIE_t)
name	type	intent	description
mandatory arguments:			
KIE_AB_val	REAL, DIMENSION(2)	IN	KIE parameters A and B
temp_t	REAL	IN	temperature
KIE_t	REAL	OUT	KIE value

description:

Calculates the KIE with the equation: KIE_t = A·exp(B/temp).

3.5 User interface

3.5.1 CH4 CTRL namelist

The control (CTRL) namelist of the CH4 submodel includes the KIE values applied in the isotopologue extension of the submodel for all four sink reactions and both isotopologues.

The KIE is represented in the form KIE $=$ A$\cdot\exp($B$/T)$, with A and B being the individual parameters and T the temperature in [K]. The namelist entries are given therefore as:

KIE_CH4_XX_YY = A, B.

XX and YY are set according to the specified reaction. XX denotes thereby the isotope in CH_4 and is 13C or D1. YY defines the reaction partner (either OH, O1D or CL) as well as the photolysis with jval. For those KIE, which are temperature independent, B is set to 0.0. The default values are A = 1.0 and B = 0.0, so that no KIE is applied.

3.5.2 CH4 CPL namelist

The coupling (CPL) namelist of the CH4 submodel sets the parameters for the applied extensions and feedback on the specific humidity. It further determines the channel objects used as the reaction partners in the CH_4 oxidation.

- i_H2O_feedback takes an integer, which controls the feedback of CH_4 oxidation on the specific humidity. Allowed values are: 0: no feedback, 1: feedback from GP and 2: feedback from LG. GP and LG denote grid-point representation and Lagrangian representation, respectively. (Default: 0)

- l_ef_re is a logical switch indicating whether the empirical formula introduced by Eichinger et al. (2015) is used (T) or not (F). (Default: F)

- L_GP and L_LG are both logical switches implying whether the Gaussian representation (GP) or Lagrangian representation (LG), or both are applied. The following namelist entries are shown for GP, however, there a identical entries for LG as well (indicated by gp and lg, respectively). (Default: L_GP = T, L_LG = F)

- c_gp_OH, c_gp_O1D, c_gp_Cl and c_gp_jCH4 define the chosen channel objects for the reaction partners of CH_4. They take two strings, the first indicates the channel, the second the object name.

- i_gp_nclass_emis_age denotes the number of emission- and age classes. It takes two integers, the first is the number of emission classes, the second is the number of age classes. (Default: i_gp_nclass_emis_age = 0, 0,)

- r_gp_age_cll is an optional entry, which adjusts the time period (in days) of one age class. This entry is only valid for ageing option 1 and 2 (see main text section 3.1). (Default: 30.44 for each age class)

- l_gp_adj_tend is a logical switch, which indicates whether the tendencies are adjusted so that the additional ~~age-~~ age and emission class tracers sum up to the master tracer CH4_fx. (Default: T)

- i_gp_ageing is an integer switch indicating the ageing method, which means the advancing of CH_4 from one age class to the next older one. It can be chosen between:

  - 0: monthly in one step
  - 1: continuously (default)
  - 2: monthly

  Note, using the first one, the Leapfrog time stepping with the Asselin-filter might cause numerical oscillations with negative values. Furthermore, the last one is not conform with the submodel TENDENCY, hence the corresponding diagnostic output created by TENDENCY is not meaningful. (Default: 1)

- l_gp_iso_C and l_gp_iso_H are logical switches. indicating whether the isotopologues of CH_4 concerning ^{13}C, D, or both are simulated. (Default: .FALSE.)

3.6 Example namelist

Namelist 1. Control (CTRL) and coupling (CPL) namelist of submodel CH4, stored in ch4.nml

```
&CTRL
!! ### KIE values for isotopologues
!! ### SYNTAX:
!! ###   KIE_*    = A, B,
!! ### with KIE(T) = A * exp(B/T)
!! ### temperature independent for B = 0._dp
!! ###
```

```
!! ### Reference KIE values:
!! ### Carbon 13 and D kinetic isotope effects in the reactions of CH4
!! ### with O1(D) and OH: New laboratory measurements and their
!! ### implications for the isotopic composition of stratospheric
!! ### methane
!! ### G. Saueressig, J. Crowley, P. Bergamaschi, C. Bruehl,
!! ### C.A.M. Brenninkmeijer and H. Fischer
!! ### [2001] Journal of Geosphysical Research
KIE_CH4_13C_OH  = 1.0039, 0.0,
KIE_CH4_13C_O1D = 1.013 , 0.0,
KIE_CH4_13C_CL  = 1.043 , 6.455,
KIE_CH4_13C_jval = 1.0 , 0.0,
KIE_CH4_D1_OH   = 1.097 , 49.0,
KIE_CH4_D1_O1D  = 1.060 , 0.0,
KIE_CH4_D1_CL   = 1.278 , 51.31,
KIE_CH4_D1_jval = 1.0, 0.0,
!
/
!
&CPL
!! ### feed back H2O tendency (= -2 * CH4-tendency) into specfic humidity?
!! ### (0: no feedback; 1: feedback from GP; 2: feedback from LG)
i_H2O_feedback = 1,
!! ### grid-point calculation
L_GP = T,
! L_LG = T,
!! ### educts and photolysis rate
c_gp_OH   = 'import_grid', 'CH4OX_OH',
c_gp_O1D  = 'import_grid', 'CH4OX_O1D',
c_gp_Cl   = 'import_grid', 'CH4OX_Cl',
c_gp_jCH4 = 'jval_gp',     'J_CH4',
!
! flag for empirical formula of Eichinger et al. (2015)
l_ef_re = T,
!
! ########################################################
! ### ADDITIONAL SECTION FOR EMISSION AND AGE CLASSES ###
! ########################################################
!
! ### n emission x m age classes
i_gp_nclass_emis_age = 48, 4, ! CAREFUL: If age / emis classes are changed
                              ! here, the tracer.nml must be updated
                              ! apropriately!
                              ! For emissions check offemis.nml,too
```

```
! ### age class duration [days] (only for ageing method 1)
!r_gp_age_cll = 1.0, 1.0, 1.0, 1.0,          ! for testing
!r_gp_age_cll = 30.44, 30.44, 30.44,30.44,  ! default
! ### adjust tendencies to sum tracer (default: true)
!l_gp_adj_tend = T,
! ### ageing method (0: monthly in one step, 1: continuous (default),
! ###                2: monthly, not TENDENCY conform)
!i_gp_ageing = 1,
i_gp_ageing = 2,
!
! ### n emission x m age classes
! i_lg_nclass_emis_age = 6, 4,
! ### age class duration [days] (only for ageing method 1)
!r_lg_age_cll = 1.0, 1.0, 1.0, 1.0,          ! for testing
!r_lg_age_cll = 30.44, 30.44, 30.44,30.44,   !
! ### adjust tendencies to sum tracer (default: true)
!l_lg_adj_tend = T,
! ### ageing method (0: monthly in one step, 1: continuous (default),
! ###                2: monthly, not TENDENCY conform)
!i_lg_ageing = 1,
! i_lg_ageing = 2,
!
! ##########################################
! ### ADDITIONAL SECTION FOR ISOTOPOLOGUES ###
! ##########################################
!
! ### Switch for isotopologues (GP)
l_gp_iso_C = .TRUE.
l_gp_iso_H = .TRUE.
! ### Switch for isotopologues (LG)
! l_lg_iso_C = .TRUE.
! l_lg_iso_H = .TRUE.
/
```

4 Documentation of the TRSYNC submodel

4.1 Introduction

The submodel TRacer SYNChronization (TRSYNC) guarantees that the physical H_2O tracers (incl. their isotopologues) receive also the correct tendencies of the corresponding chemical tracers.

The submodel ~~for~~ CH4 defines the tracer HDO, the submodel H_2O ISOtopologues (H2OISO) defines H2OISOHDOvap, and the MECCA_TAG in the MECCA defines I2H2O (or a different idiom, chosen by the user). The auxiliary submodel TRSYNC couples these tracers to combine the physical and chemical isotopic fractionation.

Without any isotopological extension solely ~~the~~ the 5th generation European Centre Hamburg general circulation model (ECHAM5) intrinsic tracer for specific humidity (q) is present. In this case, chemically produced H_2O (either from CH4 or from MECCA) directly adds optionally to q. However, in case of an isotopological extension using H2OISO, CH4 and/or MECCA_TAG the following additional tracers are defined:

- H2OISOHHOvap and H2OISOHDOvap (defined by H2OISO): The former is the total water tracer and the latter is the tracer of the rare isotopologue. Note that in H2OISO the two tracers do not add up to a master tracer, actually, H2OISOHHOvap represents and is identical to the master tracer (i.e. q).
- HDO (defined by CH4).
- I1H2O and I2H2O, representing H_2O and HDO, respectively (defined by MECCA_TAG): Both sum up to the chemical master tracer H2O.
- H2O (defined by MECCA): This tracer is originally not defined in MECCA, but is necessary in combination with MECCA_TAG for the internal scaling of I1H2O and I2H2O.

Figure S6 depicts the schematics of the coupling. At the beginning of every time step, H2OISOHHOvap is set to the current value of q, correcting any numerical deviations of H2OISOHHOvap from q caused in the previous time step. Next, basically all tracers are modified by the same physical processes: advection, vertical diffusion and convection. However, for the submodels E5VDIFF, CONVECT and CLOUD the hydrological processes are doubled in H2OISO to allow for isotope effects. The submodel Multi-phase Stratospheric Box Model (MSBM) calculates a tendency for q, which is added to H2OISOHHOvap as well. An equivalent tendency is added to H2OISOHDOvap, which is derived such that no additional fractionation by the multi-phase stratospheric chemistry is implied.

After all physical processes are complete, the submodel TRSYNC is called. It takes care that all tendencies of the previous (physical) processes of HDO and I2H2O are deleted and overwritten by the corresponding tendencies of the H2OISO equivalent H2OISOHDOvap. I1H2O is exceptional, as it must be set to the difference of the total tracer H2OISOHHOvap and the rare isotopologue H2OISOHDOvap. Note that for technical reasons the tracer H2OISOHDOvap is defined as one half of the corresponding chemical isotopological tracers HDO and I2H2O.

Next CH4 computes the CH_4 oxidation and derives the feedback onto q and HDO. At the very beginning of MECCA, the intrinsic H2O tracer is synchronized with q. Before and after the calls of the kinetic solver, I1H2O and I2H2O are scaled appropriately to add up to H2O. After this, the feedback onto H_2O is passed to q. To be precise, the sketch in Fig. S6 suggests that CH4 and MECCA are executed in the same simulation. This is indeed possible, but not necessary and it is important to note that only one of the two can provide the chemical feedback onto q, which can be arranged by corresponding switches in the namelists.

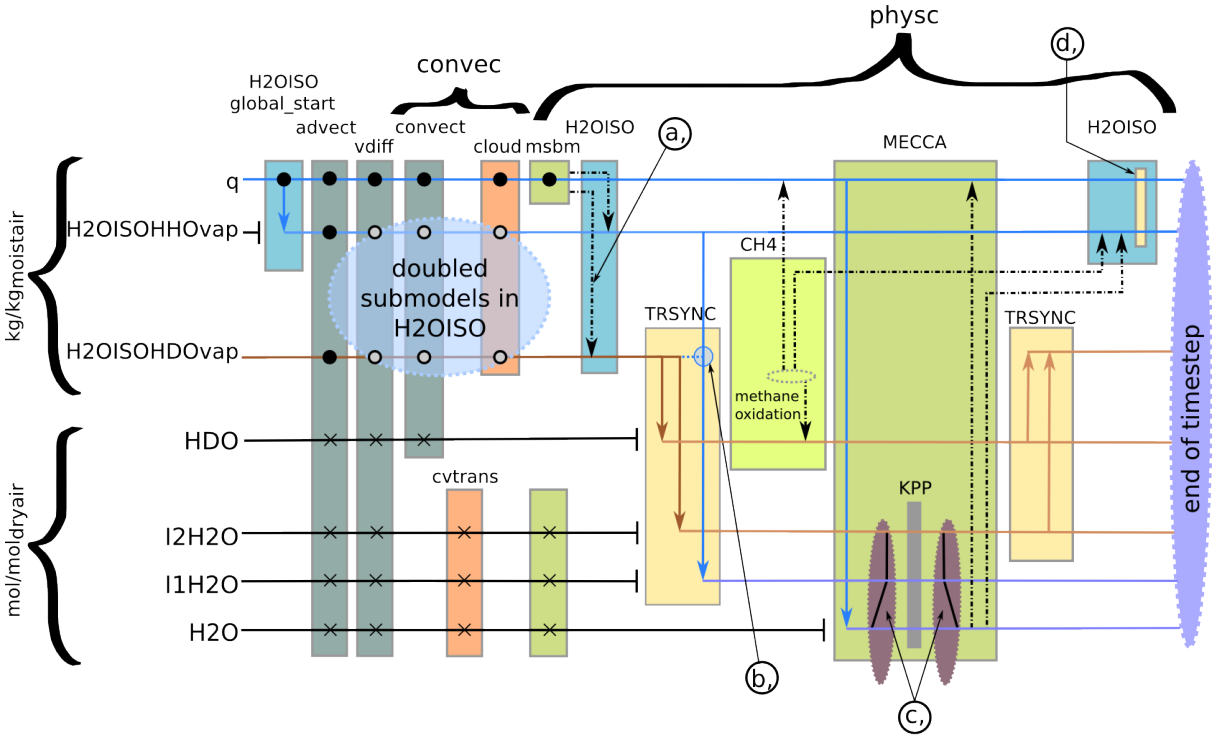

Figure S6. Sketch depicting the coupling of the hydrological cycle tracers in EMAC. q is the intrinsic variable of ECHAM5 for specific humidity. Similar, `H2OISOHHOvap` and `H2OISOHDOvap` are defined by H2OISO. q, `H2OISOHHOvap` and `H2OISOHDOvap` are in units kg of the tracer per kg of moist air (kg $kg^{-1}_{\text{moist air}}$). `HDO` is defined by CH4, `H2O` is defined by MECCA, and `I1H2O` and `I2H2O` are defined by MECCA-TAG in mol $mol^{-1}_{\text{dry air}}$. Arrows with dashed lines indicate that solely tendencies are added. Solid arrow lines correspond to a replacement of the contents. (a) relative tendency of MSBM of HHO tracer without fractionation, (b) sets `I1H2O` to the mol $mol^{-1}_{\text{dry air}}$ equivalent of `H2OISOHHOvap` - 2·`H2OISOHDOvap`, (c) adjusts `I1H2O` and `I2H2O` so that `I1H2O` + `I2H2O` = `H2O`, (d) numerical adjustment to ensure that the tendency of `H2OISOHHOvap` is equal to the tendency of q.

After the chemical processes, TRSYNC synchronizes the tracers `HDO` or `I2H2O` backward onto `H2OISOHDOvap`, and H2OISO also adds the chemical tendency of q to `H2OISOHHOvap`. As a last step H2OISO adjusts the tendency of `H2OISOHHOvap` so that it is conform to the tendency of q.

The following section documents the subroutines, which are part of the TRSYNC submodel and in the section "User interface" the entries of the corresponding namelist are explained.

4.2 MODULE messy_trsync_si: Subroutines in SMIL

These subroutines follow the general structure mandatory for MESSy submodels.

- `SUBROUTINE trsync_initialize`: Initializes the submodel, reads the coupling namelist and broadcasts necessary information to all parallel tasks.
- `SUBROUTINE trsync_init_memory`: Registers the tracers for the TENDENCY submodel, if the latter is applied.
- `SUBROUTINE trsync_init_coupling`: Sets pointers to the used tracers and checks whether the synchronized tracers are identical in terms of their molar mass.
- `SUBROUTINE trsync_init_tracer`: Initializes the tracers, hence checks whether the tracers are already initialized and accounts for a synchronized initial state.
- `SUBROUTINE trsync_physc`: This subroutine is called two times. The first time before the kinetic integrations of CH4 and MECCA and the second time after. It provides the necessary unit conversion and numerical adjustment to synchronize the chosen tracers.
- `SUBROUTINE trsync_free_memory`: Currently not necessary.

4.3 MODULE messy_trsync: Subroutines in SMCL

The following subroutines represent the core layer of the submodel.

SUBROUTINE convert_unit			(traten, case, type, molarmass, spechum, spechum_te, tracer)
name	type	intent	description
mandatory arguments:			
traten	REAL	INOUT	tracer or tendency to be converted
case	INTEGER	IN	case of conversion (1: kg/kg⇒mol/mol or 2: mol/mol⇒kg/kg)
type	INTEGER	IN	type of conversion (1: tracer or 2: tendency)
molarmass	REAL	IN	molar mass of the converted tracer
spechum	REAL	IN	specific humidity
optional arguments:			
spechum_te	REAL	IN	tendency of specific humidity
tracer	REAL	IN	additional tracer mixing ratio if traten indicates the tendency

description:

This subroutine calls the private subroutines convert_to_molmol, convert_to_kgkg, convert_to_molmol_te and convert_to_kgkg_te, depending on the chosen case and type.

4.4 Private subroutines

Private subroutines in `messy_trsync_si`

`SUBROUTINE trsync_read_nml_cpl`		`(status, iou)`	
name	type	intent	description
mandatory arguments:			
`status`	`INTEGER`	OUT	error status info
`iou`	`INTEGER`	IN	I/O unit

description:

This subroutine is used to read the CPL-namelist of the submodel.

Private subroutines in `messy_trsync`

`SUBROUTINE convert_to_kgkg`		`(tr_a, molarmass, spechum)`	
name	type	intent	description
mandatory arguments:			
`tr_a`	`REAL`	INOUT	tracer in mol $\text{mol}^{-1}_{\text{dry air}}$ to be converted
`molarmass`	`REAL`	IN	molar mass of the converted tracer
`spechum`	`REAL`	IN	specific humidity

description:

This subroutine converts the tracer `tr_a` from mol $\text{mol}^{-1}_{\text{dry air}}$ to kg $\text{kg}^{-1}_{\text{moist air}}$.

`SUBROUTINE convert_to_molmol`		`(tr_b, molarmass, spechum)`	
name	type	intent	description
mandatory arguments:			
`tr_b`	`REAL`	INOUT	tracer in kg $\text{kg}^{-1}_{\text{moist air}}$ to be converted
`molarmass`	`REAL`	IN	molar mass of the converted tracer
`spechum`	`REAL`	IN	specific humidity

description:

This subroutine converts the tracer `tr_b` from kg $\text{kg}^{-1}_{\text{moist air}}$ to mol $\text{mol}^{-1}_{\text{dry air}}$.

SUBROUTINE convert_kgkg_te			(tr_a_te, tr_a, molarmass, spechum, spechum_te)
name	type	intent	description
mandatory arguments:			
tr_a_te	REAL	INOUT	tendency in mol $\mathrm{mol}^{-1}_{\text{dry air}}$ s^{-1} to be converted
tr_a	REAL	IN	corresponding tracer of tendency to be converted
molarmass	REAL	IN	molar mass of the converted tracer
spechum	REAL	IN	specific humidity
spechum_te	REAL	IN	tendency of specific humidity
description:			
This subroutine converts the tendency tr_a_te from mol $\mathrm{mol}^{-1}_{\text{dry air}}$ s^{-1} to kg $\mathrm{kg}^{-1}_{\text{moist air}}$ s^{-1}.			

SUBROUTINE convert_molmol_te			(tr_b_te, tr_b, molarmass, spechum, spechum_te)
name	type	intent	description
mandatory arguments:			
tr_b_te	REAL	INOUT	tendency in kg $\mathrm{kg}^{-1}_{\text{moist air}}$ s^{-1} to be converted
tr_b	REAL	IN	corresponding tracer of tendency to be converted
molarmass	REAL	IN	molar mass of the converted tracer
spechum	REAL	IN	specific humidity
spechum_te	REAL	IN	tendency of specific humidity
description:			
This subroutine converts the tendency tr_b_te from kg $\mathrm{kg}^{-1}_{\text{moist air}}$ s^{-1} to mol $\mathrm{mol}^{-1}_{\text{dry air}}$ s^{-1}.			

4.5 User interface

4.5.1 TRSYNC CPL namelist

The coupling (`CPL`) namelist of the TRSYNC submodel lists the tracers to be synchronized.

`TRSYNC` takes two strings and one integer switch. The first string indicates the chemical tracer in mol $\mathrm{mol}^{-1}{}_{\mathrm{dry\ air}}$. The second string indicates the physical tracer in kg $\mathrm{kg}^{-1}_{\mathrm{moist\ air}}$. The integer string denotes, whether the synchronization is done in both ways (`0`), the chemical tracer is synchronized by the physical tracer before chemistry only (`1`), or the physical tracer is synchronized by the chemical tracer after chemistry (`2`).

4.6 Example namelist

Namelist 2. Control (CTRL) and coupling (CPL) namelists of submodel TRSYNC stored in trsync.nml

```
&CTRL
/
!
&CPL
!! ### List of tracer which should be synchronized by TRSYNC
!! ###
!! ### TRSYNC : synchronization of HDO tracer
!! ### TRSYNC(1) = 'TR_A','TR_B',i
!! ### with:
!! ###       TR_A in mol/mol_dryair
!! ###       TR_B in kg/kg_moistair
!! ###
!! ### i = 0: both ways (default)
!! ###     1: chemical tracer is synchronized with physical tracer only
!! ###     2: physical tracer is synchronized with chemical tracer only
!! ###
!! ### trsync_physc(1) will synchronize TR_A with TR_B (=> TR_A will be overwritten)
!! ### trsync_physc(2) will synchronize TR_B with TR_A (=> TR_B will be overwritten)
!! ###
TRSYNC(1) = 'HDO', 'H2OISOHDOvap',
!! ### TRSYNC(1) = 'I2H2O', 'H2OISOHDOvap', 0,
!! ### Future:
!! ### TRSYNC(2) = '','H2OISOHH18Ovap', 0,
!! ### TRSYNC(3) = '','H2OISOHH17Ovap', 0,
/
```

5 Example namelist entries for other submodels corresponding to CH4 set-up

The following snippets show namelist entries of other submodels for a MESSy set-up with the CH4 submodel.

5.1 TRACER

Namelist 3. Part of tracer.nml to import initial values of CH_4 tracer.

```
! Import from first spin-up
&regrid
infile    = "~/EMAC-x-02_____0013_restart_0005_tracer_gp.nc",  ! 2010-12-31 23:48 ...
i_latm    = "lat",          ! name of latitude axis in input file
i_latr    = -90.0,90.0,     ! range of latitude axis in input file
i_lonm    = "lon",          ! name of longitude axis in input file
i_lonr    = 0.0,360.0,      ! range of longitude axis in input file
! No time coordinate in restart files
!i_timem   = "time",         ! name of time axis in input file
i_hyam    = "hyam",     ! name of hybrid A coefficients in input file
i_hybm    = "hybm",     ! name of hybrid B coefficients in input file
i_ps      = "101325.0 Pa",
i_p0      = "1. Pa",        ! value of reference pressure in input file
pressure  = F,
! Use ALL tracers in init file
!var       =  "CH4_fx;CH4_12C;CH4_13C;CH4_D0;CH4_D1", ! CH4 tracers
! No time coordinate in restart files
!i_t       = 25,
/
```

5.2 DDEP

Namelist 4. Configuration of ddep.nml to simulate soil-loss of CH_4.

```
!## SYNTAX:
!## import_predepvel(.) = 'channel', 'object', 'tracer-name', diag. flux calc.?
!## Note: channel object is deposition flux aand must be in [molec/m^2/s]
!
!
import_predepvel(1) = 'import_grid', 'DVMETH_oxid', 'CH4_fx', T,
import_predepvel(2) = 'import_grid', 'DVMETH_oxid', 'CH4_D0', T,
import_predepvel(3) = 'import_grid', 'DVMETH_CH3D_oxid', 'CH4_D1', T,
import_predepvel(4) = 'import_grid', 'DVMETH_13CH4_oxid', 'CH4_13C', T,
import_predepvel(5) = 'import_grid', 'DVMETH_oxid', 'CH4_12C', T,
!
```

5.3 IMPORT

Namelist 5. Entries of import.nml, which import the educts (OH, Cl and O(^{1}D)) from an earlier simulation and the CH_4 emission inventory for each emission class.

```
! ************************************************************************
! CH4
! ************************************************************************
!
! PRESCRIBED EDUCTS (CH + ...): OH, O1D, Cl for methane oxidation
! QCTM data starts at Dec 1978 and ends at Nov 2014
RG_TRIG(3)  = 1,'months', 'first',0, 'CH4OX',  422,1,432,134,
        'NML=./import/MISC/QCTM/ESCiMo_DLR1.0_RC1SD-base-10_4QCTM_misc_197901-201412.nml;',
!
! ************************************************************************
! OFFEMIS
! ************************************************************************
!
! CH4_fx emissions
!
! biomass burning
RG_TRIG(20)  = 1,  'months', 'first',0, 'BB_AUS',        265,1,276,1,
        'NML=./import/offemis/CH4/EMPA/EMPA_DLR1.1_PostE_bb+AUS_CH4_199001-201212.nml; VAR=CH4;',
RG_TRIG(21)  = 1,  'months', 'first',0, 'BB_CHINA',      265,1,276,1,
        'NML=./import/offemis/CH4/EMPA/EMPA_DLR1.1_PostE_bb+CHINA_CH4_199001-201212.nml; VAR=CH4;',
RG_TRIG(22)  = 1,  'months', 'first',0, 'BB_EU',         265,1,276,1,
        'NML=./import/offemis/CH4/EMPA/EMPA_DLR1.1_PostE_bb+EU_CH4_199001-201212.nml; VAR=CH4;',
RG_TRIG(23)  = 1,  'months', 'first',0, 'BB_INDIA',      265,1,276,1,
        'NML=./import/offemis/CH4/EMPA/EMPA_DLR1.1_PostE_bb+INDIA_CH4_199001-201212.nml; VAR=CH4;',
RG_TRIG(24)  = 1,  'months', 'first',0, 'BB_NA_bor',     265,1,276,1,
        'NML=./import/offemis/CH4/EMPA/EMPA_DLR1.1_PostE_bb+NAbor_CH4_199001-201212.nml; VAR=CH4;',
RG_TRIG(25)  = 1,  'months', 'first',0, 'BB_N_AFR',      265,1,276,1,
        'NML=./import/offemis/CH4/EMPA/EMPA_DLR1.1_PostE_bb+NAFR_CH4_199001-201212.nml; VAR=CH4;',
RG_TRIG(26)  = 1,  'months', 'first',0, 'BB_NA_temp',    265,1,276,1,
        'NML=./import/offemis/CH4/EMPA/EMPA_DLR1.1_PostE_bb+NAtemp_CH4_199001-201212.nml; VAR=CH4;',
RG_TRIG(27)  = 1,  'months', 'first',0, 'BB_N_MIDEAST',  265,1,276,1,
        'NML=./import/offemis/CH4/EMPA/EMPA_DLR1.1_PostE_bb+NMIDEAST_CH4_199001-201212.nml; VAR=CH4;',
RG_TRIG(28)  = 1,  'months', 'first',0, 'BB_RUS',        265,1,276,1,
        'NML=./import/offemis/CH4/EMPA/EMPA_DLR1.1_PostE_bb+RUS_CH4_199001-201212.nml; VAR=CH4;',
RG_TRIG(29)  = 1,  'months', 'first',0, 'BB_S_AFR',      265,1,276,1,
        'NML=./import/offemis/CH4/EMPA/EMPA_DLR1.1_PostE_bb+SAFR_CH4_199001-201212.nml; VAR=CH4;',
RG_TRIG(30)  = 1,  'months', 'first',0, 'BB_SA_temp',    265,1,276,1,
        'NML=./import/offemis/CH4/EMPA/EMPA_DLR1.1_PostE_bb+SAtemp_CH4_199001-201212.nml; VAR=CH4;',
RG_TRIG(31)  = 1,  'months', 'first',0, 'BB_SA_trop',    265,1,276,1,
        'NML=./import/offemis/CH4/EMPA/EMPA_DLR1.1_PostE_bb+SAtrop_CH4_199001-201212.nml; VAR=CH4;',
```

```
RG_TRIG(32)  = 1,  'months', 'first',0, 'BB_SE_ASIA',    265,1,276,1,
        'NML=./import/offemis/CH4/EMPA/EMPA_DLR1.1_PostE_bb+SEASIA_CH4_199001-201212.nml; VAR=CH4;',
!
! anthropogenic
!
RG_TRIG(140) = 1,  'months',  'first',0, 'Mfx_an_AFRICA',  265,1,276,1,
        'NML=./import/offemis/CH4/EMPA/EMPA_DLR1.1_PostE_anth+AFRICA_CH4_199001-201212.nml; VAR=CH4;',
RG_TRIG(141) = 1,  'months',  'first',0, 'Mfx_an_AUS',     265,1,276,1,
        'NML=./import/offemis/CH4/EMPA/EMPA_DLR1.1_PostE_anth+AUS_CH4_199001-201212.nml; VAR=CH4;',
RG_TRIG(142) = 1,  'months',  'first',0, 'Mfx_an_CHINA',   265,1,276,1,
        'NML=./import/offemis/CH4/EMPA/EMPA_DLR1.1_PostE_anth+CHINA_CH4_199001-201212.nml; VAR=CH4;',
RG_TRIG(143) = 1,  'months',  'first',0, 'Mfx_an_EU',      265,1,276,1,
        'NML=./import/offemis/CH4/EMPA/EMPA_DLR1.1_PostE_anth+EU_CH4_199001-201212.nml; VAR=CH4;',
RG_TRIG(144) = 1,  'months',  'first',0, 'Mfx_an_INDIA',   265,1,276,1,
        'NML=./import/offemis/CH4/EMPA/EMPA_DLR1.1_PostE_anth+INDIA_CH4_199001-201212.nml; VAR=CH4;',
RG_TRIG(145) = 1,  'months',  'first',0, 'Mfx_an_MIDEAST', 265,1,276,1,
        'NML=./import/offemis/CH4/EMPA/EMPA_DLR1.1_PostE_anth+MIDEAST_CH4_199001-201212.nml; VAR=CH4;',
RG_TRIG(146) = 1,  'months',  'first',0, 'Mfx_an_NA',      265,1,276,1,
        'NML=./import/offemis/CH4/EMPA/EMPA_DLR1.1_PostE_anth+NA_CH4_199001-201212.nml; VAR=CH4;',
RG_TRIG(147) = 1,  'months',  'first',0, 'Mfx_an_OCEAN',   265,1,276,1,
        'NML=./import/offemis/CH4/EMPA/EMPA_DLR1.1_PostE_ship_CH4_199001-201212.nml; VAR=CH4;',
RG_TRIG(148) = 1,  'months',  'first',0, 'Mfx_an_RUS',     265,1,276,1,
        'NML=./import/offemis/CH4/EMPA/EMPA_DLR1.1_PostE_anth+RUS_CH4_199001-201212.nml; VAR=CH4;',
RG_TRIG(149) = 1,  'months',  'first',0, 'Mfx_an_SA',      265,1,276,1,
        'NML=./import/offemis/CH4/EMPA/EMPA_DLR1.1_PostE_anth+SA_CH4_199001-201212.nml; VAR=CH4;',
RG_TRIG(150) = 1,  'months',  'first',0, 'Mfx_an_SE_ASIA', 265,1,276,1,
        'NML=./import/offemis/CH4/EMPA/EMPA_DLR1.1_PostE_anth+SEASIA_CH4_199001-201212.nml; VAR=CH4;',
!
! ocean
!
RG_TRIG(151) = 1,  'months',  'first',0, 'Mfx_oc',         265,1,276,1,
        'NML=./import/offemis/CH4/EMPA/EMPA_DLR1.1_PostE_ocean_CH4_199001-201212.nml; VAR=CH4;',
!
! rice
!
RG_TRIG(152) = 1,  'months', 'first',0, 'Mfx_ri_AFR',      265,1,276,1,
        'NML=./import/offemis/CH4/EMPA/EMPA_DLR1.1_PostE_rice+AFR_CH4_199001-201212.nml; VAR=CH4;',
RG_TRIG(153) = 1,  'months', 'first',0, 'Mfx_ri_ASIA_AUS', 265,1,276,1,
        'NML=./import/offemis/CH4/EMPA/EMPA_DLR1.1_PostE_rice+ASIA+AUS_CH4_199001-201212.nml; VAR=CH4;',
RG_TRIG(154) = 1,  'months', 'first',0, 'Mfx_ri_CHINA',    265,1,276,1,
        'NML=./import/offemis/CH4/EMPA/EMPA_DLR1.1_PostE_rice+CHINA_CH4_199001-201212.nml; VAR=CH4;',
RG_TRIG(155) = 1,  'months', 'first',0, 'Mfx_ri_EU',       265,1,276,1,
        'NML=./import/offemis/CH4/EMPA/EMPA_DLR1.1_PostE_rice+EU_CH4_199001-201212.nml; VAR=CH4;',
RG_TRIG(156) = 1,  'months', 'first',0, 'Mfx_ri_INDIA',    265,1,276,1,
```

```
        'NML=./import/offemis/CH4/EMPA/EMPA_DLR1.1_PostE_rice+INDIA_CH4_199001-201212.nml; VAR=CH4;',
RG_TRIG(157) = 1,  'months', 'first',0, 'Mfx_ri_NA',       265,1,276,1,
        'NML=./import/offemis/CH4/EMPA/EMPA_DLR1.1_PostE_rice+NA_CH4_199001-201212.nml; VAR=CH4;',
RG_TRIG(158) = 1,  'months', 'first',0, 'Mfx_ri_SA',       265,1,276,1,
        'NML=./import/offemis/CH4/EMPA/EMPA_DLR1.1_PostE_rice+SA_CH4_199001-201212.nml; VAR=CH4;',
!
! termites
!
RG_TRIG(159) = 1,  'months',  'first',0, 'Mfx_te',         265,1,276,1,
        'NML=./import/offemis/CH4/EMPA/EMPA_DLR1.1_PostE_biotermites_CH4_199001-201212.nml; VAR=CH4;',
!
! volcanoes
!
RG_TRIG(160) = 1,  'months',  'first',0, 'Mfx_vo',         265,1,276,1,
        'NML=./import/offemis/CH4/EMPA/EMPA_DLR1.1_PostE_volc_CH4_199001-201212.nml; VAR=CH4;',
!
! wetlands
!
RG_TRIG(161) = 1,  'months', 'first',0, 'Mfx_wl_AUS',     265,1,276,1,
        'NML=./import/offemis/CH4/EMPA/EMPA_DLR1.1_PostE_biowetlands+AUS_CH4_199001-201212.nml; VAR=CH4;',
RG_TRIG(162) = 1,  'months', 'first',0, 'Mfx_wl_CHINA',   265,1,276,1,
        'NML=./import/offemis/CH4/EMPA/EMPA_DLR1.1_PostE_biowetlands+CHINA_CH4_199001-201212.nml; VAR=CH4;',
RG_TRIG(163) = 1,  'months', 'first',0, 'Mfx_wl_EU',      265,1,276,1,
        'NML=./import/offemis/CH4/EMPA/EMPA_DLR1.1_PostE_biowetlands+EU_CH4_199001-201212.nml; VAR=CH4;',
RG_TRIG(164) = 1,  'months', 'first',0, 'Mfx_wl_india',   265,1,276,1,
        'NML=./import/offemis/CH4/EMPA/EMPA_DLR1.1_PostE_biowetlands+INDIA_CH4_199001-201212.nml; VAR=CH4;',
RG_TRIG(165) = 1,  'months', 'first',0, 'Mfx_wl_MIDEAST', 265,1,276,1,
        'NML=./import/offemis/CH4/EMPA/EMPA_DLR1.1_PostE_biowetlands+MIDEAST_CH4_199001-201212.nml; VAR=CH4;',
RG_TRIG(166) = 1,  'months', 'first',0, 'Mfx_wl_NA_bor',  265,1,276,1,
        'NML=./import/offemis/CH4/EMPA/EMPA_DLR1.1_PostE_biowetlands+NAbor_CH4_199001-201212.nml; VAR=CH4;',
RG_TRIG(167) = 1,  'months', 'first',0, 'Mfx_wl_N_AFR',   265,1,276,1,
        'NML=./import/offemis/CH4/EMPA/EMPA_DLR1.1_PostE_biowetlands+NAFR_CH4_199001-201212.nml; VAR=CH4;',
RG_TRIG(168) = 1,  'months', 'first',0, 'Mfx_wl_NA_TEMP', 265,1,276,1,
        'NML=./import/offemis/CH4/EMPA/EMPA_DLR1.1_PostE_biowetlands+NAtemp_CH4_199001-201212.nml; VAR=CH4;',
RG_TRIG(169) = 1,  'months', 'first',0, 'Mfx_wl_RUS',     265,1,276,1,
        'NML=./import/offemis/CH4/EMPA/EMPA_DLR1.1_PostE_biowetlands+RUS_CH4_199001-201212.nml; VAR=CH4;',
RG_TRIG(170) = 1,  'months', 'first',0, 'Mfx_wl_S_AFR',   265,1,276,1,
        'NML=./import/offemis/CH4/EMPA/EMPA_DLR1.1_PostE_biowetlands+SAFR_CH4_199001-201212.nml; VAR=CH4;',
RG_TRIG(171) = 1,  'months', 'first',0, 'Mfx_wl_SA_temp', 265,1,276,1,
        'NML=./import/offemis/CH4/EMPA/EMPA_DLR1.1_PostE_biowetlands+SAtemp_CH4_199001-201212.nml; VAR=CH4;',
RG_TRIG(172) = 1,  'months', 'first',0, 'Mfx_wl_SA_TROP', 265,1,276,1,
        'NML=./import/offemis/CH4/EMPA/EMPA_DLR1.1_PostE_biowetlands+SAtrop_CH4_199001-201212.nml; VAR=CH4;',
RG_TRIG(173) = 1,  'months', 'first',0, 'Mfx_wl_se_asia', 265,1,276,1,
        'NML=./import/offemis/CH4/EMPA/EMPA_DLR1.1_PostE_biowetlands+SEASIA_CH4_199001-201212.nml; VAR=CH4;',
```

```
!
! wild animals
!
RG_TRIG(174) = 1,   'months',  'first',0, 'Mfx_wa',         265,1,276,1,
       'NML=./import/offemis/CH4/EMPA/EMPA_DLR1.1_PostE_wildlife_CH4_199001-201212.nml; VAR=CH4;',
!
```

5.4 OFFEMIS

Namelist 6. Example of the offemis.nml, which couples the imported emissions to the master CH_4 tracer `CH4_fx`, to the isotopologues, scaled according to the emission signature, and to the corresponding emission class tracers.

```
! ### SYNTAX:
!     (SPECIFIERS MUST BE UPPERCASE !)
! ###         GP=    Gridpoint  Emission Method (0,1,2) (SURFACE ONLY)
!                    0: no emission; only channel object (DEFAULT)
!                    1: 2D (SURFACE EM.) -> lowest layer
!                       3D (VOLUME  EM.) -> emission ON
!                       Nx2D (MULTI LEVEL EM.) -> internally converted to 3D
!                    SURFACE EMISSIONS ONLY:
!                    2: lower boundary condition for flux
!
! ###         LG=    Lagrangian Emission Method (0,1,2,3,4)
!                    0: no emission; only channel object (DEFAULT)
!                    1: 2D (SURFACE EM.)       -> into CELLs in lowest layer
!                       3D (VOLUME  EM.)       -> emission ON
!                       Nx2D (MULTI LEVEL EM.) -> internally converted to 3D
!                    SURFACE EMISSIONS ONLY:
!                    2: into lowest CELLs within boundary layer
!                    3: into all CELLs in boundary layer (vertical gradient)
!                    4: into all CELLs in boundary layer (no vertical gradient)
!
!NOTEs:  (1) Surface emission fluxes (2D) must be in  molecules m-2 s-1.
!        (2) Volume emissions (3D)        must be in  molecules m-3 s-1.
!        (3) Multi level emissions (Nx2D) must be in  molecules m-2 s-1.
!        (4) For volume emissions (3D), the corresponding channel object
!            must be in the GP_3D_MID representation
!        (5) The trigger for multi level emissions (Nx2D) is the presence
!            of the channel object attribute heights
!
! EMISSION: 'TRACER[_SUBNAME][,scaling];...', CHANNEL NAME, CHANNEL OBJECT,
!           EMISSION METHOD
!
! LOWER BOUNDARY CONDITIONS (SEE tnudge.nml)
```

```
!
! ########################################
! DIRECT EMISSIONS
! ########################################
!
EMIS_IN(190) = 'CH4_fx;CH4_12C,0.9894892;CH4_13C,0.0105108;CH4_D0,0.9995110;CH4_D1,0.0004890;CH4_fx_e01_a01',
                                                          'import_grid', 'Mfx_an_AFRICA_CH4', 'GP=2', ! anth.
EMIS_IN(191) = 'CH4_fx;CH4_12C,0.9894892;CH4_13C,0.0105108;CH4_D0,0.9995110;CH4_D1,0.0004890;CH4_fx_e02_a01',
                                                          'import_grid', 'Mfx_an_AUS_CH4', 'GP=2', ! anth.
EMIS_IN(192) = 'CH4_fx;CH4_12C,0.9894892;CH4_13C,0.0105108;CH4_D0,0.9995110;CH4_D1,0.0004890;CH4_fx_e03_a01',
                                                          'import_grid', 'Mfx_an_CHINA_CH4', 'GP=2', ! anth.
EMIS_IN(193) = 'CH4_fx;CH4_12C,0.9894892;CH4_13C,0.0105108;CH4_D0,0.9995110;CH4_D1,0.0004890;CH4_fx_e04_a01',
                                                          'import_grid', 'Mfx_an_EU_CH4', 'GP=2', ! anth.
EMIS_IN(194) = 'CH4_fx;CH4_12C,0.9894892;CH4_13C,0.0105108;CH4_D0,0.9995110;CH4_D1,0.0004890;CH4_fx_e05_a01',
                                                          'import_grid', 'Mfx_an_INDIA_CH4', 'GP=2', ! anth.
EMIS_IN(195) = 'CH4_fx;CH4_12C,0.9894892;CH4_13C,0.0105108;CH4_D0,0.9995110;CH4_D1,0.0004890;CH4_fx_e06_a01',
                                                          'import_grid', 'Mfx_an_MIDEAST_CH4', 'GP=2', ! anth.
EMIS_IN(196) = 'CH4_fx;CH4_12C,0.9894892;CH4_13C,0.0105108;CH4_D0,0.9995110;CH4_D1,0.0004890;CH4_fx_e07_a01',
                                                          'import_grid', 'Mfx_an_NA_CH4', 'GP=2', ! anth.
EMIS_IN(197) = 'CH4_fx;CH4_12C,0.9894892;CH4_13C,0.0105108;CH4_D0,0.9995110;CH4_D1,0.0004890;CH4_fx_e08_a01',
                                                          'import_grid', 'Mfx_an_OCEAN_CH4', 'GP=2', ! anth.
EMIS_IN(198) = 'CH4_fx;CH4_12C,0.9894892;CH4_13C,0.0105108;CH4_D0,0.9995110;CH4_D1,0.0004890;CH4_fx_e09_a01',
                                                          'import_grid', 'Mfx_an_RUS_CH4', 'GP=2', ! anth.
EMIS_IN(199) = 'CH4_fx;CH4_12C,0.9894892;CH4_13C,0.0105108;CH4_D0,0.9995110;CH4_D1,0.0004890;CH4_fx_e10_a01',
                                                          'import_grid', 'Mfx_an_SA_CH4', 'GP=2', ! anth.
EMIS_IN(200) = 'CH4_fx;CH4_12C,0.9894892;CH4_13C,0.0105108;CH4_D0,0.9995110;CH4_D1,0.0004890;CH4_fx_e11_a01',
                                                          'import_grid', 'Mfx_an_SE_ASIA_CH4', 'GP=2', ! anth.
!
! biomass burning
!
EMIS_IN(201) = 'CH4_fx;CH4_12C,0.9892048;CH4_13C,0.0107952;CH4_D0,0.9995097;CH4_D1,0.0004903;CH4_fx_e12_a01',
                                                          'import_grid', 'BB_AUS_CH4',     'GP=2', ! bb
EMIS_IN(202) = 'CH4_fx;CH4_12C,0.9892048;CH4_13C,0.0107952;CH4_D0,0.9995097;CH4_D1,0.0004903;CH4_fx_e13_a01',
                                                          'import_grid', 'BB_CHINA_CH4',     'GP=2', ! bb
EMIS_IN(203) = 'CH4_fx;CH4_12C,0.9892048;CH4_13C,0.0107952;CH4_D0,0.9995097;CH4_D1,0.0004903;CH4_fx_e14_a01',
                                                          'import_grid', 'BB_EU_CH4',     'GP=2', ! bb
EMIS_IN(204) = 'CH4_fx;CH4_12C,0.9892048;CH4_13C,0.0107952;CH4_D0,0.9995097;CH4_D1,0.0004903;CH4_fx_e15_a01',
                                                          'import_grid', 'BB_INDIA_CH4',     'GP=2', ! bb
EMIS_IN(205) = 'CH4_fx;CH4_12C,0.9892048;CH4_13C,0.0107952;CH4_D0,0.9995097;CH4_D1,0.0004903;CH4_fx_e16_a01',
                                                          'import_grid', 'BB_NA_bor_CH4',     'GP=2', ! bb
EMIS_IN(206) = 'CH4_fx;CH4_12C,0.9892048;CH4_13C,0.0107952;CH4_D0,0.9995097;CH4_D1,0.0004903;CH4_fx_e17_a01',
                                                          'import_grid', 'BB_N_AFR_CH4',     'GP=2', ! bb
EMIS_IN(207) = 'CH4_fx;CH4_12C,0.9892048;CH4_13C,0.0107952;CH4_D0,0.9995097;CH4_D1,0.0004903;CH4_fx_e18_a01',
                                                          'import_grid', 'BB_NA_temp_CH4',     'GP=2', ! bb
```

```
EMIS_IN(208) = 'CH4_fx;CH4_12C,0.9892048;CH4_13C,0.0107952;CH4_D0,0.9995097;CH4_D1,0.0004903;CH4_fx_e19_a01',
                                                          'import_grid', 'BB_N_MIDEAST_CH4',     'GP=2', ! bb
EMIS_IN(209) = 'CH4_fx;CH4_12C,0.9892048;CH4_13C,0.0107952;CH4_D0,0.9995097;CH4_D1,0.0004903;CH4_fx_e20_a01',
                                                          'import_grid', 'BB_RUS_CH4',     'GP=2', ! bb
EMIS_IN(210) = 'CH4_fx;CH4_12C,0.9892048;CH4_13C,0.0107952;CH4_D0,0.9995097;CH4_D1,0.0004903;CH4_fx_e21_a01',
                                                          'import_grid', 'BB_S_AFR_CH4',     'GP=2', ! bb
EMIS_IN(211) = 'CH4_fx;CH4_12C,0.9892048;CH4_13C,0.0107952;CH4_D0,0.9995097;CH4_D1,0.0004903;CH4_fx_e22_a01',
                                                          'import_grid', 'BB_SA_temp_CH4',     'GP=2', ! bb
EMIS_IN(212) = 'CH4_fx;CH4_12C,0.9892048;CH4_13C,0.0107952;CH4_D0,0.9995097;CH4_D1,0.0004903;CH4_fx_e23_a01',
                                                          'import_grid', 'BB_SA_trop_CH4',     'GP=2', ! bb
EMIS_IN(213) = 'CH4_fx;CH4_12C,0.9892048;CH4_13C,0.0107952;CH4_D0,0.9995097;CH4_D1,0.0004903;CH4_fx_e24_a01',
                                                          'import_grid', 'BB_SE_ASIA_CH4',     'GP=2', ! bb
!
! ocean
!
EMIS_IN(214) = 'CH4_fx;CH4_12C,0.9895891;CH4_13C,0.0104109;CH4_D0,0.9995141;CH4_D1,0.0004859;CH4_fx_e25_a01',
                                                          'import_grid', 'Mfx_oc_CH4', 'GP=2', ! ocean
!
! rice
!
EMIS_IN(215) = 'CH4_fx;CH4_12C,0.9896329;CH4_13C,0.0103671;CH4_D0,0.9995791;CH4_D1,0.0004209;CH4_fx_e26_a01',
                                                          'import_grid', 'Mfx_ri_AFR_CH4', 'GP=2', ! rice
EMIS_IN(216) = 'CH4_fx;CH4_12C,0.9896329;CH4_13C,0.0103671;CH4_D0,0.9995791;CH4_D1,0.0004209;CH4_fx_e27_a01',
                                                          'import_grid', 'Mfx_ri_ASIA_AUS_CH4', 'GP=2', ! rice
EMIS_IN(217) = 'CH4_fx;CH4_12C,0.9896329;CH4_13C,0.0103671;CH4_D0,0.9995791;CH4_D1,0.0004209;CH4_fx_e28_a01',
                                                          'import_grid', 'Mfx_ri_CHINA_CH4', 'GP=2', ! rice
EMIS_IN(218) = 'CH4_fx;CH4_12C,0.9896329;CH4_13C,0.0103671;CH4_D0,0.9995791;CH4_D1,0.0004209;CH4_fx_e29_a01',
                                                          'import_grid', 'Mfx_ri_EU_CH4', 'GP=2', ! rice
EMIS_IN(219) = 'CH4_fx;CH4_12C,0.9896329;CH4_13C,0.0103671;CH4_D0,0.9995791;CH4_D1,0.0004209;CH4_fx_e30_a01',
                                                          'import_grid', 'Mfx_ri_INDIA_CH4', 'GP=2', ! rice
EMIS_IN(220) = 'CH4_fx;CH4_12C,0.9896329;CH4_13C,0.0103671;CH4_D0,0.9995791;CH4_D1,0.0004209;CH4_fx_e31_a01',
                                                          'import_grid', 'Mfx_ri_NA_CH4', 'GP=2', ! rice
EMIS_IN(221) = 'CH4_fx;CH4_12C,0.9896329;CH4_13C,0.0103671;CH4_D0,0.9995791;CH4_D1,0.0004209;CH4_fx_e32_a01',
                                                          'import_grid', 'Mfx_ri_SA_CH4', 'GP=2', ! rice
!
! termites
!
EMIS_IN(222) = 'CH4_fx;CH4_12C,0.9896366;CH4_13C,0.0103634;CH4_D0,0.9996200;CH4_D1,0.0003800;CH4_fx_e33_a01',
                                                          'import_grid', 'Mfx_te_CH4', 'GP=2', ! termites
!
! volcanoes
!
EMIS_IN(223) = 'CH4_fx;CH4_12C,0.9893910;CH4_13C,0.0106090;CH4_D0,0.9995349;CH4_D1,0.0004651;CH4_fx_e34_a01',
                                                          'import_grid', 'Mfx_vo_CH4', 'GP=2', ! volcanoes
```

```
!
! wetlands
!
EMIS_IN(224) = 'CH4_fx;CH4_12C,0.9895934;CH4_13C,0.0104066;CH4_D0,0.9995865;CH4_D1,0.0004135;CH4_fx_e35_a01',
                                                          'import_grid', 'Mfx_wl_AUS_CH4', 'GP=2', ! wetlands
EMIS_IN(225) = 'CH4_fx;CH4_12C,0.9895934;CH4_13C,0.0104066;CH4_D0,0.9995865;CH4_D1,0.0004135;CH4_fx_e36_a01',
                                                          'import_grid', 'Mfx_wl_CHINA_CH4', 'GP=2', ! wetlands
EMIS_IN(226) = 'CH4_fx;CH4_12C,0.9895934;CH4_13C,0.0104066;CH4_D0,0.9995865;CH4_D1,0.0004135;CH4_fx_e37_a01',
                                                          'import_grid', 'Mfx_wl_EU_CH4', 'GP=2', ! wetlands
EMIS_IN(227) = 'CH4_fx;CH4_12C,0.9895934;CH4_13C,0.0104066;CH4_D0,0.9995865;CH4_D1,0.0004135;CH4_fx_e38_a01',
                                                          'import_grid', 'Mfx_wl_india_CH4', 'GP=2', ! wetlands
EMIS_IN(228) = 'CH4_fx;CH4_12C,0.9895934;CH4_13C,0.0104066;CH4_D0,0.9995865;CH4_D1,0.0004135;CH4_fx_e39_a01',
                                                          'import_grid', 'Mfx_wl_MIDEAST_CH4', 'GP=2', ! wetlands
EMIS_IN(229) = 'CH4_fx;CH4_12C,0.9895934;CH4_13C,0.0104066;CH4_D0,0.9995865;CH4_D1,0.0004135;CH4_fx_e40_a01',
                                                          'import_grid', 'Mfx_wl_NA_bor_CH4', 'GP=2', ! wetlands
EMIS_IN(230) = 'CH4_fx;CH4_12C,0.9895934;CH4_13C,0.0104066;CH4_D0,0.9995865;CH4_D1,0.0004135;CH4_fx_e41_a01',
                                                          'import_grid', 'Mfx_wl_N_AFR_CH4', 'GP=2', ! wetlands
EMIS_IN(231) = 'CH4_fx;CH4_12C,0.9895934;CH4_13C,0.0104066;CH4_D0,0.9995865;CH4_D1,0.0004135;CH4_fx_e42_a01',
                                                          'import_grid', 'Mfx_wl_NA_TEMP_CH4', 'GP=2', ! wetlands
EMIS_IN(232) = 'CH4_fx;CH4_12C,0.9895934;CH4_13C,0.0104066;CH4_D0,0.9995865;CH4_D1,0.0004135;CH4_fx_e43_a01',
                                                          'import_grid', 'Mfx_wl_RUS_CH4', 'GP=2', ! wetlands
EMIS_IN(233) = 'CH4_fx;CH4_12C,0.9895934;CH4_13C,0.0104066;CH4_D0,0.9995865;CH4_D1,0.0004135;CH4_fx_e44_a01',
                                                          'import_grid', 'Mfx_wl_S_AFR_CH4', 'GP=2', ! wetlands
EMIS_IN(234) = 'CH4_fx;CH4_12C,0.9895934;CH4_13C,0.0104066;CH4_D0,0.9995865;CH4_D1,0.0004135;CH4_fx_e45_a01',
                                                          'import_grid', 'Mfx_wl_SA_temp_CH4', 'GP=2', ! wetlands
EMIS_IN(235) = 'CH4_fx;CH4_12C,0.9895934;CH4_13C,0.0104066;CH4_D0,0.9995865;CH4_D1,0.0004135;CH4_fx_e46_a01',
                                                          'import_grid', 'Mfx_wl_SA_TROP_CH4', 'GP=2', ! wetlands
EMIS_IN(236) = 'CH4_fx;CH4_12C,0.9895934;CH4_13C,0.0104066;CH4_D0,0.9995865;CH4_D1,0.0004135;CH4_fx_e47_a01',
                                                          'import_grid', 'Mfx_wl_se_asia_CH4', 'GP=2', ! wetlands
!
! wild animals
!
EMIS_IN(237) = 'CH4_fx;CH4_12C,0.9896165;CH4_13C,0.0103835;CH4_D0,0.9995758;CH4_D1,0.0004242;CH4_fx_e48_a01',
                                                          'import_grid', 'Mfx_wa_CH4', 'GP=2', !wild animals
```

5.5 TNUDGE

Namelist 7. Example entries to nudge the tracers `CH4` and `CH4_fx` to a predefined lower boundary condition.

```
!# SYNTAX:
!#          tracer, subname, channel, object, nudging-coeff. [s],
!#          min.lat, max.lat, min.lev, max.lev, min.lon, max.lon,
!#          flux diagnostic ?
!# NOTES:
```

```
!#   - special levels: -3 boundary layer ,-2 tropopause, -1 top, 0 surface
!#   - nudging-coeff < 0: apply 'hard' nudging with coeff = model time step
!#
! GHG
TNUDGE_GP(2)  = 'CH4','',     'import_grid','TN_GHG_CH4',10800.0,-90.0,90.0,0,0,0.0,360.0,T,'','','','',0,
!
TNUDGE_GP(4)  = 'CH4','fx',   'import_grid','TN_GHG_CH4',10800.0,-90.0,90.0,0,0,0.0,360.0,T,'','','','',0,
!
```

5.6 H2OISO

Namelist 8. Namelist of the submodel H2OISO as used in the presented examples.

```
&CTRL
/
&CPL
l_steady = T          ! start from steady-state conditions
                      ! this means q, xl and xi are initialized by
                      ! H2OISOHHOvap, H2OISOHHOliq and H2OISOHHOice,
                      ! which are initialized via tracer.nml
l_noconvect_dd = F    ! set true only for sensitivity study
                      ! without influence of convect on deltaD
l_nocloud_dd   = F    ! set true only for sensitivity study
                      ! without influence of cloud on deltaD
/
```

6 ~~Isotopic signatures of emission sources~~

~~Flux in $\times 10^{12}$ g CH_4 per year (Tg CH_4 a^{-1})and signatures in ‰of CH_4 sources. Flux values are taken from the IPCC (2013) bottom-up estimate for 2000-2009. Signatures of bulk source types (other natural, agriculture & waste, and fossil fuel) are averages weighted by the individual flux strength contributions.~~ **217 -59.4 1.5** [1,2,3,4,6] **-336.2 23.8** [3,4,6] **126 -50.3 8.9 -313.3 88.9** 40 -53.8 / [3] -385.0 / [3] 15 -61.5 0.5[1] -319.0 / [5] 11 -63.3 6.5[1,2,3] -390.0 35.5 [3] 54 -40.9 0.9[1,2] -253.4 53.4 [3,7] 6 -59.0 1.0[1,2,3] -220.0 / [3] **200 -57.5 3.8 -313.8 26.5** 89 -60.2 0.3[3,4,6] -317.5 12.5 [3,4] 75 -51.7 2.5[3,4,6] -304.3 8.5[3,4,6] 36 -63.0 1.0[1,2,3,4,6] -324.3 5.5[3,4,6] **96 -41.8 7.5 -154.2 2.5** 32 -43.5 0.5[3,6] -182.5 2.5[3,6] 64 -41.0 7.0[3,6,8] -140.0 0.0[3,6] **35 -23.9 1.6** [1,2,3,4,6] **-213.0 7.5** [3,4,6] -59.0 -324.5 -41.8 -192.0 -23.9 -213.0

References

Atkinson, R.: Kinetics of the gas-phase reactions of OH radicals with alkanes and cycloalkanes, Atmos. Chem. Phys., 3, 2233–2307, 2003.

Brass, M. and Röckmann, T.: Continuous-flow isotope ratio mass spectrometry method for carbon and hydrogen isotope measurements on atmospheric methane, Atmos. Meas. Tech., 3, 1707–1721, https://doi.org/10.5194/amt-3-1707-2010, https://www.atmos-meas-tech.net/3/1707/2010/, 2010.

Brinkop, S. and Jöckel, P.: ATTILA 4.0: Lagrangian advective and convective transport of passive tracers within the ECHAM5/MESSy (2.53.0) chemistry–climate model, Geosci. Model Dev., 12, 1991–2008, https://doi.org/10.5194/gmd-12-1991-2019, https://www.geosci-model-dev.net/12/1991/2019/, 2019.

Bruhwiler, L. M. P., Michalak, A. M., Peters, W., Baker, D. F., and Tans, P.: An improved Kalman Smoother for atmospheric inversions, Atmos. Chem. Phys., 5, 2691–2702, https://doi.org/10.5194/acp-5-2691-2005, https://www.atmos-chem-phys.net/5/2691/2005/, 2005.

Eichinger, R., Jöckel, P., Brinkop, S., Werner, M., and Lossow, S.: Simulation of the isotopic composition of stratospheric water vapour - Part 1: Description and evaluation of the EMAC model, Atmos. Chem. Phys., 15, 5537–5555, https://doi.org/10.5194/acp-15-5537-2015, 2015.

Fletcher, M., E., S., Tans, P. P., Bruhwiler, L. M., Miller, J. B., and Heimann, M.: CH_4 sources estimated from atmospheric observations of CH_4 and its $^{13}C/^{12}C$ isotopic ratios: 2. Inverse modeling of CH_4 fluxes from geographical regions, Glob. Biogeochem. Cycles, 18, 1–15, https://doi.org/10.1029/2004GB002224, 2004.

Frank, F.: Atmospheric methane and its isotopic composition in a changing climate: A modelling study, Ph.D. thesis, Ludwigs Maximillian Universität München, 2018.

IPCC: Climate Change 2013: The Physical Science Basis. Contribution of Working Group I to the Fifth Assessment Report of the Intergovernmental Panel on Climate Change, Cambridge University Press, Cambridge, United Kingdom and New York, NY, USA, https://doi.org/10.1017/CBO9781107415324, www.climatechange2013.org, 2013.

Jöckel, P., Kerkweg, A., Buchholz-Dietsch, J., Tost, H., Sander, R., and Pozzer, A.: Technical Note: Coupling of chemical processes with the Modular Earth Submodel System (MESSy) submodel TRACER, Atmos. Chem. Phys., 8, 1677–1687, https://doi.org/10.5194/acp-8-1677-200, https://www.atmos-chem-phys.net/8/1677/2008/, 2008.

Kerkweg, A., Sander, R., Tost, H., and Jöckel, P.: Technical note: Implementation of prescribed (OFFLEM), calculated (ONLEM), and pseudo-emissions (TNUDGE) of chemical species in the Modular Earth Submodel System (MESSy), Atmos. Chem. Phys., 6, 3603–3609, https://doi.org/10.5194/acp-6-3603-2006, https://www.atmos-chem-phys.net/6/3603/2006/, 2006.

Kiyosu, Y.: Hydrogen isotopic compositions of hydrogen and methane from some volcanic areas in northeastern Japan, Earth and Planetary Science Letters, 62, 41–52, https://doi.org/10.1016/0012-821X(83)90069-9, 1983.

McKinney, C. R., McCrea, J. M., Epstein, S., Allen, H. A., and Urey, H. C.: Improvements in Mass Spectrometers for the Measurement of Small Differences in Isotope Abundance Ratios, The Review of Scientific Instruments, 21, 724–730, https://doi.org/10.1063/1.1745698, 1950.

Monteil, G., Houweling, S., Dlugockenky, E. J., Maenhout, G., Vaughn, B. H., White, J. W. C., and Rockmann, T.: Interpreting methane variations in the past two decades using measurements of CH_4 mixing ratio and isotopic composition, Atmos. Chem. Phys., 11, 9141–9153, 2011.

Quay, P., Stutsman, J., Wilbur, D., Snover, A., Dlugokencky, E., and Brown, T.: The isotopic composition of atmospheric methane, Glob. Biogeochem. Cycles, 13, 445–461, 1999.

Rigby, M., Manning, A. J., and Prinn, R. G.: The value of high-frequency high-precision methane isotopologue measurements for source and sink estimation, J. Geophys. Res., 117, D12 312, https://doi.org/10.1029/2011JD017384, 2012.

Röckmann, T., Brass, M., Borchers, R., and Engel, A.: The isotopic composition of methane in the stratosphere: high-altitude balloon sample measurements, Atmos. Chem. Phys., 11, 13 287–13 304, https://doi.org/10.5194/acp-11-13287-2011, 2011.

Sander, R., Baumgaertner, A., Gromov, S., Harder, H., Jöckel, P., Kerkweg, A., Kubistin, D., Regelin, E., Riede, H., Sandu, A., Taraborrelli, D., Tost, H., and Xie, Z.-Q.: The atmospheric chemistry box model CAABA/MECCA-3.0, Geosci. Model Dev., 4, 373–380, https://doi.org/10.5194/gmd-4-373-2011, 2011.

Snover, A. and Quay, P.: Hydrogen and carbon kinetic isotope effects during soil uptake of atmospheric methane and a temperate grassland, Glob. Biogeochem. Cycles, 14, 25–39, 2000.

Umezawa, T., MacHida, T., Ishijima, K., Matsueda, H., Sawa, Y., Patra, P. K., Aoki, S., and Nakazawa, T.: Carbon and hydrogen isotopic ratios of atmospheric methane in the upper troposphere over the Western Pacific, Atmos. Chem. Phys., 12, 8095–81 113, https://doi.org/10.5194/acp-12-8095-2012, 2012.

White, J., Vaughn, B., and Michel, S.: University of Colorado, Institute of Arctic and Alpine Research (INSTAAR), Stable Isotopic Composition of Atmospheric Methane (^{2}H) from the NOAA ESRL Carbon Cycle Cooperative Global Air Sampling Network, 2005-2009, Version: 2016-04-26, ftp://aftp.cmdl.noaa.gov/data/trace_gases/ch4h2/flask/, 2016.

White, J., Vaughn, B., and Michel, S.: University of Colorado, Institute of Arctic and Alpine Research (INSTAAR), Stable Isotopic Composition of Atmospheric Methane (^{13}C) from the NOAA ESRL Carbon Cycle Cooperative Global Air Sampling Network, 1998-2016, Version: 2018-01-31, ftp://aftp.cmdl.noaa.gov/data/trace_gases/ch4c13/flask/, 2017.

Whiticar, M. and Schaefer, H.: Constraining past global tropospheric methane budgets with carbon and hydrogen isotope ratios in ice., Philosophical transactions, Series A, 365, 1793–1828, https://doi.org/10.1098/rsta.2007.2048, 2007.

Zazzeri, G., Lowry, D., Fisher, R. E., France, J. L., Lanoisell, M., and Nisbet, E. G.: Plume mapping and isotopic characterisation of anthropogenic methane sources, Atmos. Environ., 110, 151–162, https://doi.org/10.1016/j.atmosenv.2015.03.029, 2015.